

國立交通大學

機械工程學系

博士論文

電氣紡絲成形之生醫薄膜研發應用

**Development and Application of Electrospinning Formed
Biomedical Thin Films**

研究生：林耀楠

指導教授：徐瑞坤 教授

中華民國一百年五月

電氣紡絲成形之生醫薄膜研發應用

**Development and Application of Electrospinning Formed
Biomedical Thin Films**

研究生：林耀楠

Student：Yao-Nan Lin

指導教授：徐瑞坤

Advisor：Ray-Quan Hsu

國立交通大學

機械工程學系

博士論文



Submitted to Department of Mechanical Engineering
College of Engineering

National Chiao Tung University

in partial Fulfillment of the Requirements

for the Degree of

Doctor of Philosophy

In

Mechanical Engineering

May 2011

Hsinchu, Taiwan, Republic of China

中華民國一百年五月

電氣紡絲成形之生醫薄膜研發應用

研究生：林耀楠

指導教授：徐瑞坤 教授

國立交通大學機械工程學系博士班

摘 要

電氣紡絲是一種簡單且方便的方法用來製備纖維，以靜電力使聚合物噴向收集板產生連續纖維，纖維直徑可從幾奈米到微米。電氣紡絲是一種有趣的技術用來製備聚乳酸/複合材料。在聚合物噴向收集板過程中，可藉此設計纖維的表面形貌和孔隙度，以提供最適當的纖維薄膜應用於生物醫學。

在過去的幾十年裡，高分子複合材料取代了許多傳統金屬材料的各種應用。這可能是因為高分子複合材料比起傳統材料具有許多優勢。最重要的優勢之一是高分子複合材料易於加工，可大量生產，降低成本。在大多數的這些應用中，高分子可藉由添加填料來改變其性能，以達到提升材料強度與特殊性能需求。比起其他常規材料高分子複合材料在改變材料性能上更具有優勢。目前這些高分子複合材料已應用在不同領域，從家電製品到航太科技比比皆是。在生醫應用方面本研究以電氣紡絲製備聚左乳酸/chlorhexidine (CHX)-gluconate 可生物降解藥物釋放薄膜，能持續穩定地抑制細菌生長。藉由細菌生長曲線來即時評估藥物釋放薄膜釋放出藥物的速率與細菌生長的關係。另外本研究提出了一種新的想法，以添加碳酸鈣及其同質異構物於聚左乳酸中，並以電氣紡絲製備生物可降解引導組織再生

膜或引導骨頭再生膜。碳酸鈣具備良好的生物相容性，而其同質異構物因有不同的晶格結構，意味著具備不同的力學性能。實驗結果顯示碳酸鈣及其具有不同晶格結構的同質異構物，能製備不同機械強度的生物可降解引導組織再生膜或引導骨頭再生膜。此再生膜的機械性質實驗結果顯示，聚左乳酸添加 5% 霰石較純的聚左乳酸薄膜的降伏強度高出 35%。此結果提供一新的觀念，未來將可視需求而選擇合適的碳酸鈣或其同質異構物，藉由添加不同晶體結構的碳酸鈣比例來製備所需強度的生物可降解引導組織再生膜或引導骨頭再生膜以達到更廣泛的生物醫學應用。

本實驗另以電氣紡絲製備抗紫外線高分子微米纖維。而此抗紫外線纖維薄膜以聚左乳酸和常用紫外線吸收劑二苯甲酮-12 與抗氧化劑 Chemfos - 168 來製備抗紫外線高分子微米纖維。結果顯示，添加紫外線吸收劑二苯甲酮-12 與抗氧化劑 Chemfos - 168 雖然能皆具備良好的抗紫外線能力，但在降解速率上添加紫外線吸收劑二苯甲酮-12 抗紫外線高分子纖維薄膜卻遠不及抗氧化劑 Chemfos - 168 抗紫外線高分子納米纖維薄膜。

關鍵字：高分子複合薄膜，電氣紡絲，抑菌，碳酸鈣，生物礦化，同質異構物，方解石，霰石，抗紫外線薄膜

Development and Application of Electrospinning Formed Biomedical Thin Films

Student : Yao-Nan Lin

Advisor : Dr. Ray-Quen Hsu

Department of Mechanical Engineering
National Chiao Tung University

ABSTRACT

Electrospinning is a simple and versatile method for fibers preparation, which employs electrostatic forces that strength a polymer jet to generate continuous fibers with diameters ranging from micrometers down to several nanometers. Electrospinning is an interesting technique for spinning PLLA / composites. The process offers an excellent opportunity for designing the surface morphology and porosity of the fibers to provide the most appropriate interface for biomedical application.

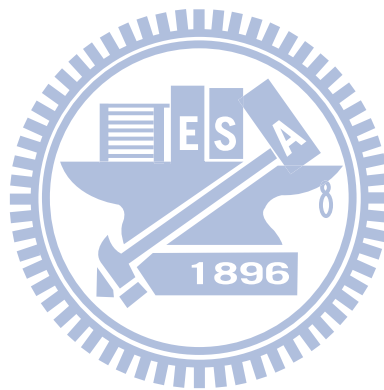
Over the past few decades, polymer composites have replaced many of the conventional metals/materials in various applications. This trends may arise from the advantages polymer composites offer over conventional materials. The most important advantages of using polymer composites are the ease of processing, productivity, and cost reduction. In many of these applications, the properties of polymers composites are modified using fillers and fibers to suit the high strength/specific properties requirements. Polymer composites offer advantages over other conventional materials when specific properties are required. These composites are finding applications in diverse fields from electronic appliances to spacecrafts. These research presents some possible applications in the field of biomedical thin films.

The study found that biodegradable drug delivery membranes that were fabricated from Poly(α -L-alanine) (PLLA) and chlorhexidine (CHX)-gluconate via electrospinning could steadily and continuously inhibit the growth of bacteria. Bacterial growth curves were used to evaluate on a real-time basis the relationship between drug delivery speeds of the membranes and growth rates of bacteria in different phases.

Besides, this paper proposes a novel idea, i.e. to produce bio-degradable GTR or GBR membranes with calcium carbonate and its polymorphism, aragonite, through electrospinning. Calcium carbonate enjoys fair bio-compatibility, while its polymorphism has a different lattice structure which means different mechanical properties. We can tell that PLLA with 5% aragonite offered a yield strength than pure PLLA by approximately 35%. There is a potential that adding calcite or aragonite of different percentage can produce membranes with different mechanical strength for wider applications.

This article provides a comprehensive review of the ultraviolet resistance ability, bio-degradation and structural differences of UV absorption and anti-oxidation agents. We use the elements (UV absorption and anti-oxidation agents) composite with PLLA by electrospinning in our study. We observed the PLLA/UV absorption (Benzophenone-12) fiber membranes higher than PLLA membrane 14.9% in UVA ratio. In this experiment, although both are bio-degradable membranes, the the PLLA/UV absorption (Benzophenone-12) fiber membranes higher than PLLA membrane 61.6% in I875/I1452 Raman intensity ratio. So PLLA Add UV absorption (Benzophenone-12) fiber membranes can achieve good UV resistance and fast bio-degradation.

Keyword : Polymer Composites membranes, Electrospinning, Bacteriostatic,
Calcium Carbonate, Biomineralization, Polymorphism, Calcite, Aragonite,
Ultraviolet resistance membrane



誌 謝

本論文得以順利完成，首先要感謝我的指導教授徐瑞坤老師對我論文上的指導，也因為有老師不斷灌輸我們做研究的方法及態度，論文才能順利完成。感謝論文口試委員台灣科技大學向四海教授、交通大學洪景華教授、陳仁浩教授、楊秉祥教授與新竹教育大學林志明教授對我論文詳細審閱，匡正謬誤，讓論文更臻完善。

感謝在成形實驗室的所有研究伙伴，論文實驗的部分在學弟的協助下能夠快速完成，在此特別感謝李柏德、梁達嵐、江維堂、王奕超、鄭凱文、陳皇洲、陳鈞源、邱添煌、吳勇霖、李艾聰、徐啟峰、黃大益、曾仕駿、李昱劭、陳立群給予我實驗研究上的幫助，感謝實驗室的學弟妹，謝謝你們，讓實驗室總是天天都很開心，讓我博士班求學期間生活更加精采與順利。感謝海洋大學張建仁教授、鄭煥琨、黃瑩玉醫師、陳維揚、林志杰、黃怡禎與交通大學材料工程學系葉孝蔚博士、張凱明學長、陳永昌、蘇祥溢在我求學期間給予精神鼓勵與支持，僅此深致謝忱

最後最重要的，感謝我的家人，感謝爸爸媽媽對我的付出與養育之恩，讓我在求學的路上順利沒有牽掛，謝謝你們。

謹以此文獻給所有關愛我、照顧我的師長與親友。

耀楠 謹識

2011.5

Contents

摘要	ii
ABSTRACT	iv
誌謝	vii
Contents	viii
Table of contents	x
Figure of contents	xi
Chapter 1 General Introduction	1
1.1 The background of the research	1
1.2 Biodegradable materials	2
1.3 Electrospinning biodegradable PLA	4
1.4 Objectives of research	6
Chapter 2 Electrospinning	13
2.1 Introduction	13
2.2 Taylor cone	15
2.3 Major processing parameters	16
2.3.1 Voltage	17
2.3.2 Feed rate	17
2.3.3 Effect of Collector	18
2.3.4 Diameter of Pipette Orifice / Needle	18
2.3.5 Distance between Tip and Collector	18
2.4 Important features of electrospinning	20
2.5 Biodegradable polymer	21
2.6 Optimum conditions for electrospinning PLLA fibers	22
Chapter 3 Membranes for Drug Delivery and Antibacterial	25
3.1 Introduction	25
3.2 Experimental procedure	29
3.2.1 Materials and Methods	29
3.2.2 Fabrication of bacteriostatic Fibers	29
3.2.3 Physical and chemical properties	30
3.2.4 Antibacterial Test	31
3.3 Results and Discussion	32
Chapter 4 Membranes for Guided Bone Regeneration	43
4.1 Introduction	43
4.2 Experimental procedure	49

4.2.1	Materials and Methods	49
4.2.2	Fabrication of Calcium Carbonate Particles	49
4.2.3	Fabrication of Guided Bone Regeneration membranes	50
4.2.4	Physical and chemical properties	50
4.2.5	Analysis of mechanical properties	51
4.3	Results and Discussion	52
Chapter 5 Ultraviolet Resistant and Degradable Membranes		61
5.1	Introduction	61
5.2	Experimental procedure	66
5.2.1	Materials and Methods	66
5.2.2	Fabrication of Composite ultraviolet resistant and high degree of degradable membranes	68
5.2.3	Physical and chemical properties	69
5.2.4	Ultraviolet Protection Factor (UPF).....	69
5.2.5	UVA Effectiveness - The Boot's Star System.....	70
5.2.6	UVA Effectiveness - Critical Wavelength.....	71
5.3	Results and Discussion	72
Chapter 6 Conclusions		82
Chapter 7 Future work.....		87
References		88

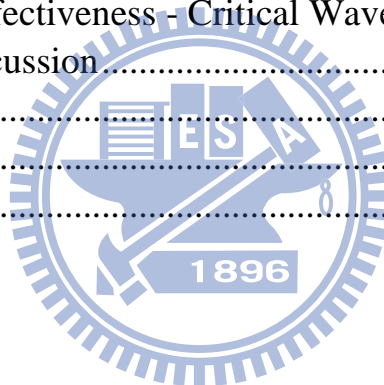


Table of contents

Table 4- 1: Mechanical properties of the electrospun PLLA, PLLA/calcite and PLLA/aragonite fiber.....	60
Table 5- 1 Ultraviolet wave-lengths of maximum sensitivity for typical commercial polymers[62].....	62
Table 5- 2 UPF classification system of sun protective clothing[96]	70
Table 5- 3 UVA Effectiveness[96].....	71
Table 5- 4 Level of Protection (Critical Wavelength)[96]	72
Table 5- 5 UVA Effectiveness - UPF and Critical Wavelength.....	81



Figure of contents

Figure 1- 1 Composite Reinforcement	2
Figure 1- 2 General molecular structure of poly(α -hydroxyl acid) family[9, 13]	4
Figure 1- 3 Polylactide synthesis[9, 13]	4
Figure 1- 4 scope of experiments.....	12
Figure 2- 1 Electrospinning Device Setup.....	14
Figure 2- 2 (a) high voltage power supply (b) KDS100 syringe pump (c) 22 needle gauge	15
Figure 2- 3 Taylor cone[17-18]	16
Figure 2- 4 SEM images showing the variation of beaded fibers at different feeding rates: (a) 20 ml/min; (b) 75 ml/min[21].....	17
Figure 2- 5 Nylon 6,6 at (a) 2 cm deposition distance and (b) 0.5cm deposition distance[21].....	20
Figure 2- 6 High-speed camera observed the fiber spraying process of electrospun	23
Figure 2- 7 The optimum conditions for Electrospinning PLLA fibers.....	24
Figure 3- 1 The structure of Chlorhexidine[36, 74]	26
Figure 3- 2 Field Emission Scanning electron micrographs of the electrospinning fibers: (a) PLLA fibers, (b) PLLA/CHX fibers image (50:50).....	32
Figure 3- 3 Fourier Transform Infrared Spectra of PLLA fibers and PLLA/CHX fibers (50:50).....	33
Figure 3- 4 Micro-Raman spectra of PLLA fibers and PLLA/CHX fibers.....	34
Figure 3- 5 (a) (b) (c) are illustrations of interaction between drug released	

by drug delivery membranes and growth rates of *XL1-Blue* in the (a) zero to third hours (b) fourth to ninth hours (c) tenth to twelfth hours (yellow membrane: PLLA/CHX(50:50 volume ratio), Green bacterial: *XL1-Blue*) (d) Growth curves of *XL1-Blue* in LB medium inoculated with 10^7 CFU of bacteria. The presence of different concentrations of (▲) PLLA/CHX fibers (90:10) and (●) PLLA/CHX fibers (50:50). Another two curves: one is only (▼) poly(L-lactic acid)s fibers; the other is (■) ampicillin-added 100 $\mu\text{g/mL}$ 37

Figure 3- 6 (a) (b) (c) are illustrations of interaction between drug released by PLLA/CHX(50:50) membranes and growth rates of *TOPO XL1-Blue* in the (a) zero to fourth hours (b) fifth to tenth hours (c) eleventh to twelfth hours (yellow membrane: PLLA/CHX(50:50 volume ratio), Green bacterial: *TOPO XL1-Blue*).(d) Growth curves of *TOPO XL1-Blue* in LB medium inoculated with 10^7 CFU of bacteria. The presence of different concentrations of (▲) PLLA/CHX fibers (90:10) and (●) PLLA/CHX fibers (50:50). Another two curves: one is only (▼) poly(L-lactic acid)s fibers; the other is (■) ampicillin-added 100 $\mu\text{g/mL}$ 41

Figure 4- 1 Guided bone regeneration (GBR) membranes[40-42] 45

Figure 4- 2 Calcium carbonate phase diagram[56] 47

Figure 4- 3 Calcium carbonate Interaction diagram[42, 48] 48

Figure 4- 4 lattice structure of (a)calcite and (b)aragonite[57] 48

Figure 4- 5 Calcium carbonate of (a)calcite and (b)aragonite..... 48

Figure 4- 6 FTIR spectra of calcite and aragonite showing their characteristic carbonate vibrational bands.....	53
Figure 4- 7 Powder X-ray diffractograms of calcite and aragonite.....	54
Figure 4- 8 Field Emission Scanning electron micrographs of the electrospinning fibers: (a) PLLA fibers, (b) PLLA/calcite fibers(c) PLLA/aragonite fibers image.	54
Figure 4- 9 Micro-Raman spectra of the synthetically prepared PLLA fibers, PLLA/calcite fibers and PLLA/aragonite fibers.....	56
Figure 4- 10 Tensile tests (a) specimen size 25 mm× 70mm× 0.1mm (b) Instrument setup.....	57
Figure 4- 11 Stress-strain curves of electrospun of PLLA, PLLA/calcite and PLLA/aragonite fiber.....	57
Figure 5- 1 The Ultraviolet resistance structure of (a) 2-Hydroxy-4-Octyloxy Benzophenone, (b) 2-(2'-hydroxy-5'-methylphenyl) benzotriazole, (c) Tetrakis [Methylene(3',5'-Di-tert-Butyl-4-hydroxyphenyl) Propionate] methane, and (d) Tris(2,4-di-tert-butylphenyl) phosphate	67
Figure 5- 2: SEM Image (a) PLLA , (b) PLLA/Benzophenone-12 , (c) PLLA/Chemfos-168(d) PLLA/Chemsorb-p.....	73
Figure 5- 3 Micro-Raman spectra of PLLA fibers, PLLA/Benzophenone-12 fibers, PLLA/Chemfos-168 fibers and PLLA/ Chemsorb-p fibers.	78
Figure 5- 4 The transmission spectra of (A) PLA , (B) PLA/Benzophenone-12 , (C) PLA/ Chemfos-168 fibers.	80

Chapter 1 General Introduction

1.1 The background of the research

Composites are combination of two distinct material phases, a bulk phase, also known as a matrix and a reinforcement phase. It is the combination of the strength of the reinforcement and the toughness of the matrix that gives composite its superior properties that are not available in any single conventional material[1-2]. Both matrix and reinforcement phases can be metal, ceramic or polymer. Generally, the matrix binds the reinforcement together to give the composite its shape, surface appearance and resistance to environmental damage. While the matrix is usually ductile or tough, the reinforcements are strong with low densities. It is the reinforcement that carries most of the load thus giving the composite its stiffness and strength[3]. When fiber reinforcements of less than 100nm are used, it is possible to produce transparent composites[4] although they are generally opaque due to light scattering. In most cases, composites are designed for loadbearing applications although there are other classes of composites that are used for their interesting electrical, thermal or magnetic properties[5-8].

There are generally two types of composite reinforcements, fibrous reinforcement and particulate reinforcement. In fibrous reinforcement, the fibers arrangement can be of many different forms. The simplest arrangement of the fibers in the matrix is to have the fibers aligned in a certain direction to form a laminate composite. Thin sheets of unidirectional composites can be stacked in an arrangement such that the fibers are oriented at 0° , 90° and $+45^\circ$

directions. Such composite laminates are strong in all directions within the plane containing the fibers but are weak in the direction normal to the plane of the laminates[1-2]. Other types of fiber arrangements include weaving to produce fabrics of different shapes and weave configurations, knitting as well as braiding as seen in Figure 1-1. Depending on the application of the composite, different fiber arrangements are used as reinforcement in the composite. For example, braided fiber can be used as reinforcement for composite where high torsional stiffness is desired. Randomly distributed fibers in the form of non-woven mat can also be used as reinforcement in composite[3].

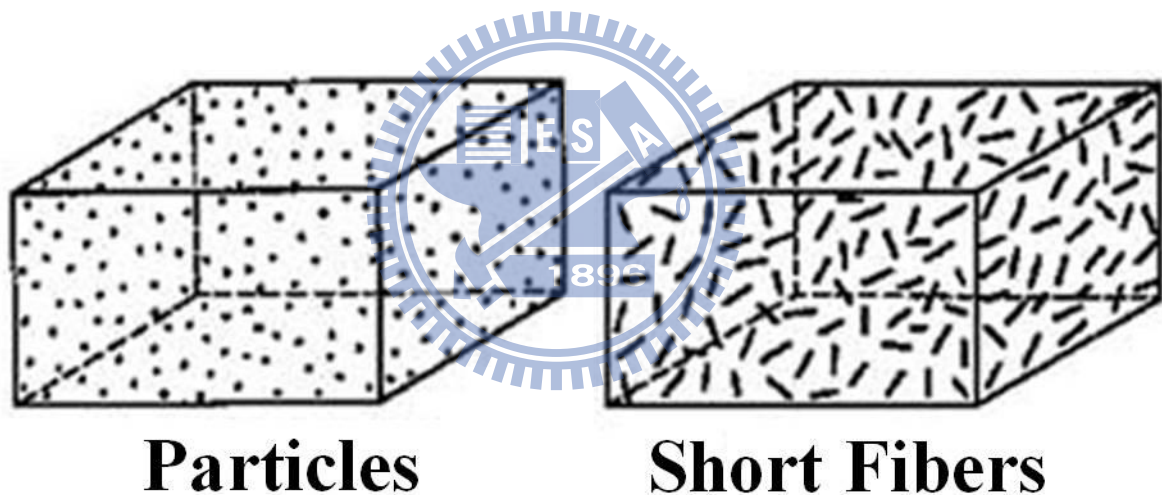


Figure 1- 1 Composite Reinforcement

1.2 Biodegradable materials

Polylactic acid or polylactide (PLA) is a biodegradable, thermoplastic, aliphatic polyester derived from renewable resources, such as corn starch or sugarcane[9]. PLA is a sustainable alternative to petrochemical-derived products, since the lactides from which it is ultimately produced can be

derived from the fermentation of agricultural by-products such as corn starch or other carbohydrate-rich substances like maize, sugar or wheat. PLA has a crystallinity of around 37%, a glass transition temperature between 50-80 °C and a melting temperature between 173-178 °C[10]. PLA has similar mechanical properties to PETE polymer, but has a significantly lower maximum continuous use temperature[11-12]. Due to the chiral nature of lactic acid, several distinct forms of polylactide exist: Poly(α -L-alanine) (PLLA) is the product resulting from polymerization of L, L-lactide (also known as L-lactide). The melting temperature of PLLA can be increased 40-50 °C and its heat deflection temperature can be increased from approximately 60°C to up to 190 °C by physically blending the polymer with PDLA (poly-D-lactide). Polymerization of a racemic mixture of L- and D-lactides[13] usually leads to the synthesis of poly-DL-lactide (PDLLA) which is amorphous. The degree of crystallinity, and hence many important properties, is controlled by the ratio of D to L enantiomers used.

PLA belongs to the poly(α -hydroxyl acid) family (Figure 1-2) with a methyl group attached to the R position, which makes it the second simplest poly(α -hydroxyl acid) after polyglycolide which has only one hydrogen atom in the R position. PLA can be obtained by polycondensation or by step-growth polymerization of lactic acid. High molecular weight PLA is, however, normally formed by a ring-opening polymerization of lactide, or the dimer of lactic acid, as is shown in figure 1-3.

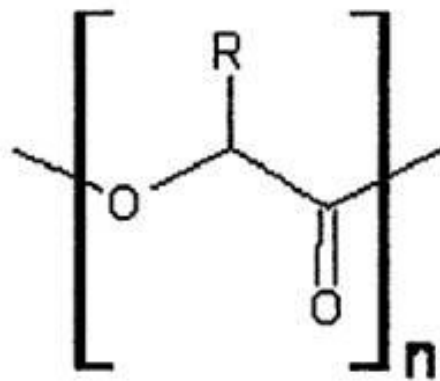


Figure 1- 2 General molecular structure of poly(α -hydroxy acid) family[9, 13]

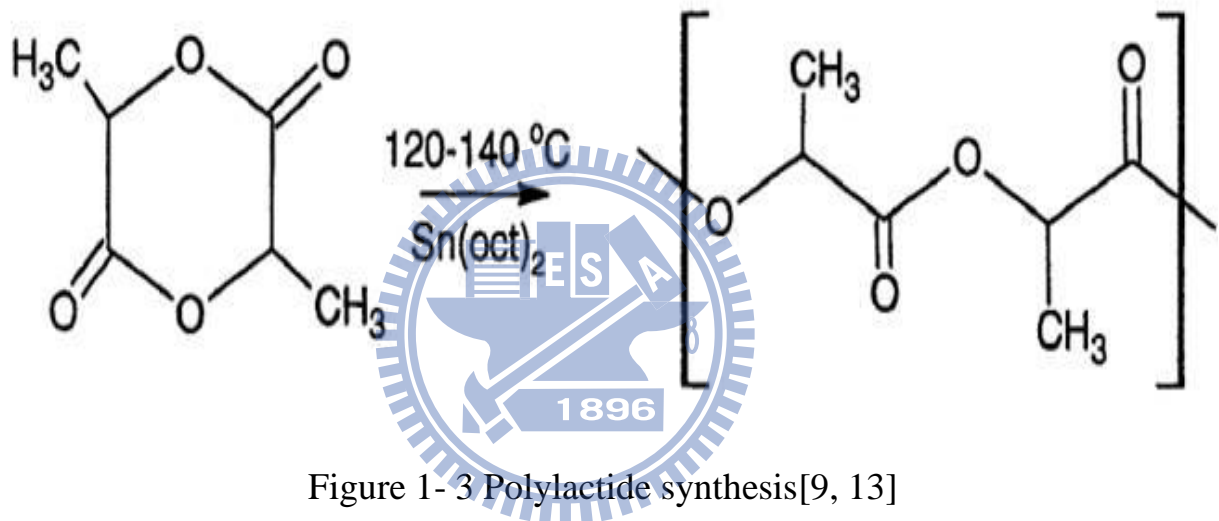


Figure 1- 3 Polylactide synthesis[9, 13]

PLA is currently used in a number of biomedical applications, such as sutures, stents, dialysis media and drug delivery devices. It is also being evaluated as a material for tissue engineering. Because it is biodegradable, it can also be employed in the preparation of bioplastic, useful for producing loose-fill packaging, compost bags, food packaging, and disposable tableware. In the form of fibers and non-woven textiles, PLA also has many potential uses, for example as upholstery, disposable garments, awnings, feminine hygiene products, and nappies[9, 13].

1.3 Electrospinning biodegradable PLA

In the late 1500s William Gilbert set out to describe the behaviour of magnetic and electrostatic phenomena. He observed that when a suitably electrically charged piece of amber was brought near a droplet of water it would form a cone shape and small droplets would be ejected from the tip of the cone: this is the first recorded observation of electrospaying. The process of electrospinning was patented by J.F Cooley in February 1902[14] and by W.J. Morton in July 1902[15]. In 1914 John Zeleny, published work on the behaviour of fluid droplets at the end of metal capillaries. His effort began the attempt to mathematically model the behaviour of fluids under electrostatic forces[16].

Between 1964 and 1969 Sir Geoffrey Ingram Taylor produced the theoretical underpinning of electrospinning[17-18]. Taylor's work contributed to electrospinning by mathematically modelling the shape of the cone formed by the fluid droplet under the effect of an electric field; this characteristic droplet shape is now known as the Taylor cone. He further worked with J. R. Melcher to develop the "leaky dielectric model" for conducting fluids[18]. In the early 1990s several research groups (notably that of Reneker and Rutledge who popularised the name electrospinning for the process)[19] demonstrated that many organic polymers could be electrospun into nanofibers. Since then, the number of publications about electrospinning has been increasing exponentially every year[20].

The electrospinning process, in its simplest form consisted of a pipette to hold the polymer solution, two electrodes and a DC voltage supply in the kV range. The polymer drop from the tip of the pipette was drawn into a fiber due to the high voltage. The jet was electrically charged and the charge caused the

fibers to bend in such a way that every time the polymer fiber looped, its diameter was reduced. The fiber was collected as a web of fibers on the surface of a grounded target[21].

Electrospinning is a simple and versatile method for fibers preparation, which employs electrostatic forces that strength a polymer jet to generate continuous fibers with diameters ranging from micrometers down to several nanometers[22-23]. Electrospinning is an interesting technique for spinning PLLA[24]. The process offers an excellent opportunity for designing the surface morphology and porosity of the fibers to provide the most appropriate interface for biomedical application[10, 12, 25-27].

1.4 Objectives of research

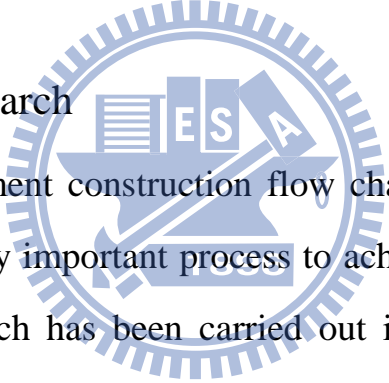


Figure 1-4 Experiment construction flow chart. Research on Controlled release of drugs is a very important process to achieve the highest therapeutic efficiency. Much research has been carried out in order to develop of new and/or improved drug therapies that are more efficient and, most importantly, more cost-effective. The conventional definition of controlled release is a constant level of drugs in suitable systems. Electrospun fibers was a novel process to prepare and the release characteristics should depend on interaction between polymer and drug pair as much as on the sizes of fibers[28]. Polymeric drug delivery systems plays an important role in conventional dosage forms, such as improved therapeutic effect, reduced toxicity, convenience, and so on. In previous study, the drugs can be capsulated directly into electrospun fibers and these systems show nearly zero-order kinetics of drug release[29].

Previous studies fabricated effective bacteria inhibiting fiber membranes from Polymer/Silver nanoparticles[30-31] & Polymer/chitosan[32-34] via electrospinning. In addition, when it comes to bacteria inhibiting drug, such as CHX[35], CHX-CA[36], CHX-Digluconate[37], and CHX-gluconate, only the delivery efficiency of Polymer/CHX, or just that of CHX, has been discussed[36-37]. Tests on the inhibiting capability (Inhibition Zone) of Polymer/CHX matrix were rarely done. Evaluations of bacteria inhibiting capability based on Inhibition Zone were only qualitative, not quantitative. This study aimed to discuss whether biodegradable inhibiting drug delivery membranes fabricated from PLLA/CHX via electrospinning possessed the characteristics of drug delivery systems and whether CHX could still inhibit bacteria after being released from PLLA. This experiment quantitatively evaluated bacteria growth in liquid culture by observing Optical Density 600nm (OD) at one-hour intervals, and used the growth curves thus derived to evaluate on a real-time the impacts of drug delivery speeds on the growth rates of bacteria in different phases. Competent cell and plasmid inserted competent cell, bacteria that are of the same strain but grow at different speeds were utilized to interact with biodegradable CHX delivery membranes fabricated via electrospinning to determine whether such drug delivery membranes are a rate-preprogrammed drug delivery system.

A major goal of periodontal regeneration therapy is the regeneration of lost supporting tissue, including the alveolar bone, periodontal ligament, and cementum around a previously diseased tooth root[38-39]. Guided tissue regeneration (GTR) has accomplished this goal, and has become a standard

procedure for periodontal regeneration therapy since it was initially suggested for such therapy[40-42]. In addition, it has been applied to bone and peri-implant defects, and for bone augmentation procedures prior to implant placement. In such situations, it is sometimes termed guided bone regeneration (GBR)[42-44]. For the membrane to be effective, it must satisfy criteria such as excellent biocompatibility, controllable biodegradability, cytocompatibility, suitable microstructure (pore size and porosity) and mechanical properties[45-47].

In previous studies, although present polymeric products show positive results in clinical studies, their weak mechanical properties and poor bone regeneration capacity are still major challenges[42]. To overcome these problems, recent research efforts have included the incorporation of bone-like ceramics into the membranes, e.g. hydroxyapatite, tricalcium phosphate and calcium carbonate[42, 44, 48-49]. Hydroxyapatite ($\text{HA}, \text{Ca}_{10}[\text{PO}_4]_6[\text{OH}]_2$) is the main mineral component of natural bone and has good biocompatibility, osteoconductivity and bioactivity, and thus it is suitable for making the guided bone regeneration membranes[50]. However, the brittleness of hydroxyapatite limits its applicability[51]. The co-precipitation of HA nanocrystals in soluble collagen has met with partial success in the fabrication of HA–collagen nanocomposites similar to the nanostructure of real bone[52], though with weaker mechanical properties. Calcium carbonate has been recognized as bone filling material and its good osteoconductivity has been approved in recent studies[44, 53-55].

Polymorphism in materials science is the ability of a solid material to exist in more than one form or crystal structure. Polymorphism can potentially be

found in any crystalline material. Calcium carbonate is one of the most common biological minerals and has polymorphs of calcite, aragonite, and to a less extent amorphous state, vaterite or monohydrate in calcareous structures of organisms[56]. Calcium carbonate can be precipitated in aqueous solution as three anhydrous polymorphs, calcite, aragonite and vaterite, and three hydrated forms, amorphous calcium carbonate, calcium carbonate hexahydrate and calcium carbonate monohydrate[57-58].

The calcite has a trigonal and the aragonite has an orthorhombic crystal structure. The latter has typically higher elasticity modulus than the powder, better dispersibility due to the surface treatment, increased impact strength, tensile strength and elongation at break[59]. So far, most GTR/GBR membranes are made in the shape of porous foam, created by traditional methods such as particulate leaching, solvent casting or gas foaming[60]. Electrospinning is a simple and versatile method for fibers preparation, which employs electrostatic forces that strength a polymer jet to generate continuous fibers with diameters ranging from micrometers down to several nanometers[22]. Fibers obtained from electrospinning are in the range of 50 nm to a few microns in diameter and generally collected in the form of a non-woven structure[23]. It has already been shown that electrospun membranes have the potential to promote osteoblastic cell function and bone regeneration[42].

When plastics are used for outdoor applications, they often deteriorate fairly rapidly. Theoretical explanation is based upon absorption of ultraviolet energy, raising some bonds to an energy level which exceeds their stability, and thus initiating their breakdown, usually involving atmospheric oxidation and

sometimes hydrolysis as well. Many of the newer engineering plastics offer high performance in their mechanical, thermal, and chemical properties, but still cannot be recommended for use out-of-doors[61].

Ultraviolet radiation can be classified into UV-A, UV-B, and UV-C regions. Much less is known about the biological effects of UV-A radiation (320–400 nm), which adjoins the visible light, so the waveband is usually not a topic of discussion. Most observed biological effects of UV-B (280–320 nm) radiation are extremely detrimental to living organisms[62]. Because solar UVR below wavelengths of 290 nm is effectively absorbed by stratospheric ozone, and no such radiation reaches living organisms from natural sources, the wavelength in the UV-C region (200–280 nm) is considered of little detriment to human beings. Ultraviolet radiation (UV-A · UV-B · UV-C) can cause damage to C-H, C-C, O-H, C-Cl, etc. in living organisms, and substance with the same bond energy. In order to solve the polymer composite material is not suitable for outdoor issues, often in the processing additives are added to solve this problem a little[61-63]. Many common additives, such as : UV Absorber : Benzophenone · Phosphite Antioxidant · Hindered Amine Light Stabilizers (HALS) : Hindered Amine Light Stabilizer[64] ·

Poly lactide (PLA) is one of the most promising biodegradable polymers owing to its mechanical property profile, thermoplastic processibility and biological properties, such as biocompatibility and biodegradability. The use of synthetic degradable polyesters in surgery as suture materials and bone fixation devices has three decades of history. Degradable polyesters derived from three monomers, lactide, glycolide and caprolactone, are commonly used clinically.

They are characterized by degradation times ranging from days to years, depending on formulation and initial molecular weight[10].

The majority of the studies on electrospinning fibers of PLLA to add Benzophenone -12[65-68] and Chemfos-168[69-70] from solutions, we have reported that molecular structures and antiultraviolet of electrospinning nanofibers. Benzophenone can be used as a photo initiator in UV-curing applications such as inks, imaging and clear coatings in the printing industry. Benzophenone prevents ultraviolet (UV) light from damaging scents and colours in products such as perfumes and soaps. It can also be added to the plastic packaging as a UV blocker. This allows manufacturers to package the product in clear glass or plastic. Without it, opaque or dark packaging would be used. In laboratories, solvents are often distilled with sodium and benzophenone as desiccants. The product of these two chemicals in the absence of air and water is a dark blue ketyl; a solution of this ketyl can be used to qualitatively test for the absence of air and water. Chemfos-168 is an antioxidant is a molecule capable of slowing or preventing the oxidation of other molecules. Oxidation is a chemical reaction that transfers electrons from a substance to an oxidizing agent. Oxidation reactions can produce free radicals, which start chain reactions that damage cells. Antioxidants terminate these chain reactions by removing free radical intermediates, and inhibit other oxidation reactions by being oxidized themselves. As a result, antioxidants are often reducing agents such as thiols or polyphenols.

In this study, we investigated ultraviolet resistance of the PLLA, PLLA / UV absorption and PLLA / anti-oxidation agents by electrospinning. It is believed that this study could provide a good insight into ultraviolet resistance

properties of the electrospinning polymer. We also hope to make the ultraviolet resistance electrospinning fibers and have high degree of degradability.

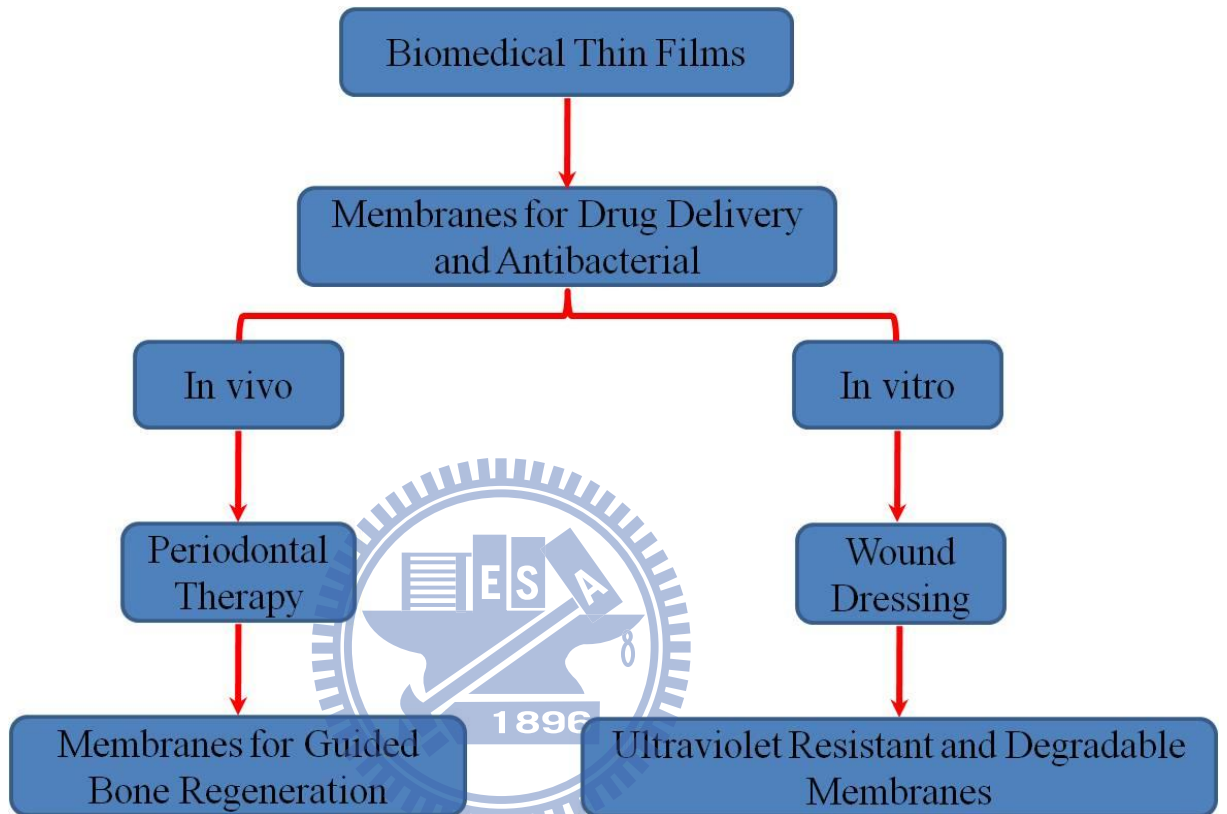


Figure 1- 4 scope of experiments

Chapter 2 Electrospinning

2.1 Introduction

In the late 1500s William Gilbert set out to describe the behaviour of magnetic and electrostatic phenomena. He observed that when a suitably electrically charged piece of amber was brought near a droplet of water it would form a cone shape and small droplets would be ejected from the tip of the cone: this is the first recorded observation of electrospinning. The process of electrospinning was patented by J.F Cooley in February 1902[14] and by W.J. Morton in July 1902[15]. In 1914 John Zeleny, published work on the behaviour of fluid droplets at the end of metal capillaries. His effort began the attempt to mathematically model the behaviour of fluids under electrostatic forces[16].

Between 1964 and 1969 Sir Geoffrey Ingram Taylor produced the theoretical underpinning of electrospinning[17-18]. Taylor's work contributed to electrospinning by mathematically modelling the shape of the cone formed by the fluid droplet under the effect of an electric field; this characteristic droplet shape is now known as the Taylor cone. He further worked with J. R. Melcher to develop the "leaky dielectric model" for conducting fluids[18]. In the early 1990s several research groups (notably that of Reneker and Rutledge who popularised the name electrospinning for the process)[19] demonstrated that many organic polymers could be electrospun into nanofibers. Since then, the number of publications about electrospinning has been increasing exponentially every year[20].

The electrospinning process, in its simplest form consisted of a pipette to hold the polymer solution, two electrodes and a DC voltage supply in the kV

range. The polymer drop from the tip of the pipette was drawn into a fiber due to the high voltage. The jet was electrically charged and the charge caused the fibers to bend in such a way that every time the polymer fiber looped, its diameter was reduced. The fiber was collected as a web of fibers on the surface of a grounded target[21] (Figure 2-1).

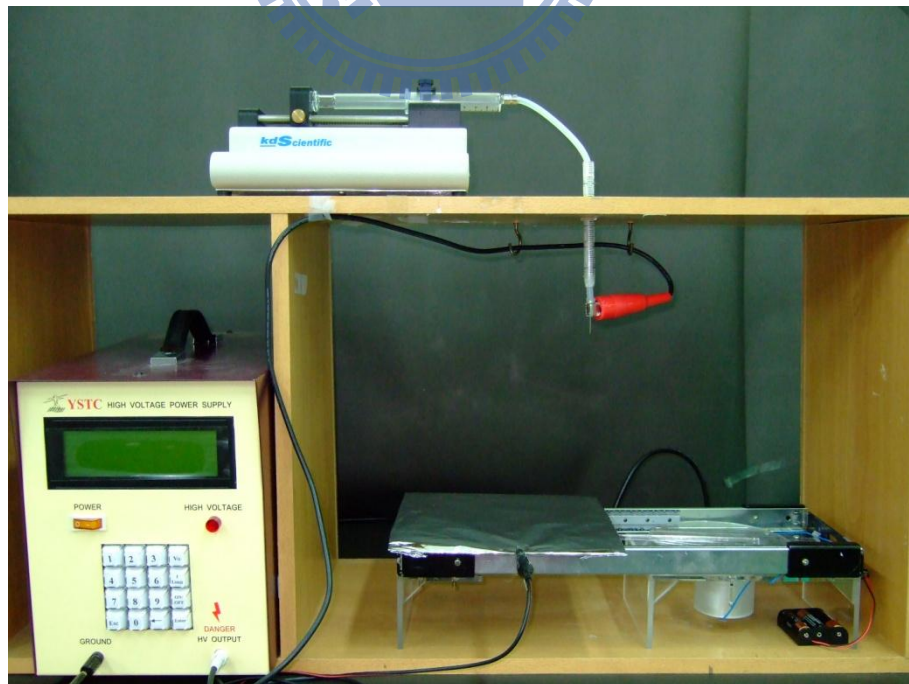
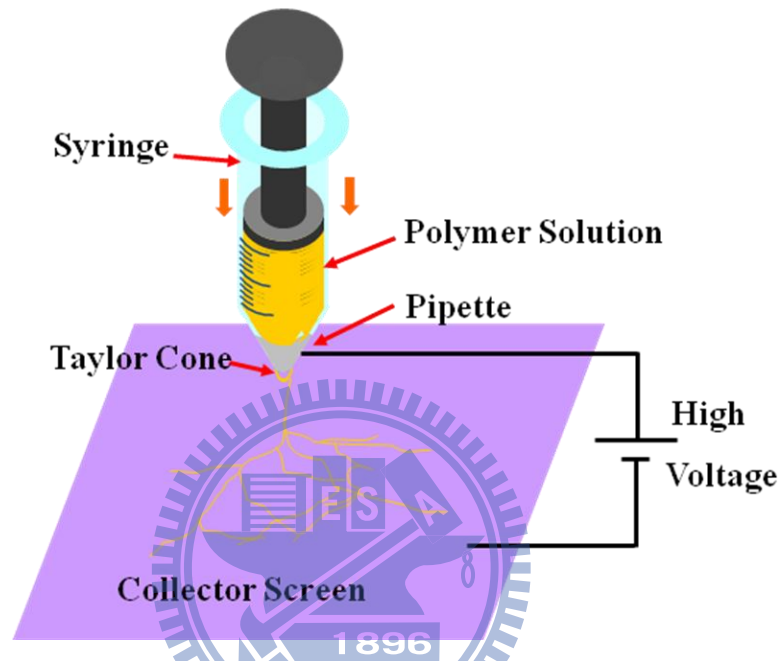


Figure 2- 1 Electrospinning Device Setup

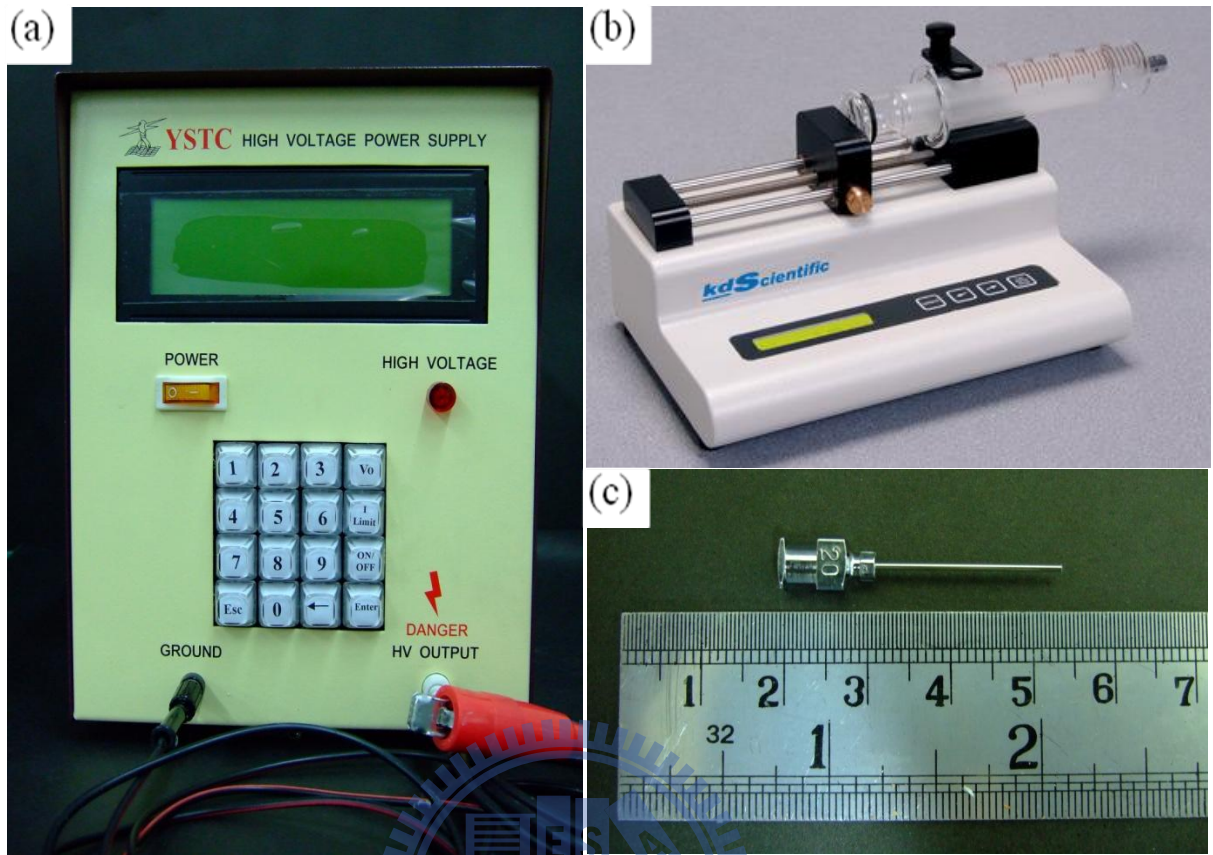


Figure 2- 2 (a) high voltage power supply (b) KDS100 syringe pump (c) 22 needle gauge

2.2 Taylor cone

In electrospinning, a high voltage is applied to a polymer fluid such that charges are induced within the fluid. When charges within the fluid reached a critical amount, a fluid jet will erupt from the droplet at the tip of the needle resulting in the formation of a Taylor cone[17-18]. The electrospinning jet will travel towards the region of lower potential, which in most cases, is a grounded collector. There are many parameters that will influence the morphology of the resultant electrospun fibers. The parameters affecting electrospinning and the fibers may be broadly classified into polymer solution

parameters, processing conditions which include the applied voltage, temperature and effect of collector, and ambient conditions. With the understanding of these parameters, it is possible to come out with setups to yield fibrous structures of various forms and arrangements. It is also possible to create nanofiber with different morphology by varying the parameters.

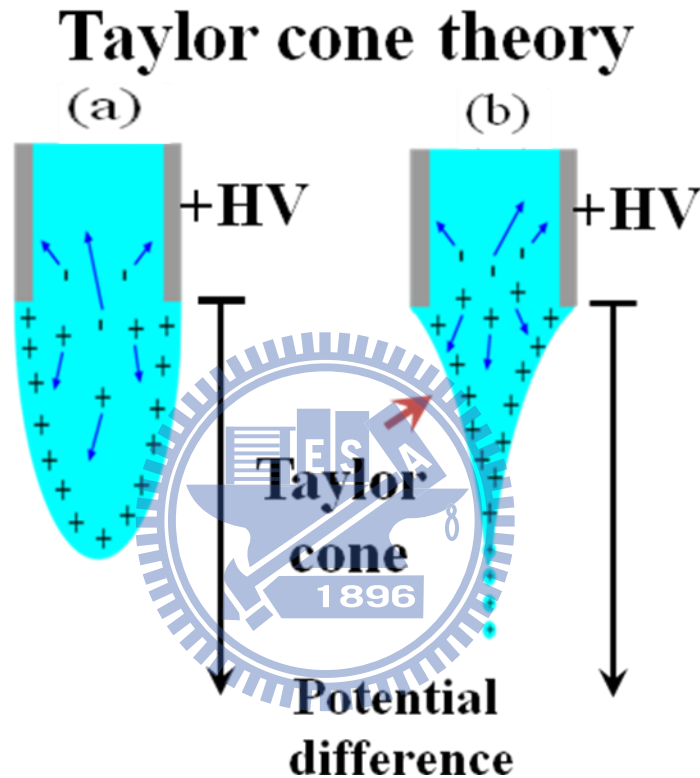


Figure 2- 3 Taylor cone[17-18]

2.3 Major processing parameters

Another important parameter that affects the electrospinning process is the various external factors exerting on the electrospinning jet. This includes the voltage supplied, the feedrate, temperature of the solution, type of collector, diameter of needle and distance between the needle tip and collector. These parameters have a certain influence in the fiber morphology.

2.3.1 Voltage

A crucial element in electrospinning is the application of a high voltage to the solution.. The high voltage will induce the necessary charges on the solution and together with the external electric field, will initiate the electrospinning process when the electrostatic force in the solution overcomes the surface tension of the solution. Generally, both high negative or positive voltage of more than 10kV is able to cause the solution drop at the tip of the needle to distort into the shape of a Taylor Cone during jet initiation[17].

2.3.2 Feed rate

The feedrate will determine the amount of solution available for electrospinning. For a given voltage, there is a corresponding feedrate if a stable Taylor cone is to be maintained. When the feedrate is increased, there is a corresponding increase in the fiber diameter or beads size as shown in Figure 2-3[21].

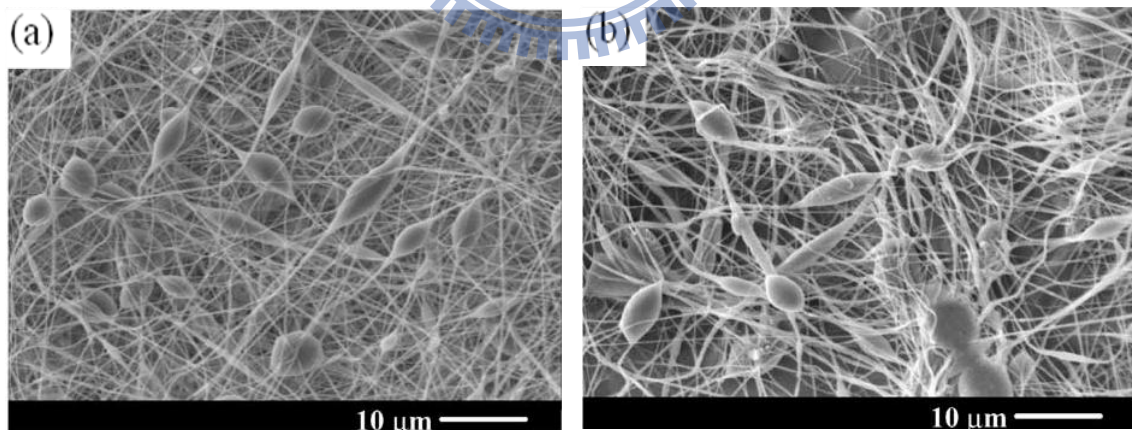


Figure 2- 4 SEM images showing the variation of beaded fibers at different feeding rates: (a) 20 ml/min; (b) 75 ml/min[21].

However, there is a limit to the increase in the diameter of the fiber due to higher feedrate. If the feed rate is at the same rate which the solution is carried

away by the electrospinning jet, there must be a corresponding increased in charges when the feed rate is increased. Thus there is a corresponding increased in the stretching of the solution which counters the increased diameter due to increased volume. Due to the greater volume of solution drawn from the needle tip, the jet will takes a longer time to dry. As a result, the solvents in the deposited fibers may not have enough time to evaporate given the same flight time. The residual solvents may cause the fibers to fuse together where they make contact forming webs. A lower feedrate is more desirable as the solvent will have more time for evaporation.

2.3.3 Effect of Collector

There must be an electric field existed between the source and the collector for electrospinning to initiate. Thus in most electrospinning setup, the collector plate is made out of conductive material such as aluminum foil which is electrically grounded so that there is a stable voltage potential difference between the source and the collector.

2.3.4 Diameter of Pipette Orifice / Needle

The internal diameter of the needle or the pipette orifice has a certain effect on the electrospinning process. A smaller internal diameter was found to reduce the clogging as well as the amount of beads on the electrospun fibers.

2.3.5 Distance between Tip and Collector

In several cases, the flight time as well as the electric field strength will

affect the electrospinning process and the resultant fibers. Varying the distance between the tip and the collector will have a direct influence in both the flight time and the electric field strength. For independent fibers to form, the electrospinning jet must be allowed time for most of the solvents to be evaporated. When the distance between the tip and the collector is reduced, the jet will have a shorter distance to travel before it reaches the collector plate. Moreover, the electric field strength will also increase at the same time and this will increase the acceleration of the jet to the collector. As a result, there may not have enough time for the solvents to evaporate when it hits the collector. When the distance is too low, excess solvent may cause the fibers to merge where they contact to form junctions resulting in inter and intra layer bonding as shown in Figure 2-4[21].

This interconnected fiber mesh may provide additional strength to the resultant scaffold. Depending on the solution property, the effect of varying the distance may or may not have a significant effect on the fiber morphology. In some cases, changing the distance has no significant effect on the fiber diameter. However, beads were observed to form when distance was too low. The formation of beads may be the result of increased field strength between the needle tip and the collector. Decreasing the distance has the same effect as increasing the voltage supplied and this will cause an increased in the field strength. As mentioned earlier, if the field strength is too high, the increased instability of the jet may encourage beads formation. However, if the distance is such that the field strength is at an optimal value, there is less beads formed as the electrostatic field provides sufficient stretching force to the jet.

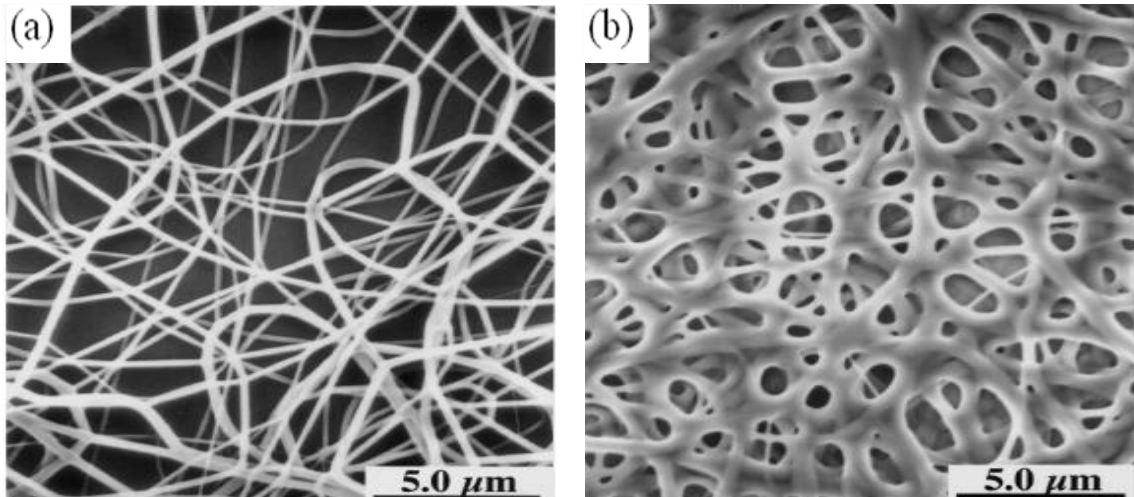


Figure 2- 5 Nylon 6,6 at (a) 2 cm deposition distance and (b) 0.5cm deposition distance[21].

2.4 Important features of electrospinning

1. Suitable solvent should be available for dissolving the polymer.
2. The vapor pressure of the solvent should be suitable so that it evaporates quickly enough for the fiber to maintain its integrity when it reaches the target but not too quickly to allow the fiber to harden before it reaches the nanometer range.
3. The viscosity and surface tension of the solvent must neither be too large to prevent the jet from forming nor be too small to allow the polymer solution to drain freely from the pipette.
4. The power supply should be adequate to overcome the viscosity and surface tension of the polymer solution to form and sustain the jet from the pipette.
5. The gap between the pipette and grounded surface should not be too small to create sparks between the electrodes but should be large enough for the solvent to evaporate in time for the fibers to form.

2.5 Biodegradable polymer

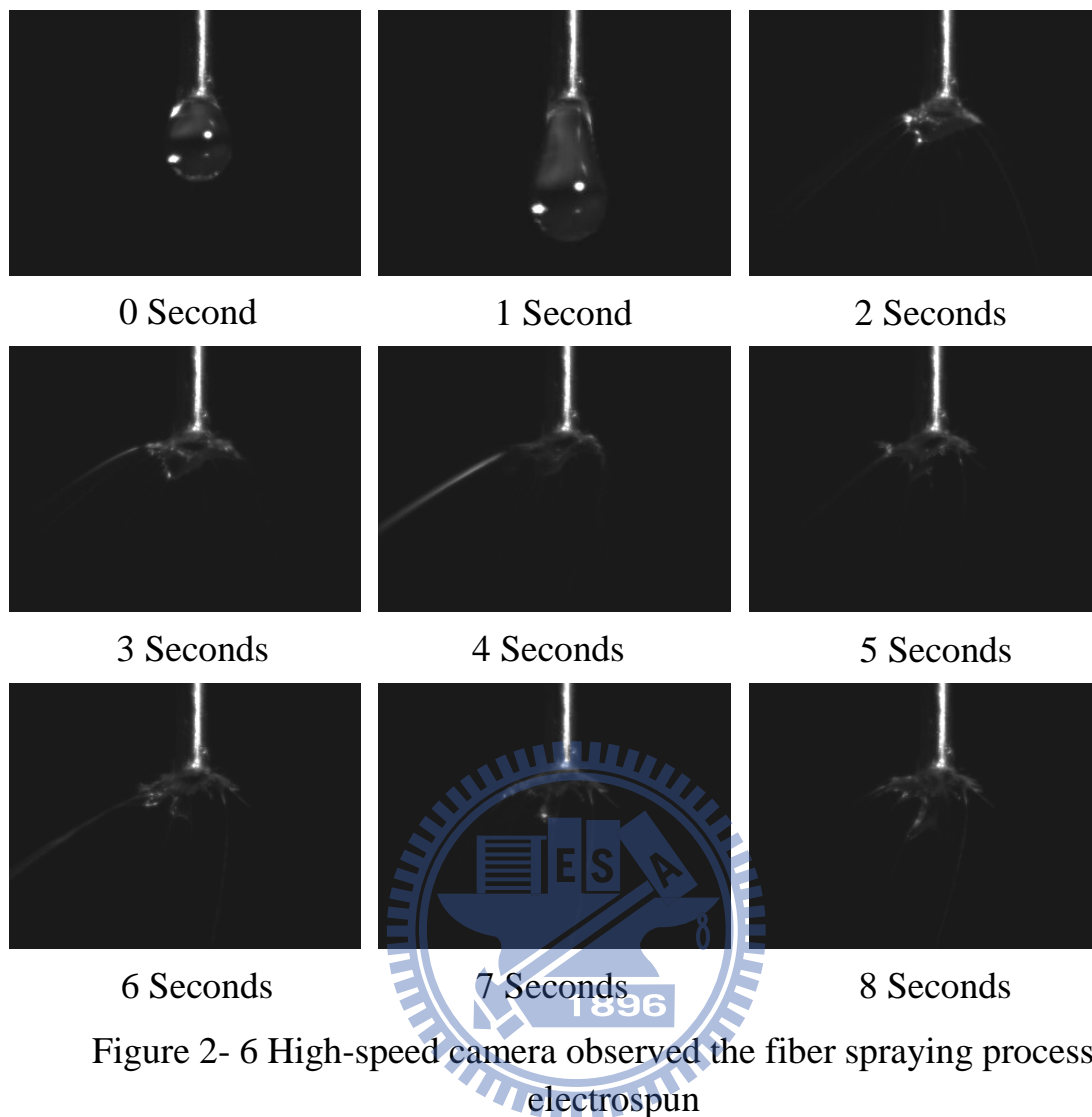
Poly(lactic acid) or polylactide (PLA) is a thermoplastic aliphatic polyester derived from renewable resources, such as corn starch (in the United States), tapioca products (roots, chips or starch mostly in Asia) or sugarcane (in the rest of world). It can biodegrade under certain conditions, such as the presence of oxygen, and is difficult to recycle.

Due to the chiral nature of lactic acid, several distinct forms of polylactide exist: poly-L-lactide (PLLA) is the product resulting from polymerization of L,L-lactide (also known as L-lactide). PLLA has a crystallinity of around 37%, a glass transition temperature between 60-65 °C, a melting temperature between 173-178 °C and a tensile modulus between 2.7-16 GPa. PLA has similar mechanical properties to PETE polymer, but has a significantly lower maximum continuous use temperature. Polylactic acid can be processed like most thermoplastics into fiber (for example using conventional melt spinning processes) and film. The melting temperature of PLLA can be increased 40-50 °C and its heat deflection temperature can be increased from approximately 60°C to up to 190 °C by physically blending the polymer with PDLA (poly-D-lactide). PDLA and PLLA form a highly regular stereocomplex with increased crystallinity. The temperature stability is maximised when a 50:50 blend is used, but even at lower concentrations of 3-10% of PDLA, there is still a substantial improvement. In the latter case, PDLA acts as a nucleating agent, thereby increasing the crystallization rate. Biodegradation of PDLA is slower than for PLA due to the higher crystallinity of PDLA. PDLA has the useful property of being optically transparent.

2.6 Optimum conditions for electrospinning PLLA fibers

The polymer fibers were injected in by using a 10mL glass syringe with a 22 needle gauge (0.7mm OD×0.4mm ID) at a flow rate of 0.2mL/hour, which was controlled by using a KDS100 pump from YEONG-SHIN CO., LTD. Hsinchu, Taiwan. The high voltage power supply used was a 30KV/15W model purchased from YOU-SHANG TECHNICAL CORP. Kaohsiung, Taiwan. The equipment was attached to the needle tip through an alligator clip and voltage was 20KV; the tinfoil grounded target was placed at 15cm away from the needle tip. It could be observed by the High-speed camera that in Figure 2-6.

Poly(α -L-alanine) (CAS No:77160-91-9, $C_3H_7NO_2$, PLLA) is a biodegradable, thermoplastic, aliphatic polyester derived from renewable resources, such as corn starch or sugarcane. PLLA, purchased from Sigma, Taiwan, has a molecular weight of 180~200 KDa with a volume concentration of 12%, i.e. 12g PLLA dissolved in 100ml ACS grade >99.8% chloroform.



The polymer fibers were injected in by using a 10mL glass syringe with a 22 needle gauge (0.7mm OD×0.4mm ID) at a flow rate of 0.2mL/hour, which was controlled by using a KDS100 pump from YEONG-SHIN CO., LTD. Hsinchu, Taiwan. The high voltage power supply used was a 30KV/15W model purchased from YOU-SHANG TECHNICAL CORP. Kaohsiung, Taiwan. The equipment was attached to the needle tip through an alligator clip and voltage difference in 15KV, 20KV and 25KV was used; the tinfoil grounded target was placed at 15cm away from the needle tip. Poly(α -L-alanine) (CAS No:77160-91-9, $C_3H_7NO_2$, PLLA) is a biodegradable, thermoplastic, aliphatic

polyester derived from renewable resources, such as corn starch or sugarcane. PLLA, purchased from Sigma, Taiwan, has a molecular weight of 180~200 KDa with a volume concentration of 6%, 10%, 12%, and 20%. It could be observed by the optical microscope that in Figure 2-7. We recognize the optimum conditions for electrospinning PLLA fibers at 20KV 12% PLLA 15cm 25°C 0.2mL/hour 22 needle gauge (0.7mm OD×0.4mm ID).

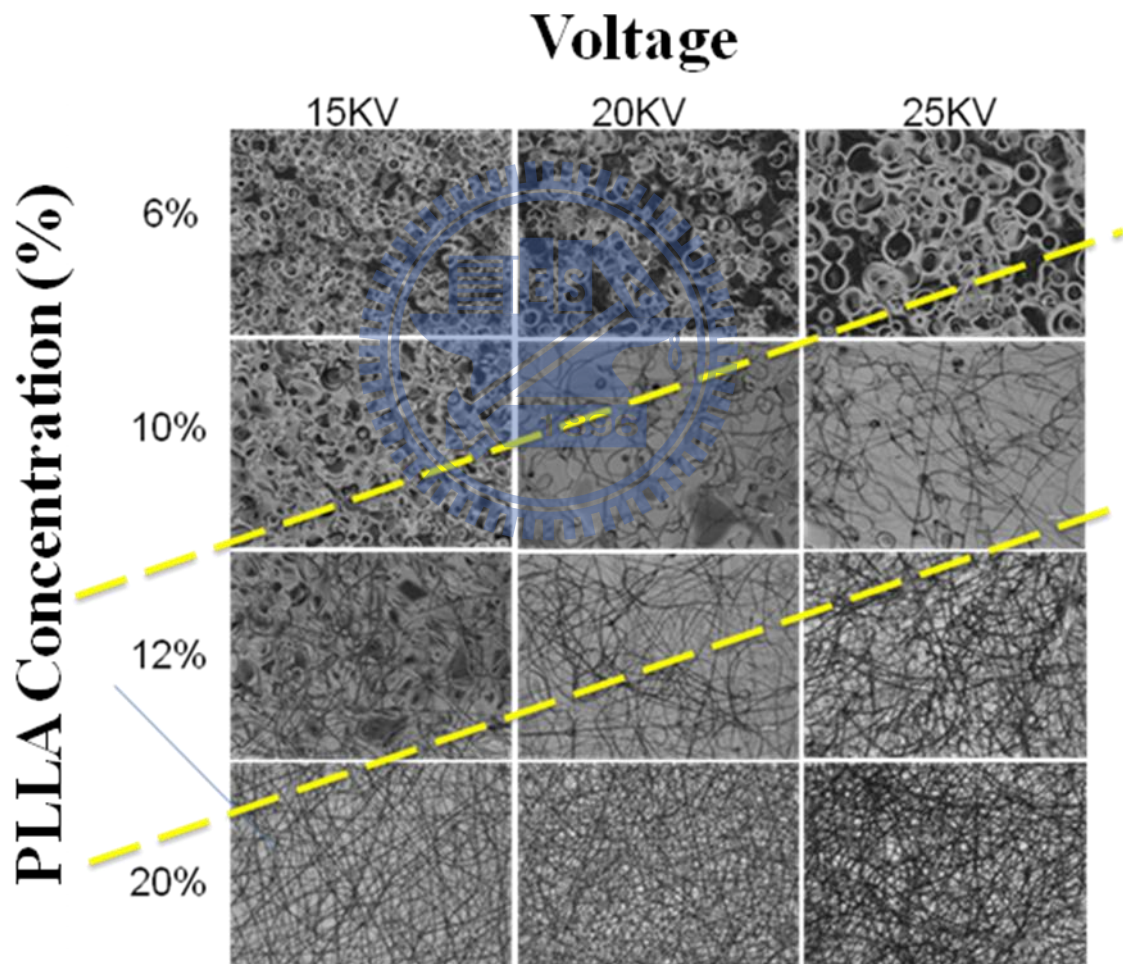


Figure 2- 7 The optimum conditions for Electrospinning PLLA fibers

Chapter 3 Membranes for Drug Delivery and Antibacterial

3.1 Introduction

Development of new drug molecule is expensive and time consuming. Improving safety efficacy ratio of “old” drugs has been attempted using different methods such as individualizing drug therapy, dose titration and therapeutic drug monitoring. Delivering drug at controlled rate, slow delivery, targeted delivery are other very attractive methods and have been pursued very vigorously. Drug delivery is playing a significant role in the pharmaceutical industry such that new drug delivery systems and a diverse range of technology options have emerged. A recent industry survey estimated that there are more than 300 companies engaged in the development and licensing of drug delivery technology. The drug delivery market is currently estimated to be worth approximately \$50 billion, and worldwide sales could reach as much as \$100 billion by 2005[71].

Currently available polymers for controlled release can be classified into four major categories: (1) diffusion-controlled systems, (2) solvent-activated systems, (3) chemically controlled systems, and (4) magnetically controlled systems[72-73].

Chlorhexidine (CHX) (Figure 3-1) has been widely used as an effective antibacterial agent in applications that range from common disinfectants to bactericidal agents in dentistry; this is largely due to its broad range of antimicrobial activities against bacteria and fungi, high killing rate and nontoxicity toward mammalian cells[36, 74].

The commonly cited mechanism of action of CHX is that two

symmetrically positioned chlorophenyl guanide groups can penetrate through the cellular wall of bacteria and irreversibly disrupt the bacterial membrane, thus killing the microorganism. In most materials that include CHX as the biocide, CHX is simply enmeshed within the material and gradually leaches out to kill the bacteria[36].

In the past 30 years, chlorhexidine, a bacterial membrane permeabilizing agent and its water-soluble derivative chlorhexidine digluconate has been used extensively in mouth rinses to control bacteria biofilms on teeth[37, 75].

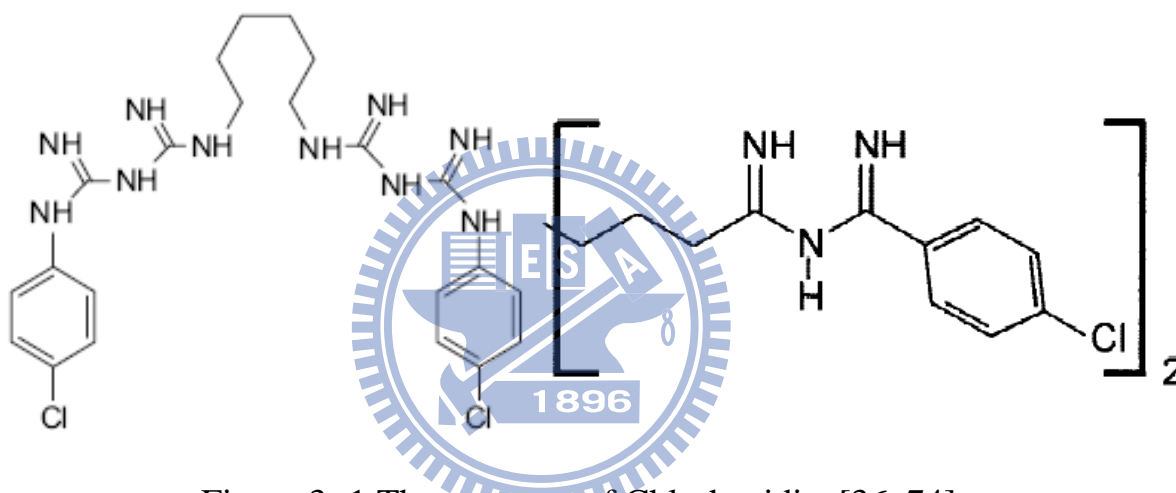


Figure 3- 1 The structure of Chlorhexidine[36, 74]

Research on Controlled release of drugs is a very important process to achieve the highest therapeutic efficiency. Much research has been carried out in order to develop of new and/or improved drug therapies that are more efficient and, most importantly, more cost-effective. The conventional definition of controlled release is a constant level of drugs in suitable systems. Electrospun fibers was a novel process to prepare and the release characteristics should depend on interaction between polymer and drug pair as much as on the sizes of fibers[28].

Polymeric drug delivery systems plays an important role in conventional

dosage forms, such as improved therapeutic effect, reduced toxicity, convenience, and so on. In previous study, the drugs can be encapsulated directly into electrospun fibers and these systems show nearly zero-order kinetics of drug release[29].

Electrospinning is a simple and versatile method for fibers preparation, which employs electrostatic forces that strength a polymer jet to generate continuous fibers with diameters ranging from micrometers down to several nanometers[23, 25].

Poly(α -L-alanine) (PLLA) is one of the most promising biodegradable polymers owing to its mechanical property profile, thermoplastic processibility and biological properties, such as biocompatibility and biodegradability. Electrospinning is an interesting technique for spinning PLLA. The process offers an excellent opportunity for designing the surface morphology and porosity of the fibers to provide the most appropriate interface for biomedical application[12, 25-27].

Chlorhexidine (CHX) is a bactericidal agent. Its effect on *E. coli* and *S. aureus* is dependent on CHX concentration and pH. It's found that, by using C¹⁴ chlorhexidine gluconate, the uptake by bacteria becomes extremely rapid, with a maximum effect occurring within 20 seconds[75]. Damage to outer cell layers takes place but is insufficient to induce lysis or cell death. The agent then crosses cell walls or outer membranes, presumably by passive diffusion, and subsequently attacks bacterial cytoplasmic or inner membranes. In previous studies, interaction of chlorhexidine with carboxyl, sulfate, and phosphate groups was studied in vitro, including factors that might interfere with these interactions. The properties of cetylpyridine in the same systems also were

investigated for comparison, as this is a basic antibacterial agent with virtually no plaque inhibiting effect[36-37, 74-75].

Previous studies fabricated effective bacteria inhibiting fiber membranes from Polymer/Silver nanoparticles[30-31] & Polymer/chitosan[32-34] via electrospinning. In addition, when it comes to bacteria inhibiting drug, such as CHX[35], CHX-CA[36], CHX-Digluconate[37], and CHX-gluconate, only the delivery efficiency of Polymer/CHX, or just that of CHX, has been discussed[36-37]. Tests on the inhibiting capability (Inhibition Zone) of Polymer/CHX matrix were rarely done. Evaluations of bacteria inhibiting capability based on Inhibition Zone were only qualitative, not quantitative. This study aimed to discuss whether biodegradable inhibiting drug delivery membranes fabricated from PLLA/CHX via electrospinning possessed the characteristics of drug delivery systems and whether CHX could still inhibit bacteria after being released from PLLA. This experiment quantitatively evaluated bacteria growth in liquid culture by observing Optical Density 600nm (OD) at one-hour intervals, and used the growth curves thus derived to evaluate on a real-time the impacts of drug delivery speeds on the growth rates of bacteria in different phases. Competent cell and plasmid inserted competent cell, bacteria that are of the same strain but grow at different speeds were utilized to interact with biodegradable CHX delivery membranes fabricated via electrospinning to determine whether such drug delivery membranes are a rate-preprogrammed drug delivery system.

3.2 Experimental procedure

3.2.1 Materials and Methods

Poly(α -L-alanine) (CAS No:77160-91-9, $C_3H_7NO_2$, PLLA) is a biodegradable, thermoplastic, aliphatic polyester derived from renewable resources, such as corn starch or sugarcanes. PLLA, purchased from Sigma, Taiwan, has a molecular weight of 180~200 KDa with a volume concentration of 12%, i.e. 12g PLLA dissolved in 100ml ACS grade>99.8% chloroform. chlorhexidine gluconate, acquired from J.T. Backer, has a volume concentration of 0.5%, i.e. 5mg chlorhexidine gluconate dissolved in 1000ml 70% Isopropyl Alcohol.

3.2.2 Fabrication of bacteriostatic Fibers

The polymer fibers were injected in by using a 10mL glass syringe with a 22 needle gauge (0.7mm OD×0.4mm ID) at a flow rate of 0.2mL/hour, which was controlled by using a KDS100 pump from YEONG-SHIN CO., LTD. Hsinchu, Taiwan. The high voltage power supply used was a 30KV/15W model purchased from YOU-SHANG TECHNICAL CORP. Kaohsiung, Taiwan. The equipment was attached to the needle tip through an alligator clip and voltage difference of 20KV was used; the tinfoil grounded target was placed at 15cm away from the needle tip.

First, PLLA, PLLA/CHX (90:10 in terms of volume), and PLLA/CHX (50:50 in terms of volume) solution were injected into 10mL syringes. Next, a syringe pump was used to control the 10mL syringes with PLLA/CHX solution to flow at 0.2mL/hour. The syringe needle was stainless steel, while the

collector was tinfoil paper. The distance between the syringe tip and the collector was 15cm. Then, the high power supply was connected to the syringe tip and the collector; the positive electrode was on the syringe tip side, and the negative electrode was on the collector side. The high power supply was turned on to 20KV to observe the spinning fibers on the collector. The structural and optical properties were investigated by a Scanning Electron Microscope (SEM), micro-Raman system and tensile tests. All the experiments were performed at room temperature, about 25°C .

3.2.3 Physical and chemical properties

The fibers were examined by a Field Emission Scanning Electron Microscope (FE-SEM) to visualize their morphology by using a JSM-6700F (JEOL Ltd.). The fiber samples were coated with a thin layer of palladium in 100sec at 20mA by the auto fine coater JFC-1600 (JEOL Ltd.). The fibers were examined by a Fourier Transform Infrared Spectroscopy (FTIR) to analysis of chemical compound by using a Perkin-Elmer Spectrum One FTIR Spectroscopy (Analytical & Bio Science Instrument Co., Ltd., Taipei, Taiwan). The Fourier Transform Infrared Spectroscopy was used and set at absorbance mode, 500 (cm^{-1}) to 2000 (cm^{-1}) wavelength with a resolution of 4 cm^{-1} . Raman scattering measurements were performed in the TRIAX 550 micro-Raman system. The 5145 Å line with a power of 0.2 W from the Coherent Innova Argon ion laser was focused to about 2 ~ 4 μm on the sample surface. The back-scattered signal was collected by a microscopic system and recorded with a JOBIN-YVON SPEX SPECTRUM ONE liquid nitrogen cooled CCD detector. All spectra were recorded by an OLYMPUS microscope objective and 3 accumulations at 300

seconds integration time with ~50 mW power on the sample for each Raman spectrum. Frequencies were to $\pm 2 \text{ cm}^{-1}$ accurately as determined from plasma emission lines. The frequency of each Raman band reported in this study was obtained using Lorentzian curve fitting.

3.2.4 Antibacterial Test

The competent cells used in this experiment, XL1-Blue Escherichia coli (E. coli) Strain from Stratagene, were purchased from Invitrogene, the same company from which TOPO plasmid was obtained. TOPO XL1-Blue were XL1-Blue inserted with TOPO plasmid by means of heat shock. XL1-blue Escherichia coli and TOPO XL1-Blue were cultured in Luria-Bertani (LB) broth (from Difco Co Ltd, Taipei, Taiwan) and LB agar plates were supplemented with 100 $\mu\text{g}/\text{mL}$ of ampicillin for cloning and maintenance. The cells were grown at 37°C and 200 rpm to mid-logarithmic phase (Optical Density 600nm of 0.8) Growth rates and bacterial concentrations were determined by measuring optical density (OD) at 600 nm each 30 min (OD of 0.1 corresponds to a concentration of 10^8 cells per cm^3). PLLA, PLLA/CHX(90:10) and PLLA/CHX(50:50) membrane size is 18×18mm, similar to the size of cover slip.

XL1-Blue and TOPO XL1-Blue were used to evaluate the bacteria/plague inhibiting capability of the CHX releasing membranes by observing their bacteria growth curves. First of all, one colony from the LB agar plate of XL1-Blue and one colony from that of TOPO XL1-Blue were collected and respectively placed into culture tubes containing 5mL of Luria-Bertani (LB) broth. The tubes were then put in an incubator at 37°C at 200rpm for six to eight hours (until Optical Density=0.8). Next, ten 1L Erlenmeyer flasks containing

500mL of LB broth medium, sterilized by Autoclave at 120°C under 1.2 kgf/cm² for 15 minutes, and cooled down for 3 hours, were prepared. The ten flasks were divided into two groups of five. One group was added with 0.2mL of XL1-Blue (Optical density=0.8), while the other was added with 0.2mL of TOPO XL1-Blue (Optical density=0.8). In each group, only the first flask (control group) was not added with the drug delivery membranes and PLLA fibers, PLLA/CHX fibers (50:50), PLLA/CHX fibers (90:10), and 100 µg/mL of ampicillin solution were respectively added into the other four flasks.

3.3 Results and Discussion

It could be observed by the electronic microscope that, in Figure 3-2(a), the fiber diameter of PLLA was approximately 3~5µm and on the surface of the fibers were pores at the size of around 10nm. In Figure 3-2(b), the fiber diameter of PLLA/CHX was approximately 600~900nm and the surface was smooth. It was further observed that PLLA/CHX fibers tended to overlap and formed a structure of 2~3 fiber tubes.

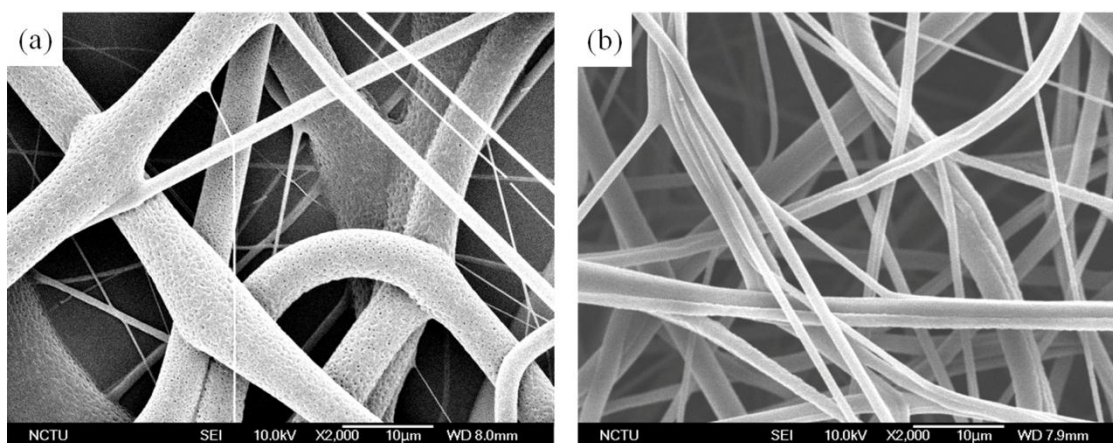


Figure 3- 2 Field Emission Scanning electron micrographs of the electrospinning fibers: (a) PLLA fibers, (b) PLLA/CHX fibers image (50:50).

In this experiment, the original intent was to understand, by means of FTIR & Raman Spectroscopy, if CHX was successfully mixed with PLLA solution to fabricate via electrospinning biodegradable PLLA fiber membranes that contained CHX. FTIR spectra of analyzed polymers were demonstrated in Figure 3-3. The band originating from C=O stretching vibrations was situated at 1745 cm^{-1} for Poly lactide[76]. In the range $1050\text{-}1250\text{ cm}^{-1}$ C-O and C-O-C stretching vibrations could be attributed. There were three bands in the range $1300\text{-}1500\text{ cm}^{-1}$ in PLLA spectrum that might attribute to symmetric and asymmetric deformational vibrations of C-H in CH_3 groups[13].

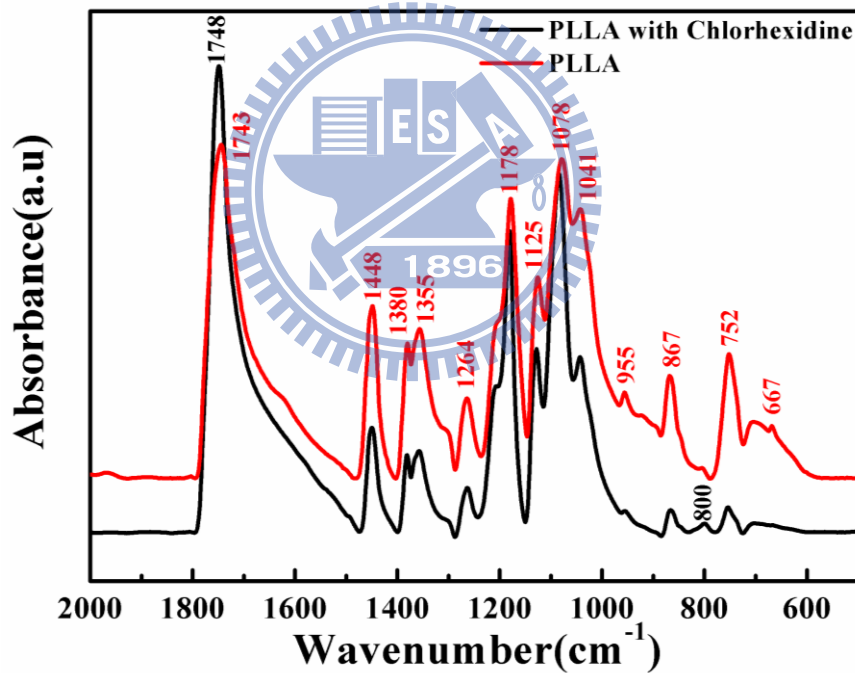


Figure 3- 3 Fourier Transform Infrared Spectra of PLLA fibers and PLLA/CHX fibers (50:50).

However, in the FTIR experiment, the characteristic IR peaks of CHX were observed between 1500 cm^{-1} and 1650 cm^{-1} (C=N stretching and aromatic C=C bending vibrations, respectively)[36] and PLLA demonstrated a

very strong peak $\nu\text{C}=\text{O}$ at 1760 cm^{-1} , so we could not confirm via FTIR whether the biodegradable PLLA fiber membranes contained CHX. FTIR could at most confirm that PLLA was used in the experiment. (In the FTIR spectrum of the PLLA film, the most pronounced difference with the spectra of individual homopolymers was the disappearance of the absorption peak at 1270 cm^{-1} . [13, 76])

Therefore, to confirm the existence of CHX in the fiber membranes, Micro-Raman Spectroscopy was utilized to conduct fiber membrane analyses at CH_3 and CH bending region. The CH_3 asymmetric deformation modes appeared at about $1450\pm 2\text{ cm}^{-1}$ as intense Raman and IR bands in all the compounds [76-77].

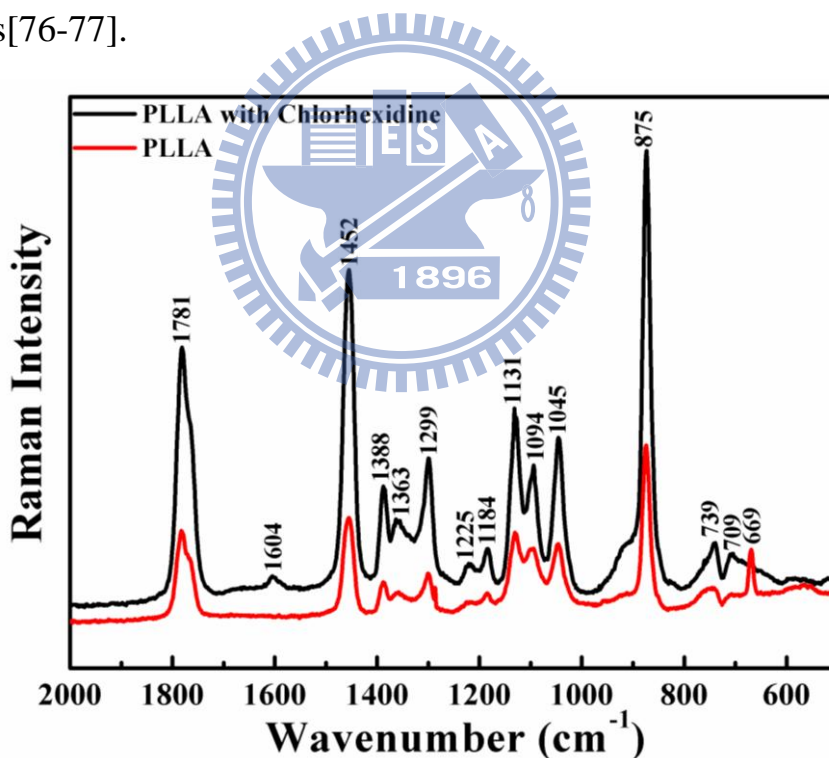


Figure 3- 4 Micro-Raman spectra of PLLA fibers and PLLA/CHX fibers.

In the Raman spectra of the PLLA/CHX fibers, the characteristic CHX peak at 1604 cm^{-1} , as indicated by an arrow in Figure 3-4, was observed. The

peak shifted 34 cm^{-1} to higher wavenumbers compared to that of pure CHX powders (1570 cm^{-1})[35-36], which could be attributed to the interaction between CHX and the polymer matrix in the fibers. As mentioned in previous literature, the I875/I1452 Raman intensity ratio signaled results of bio-degradation and structural differences[76-77]. In this experiment, although both were bio-degradable membranes, the I875/I1452 Raman intensity ratio of PLLA fiber membranes was 1.494 while that of PLLA/CHX fiber membranes was 1.304.

Figure 3-5(a)(b)(c) illustrated the interactions between the PLLA/CHX (50:50) drug releasing membranes and XL1-Blue. Figure 3-5(d) was the bacteria growth curves derived by observing the ODs (Optical Density 600nm) of the 1mL broth extracted from flasks of various conditions at one-hour intervals. As ampicillin, a form of antibiotics, could effectively inhibit the growth of XL1-Blue, no growth was observed (Optical Density 600nm = 0.002) in XL1-Blue added with ampicillin solution $100\mu\text{g/mL}$. No obvious growth was observed in the zero to third hours in the Lag Phase. Only PLLA and PLLA/CHX (90:10) experienced some minor growth in OD (Optical Density 600nm = 0.018, 0.016) in the third hour. The OD of PLLX/CHX (50:50) in the zero to third hours was 0.002, which signaled that the growth of bacteria was effectively inhibited. PLLA/CHX (50:50) PLLA was non-toxic and biocompatible. Even though PLLA/CHX (90:10) contained CHX, the concentration is very low (0.05%). Therefore, bacteria also started to grow in the third hour. In the fourth to ninth hours, the growth curves of PLLA and PLLA/CHX (90:10) entered the Log Phase, a period featured by exponential multiple growth in terms of the number of XL1-Blue. During this phase,

PLLA/CHX (50:50) still could release CHX steadily, maintaining the concentration level of CHX in the flasks and thus inhibiting the growth of XL1-Blue (average Optical Density 600nm = 0.006). Figure 2-4(b) was a further illustration of the growth curves resulted from the interactions between PLLA/CHX (50:50) membranes and XL1-Blue in the fourth to ninth hours. During the Log Phase, bacteria could grow in exponential multiples, but as PLLA/CHX (50:50) steadily released CHX, the concentration within the flasks was thus maintained at a level that could effectively inhibit XL1-Blue from growing. In the tenth to twelfth hours, it was observed from the growth curves of PLLA and PLLA/CHX (90:10) that the Stationary Phase was initiated. During this period of time, PLLA/CHX (50:10) could no longer effectively inhibit the growth of XL1-Blue. The OD (600nm) was 0.065 in the tenth hour, 0.251 in the eleventh hour, and 0.461 in the twelfth hour. Figure 2-4(c), the growth curves of PLLA/CHX membranes in the tenth to twelfth hours, further manifested such results. Theoretically, if the concentration of CHX released by PLLA/CHX (50:50) into the flasks was high enough to inhibit bacteria, XL1-Blue would not grow. However, the ODs proved that CHX concentration in the flasks was not high enough to inhibit the growth of XL1-Blue (from the tenth hour and beyond).

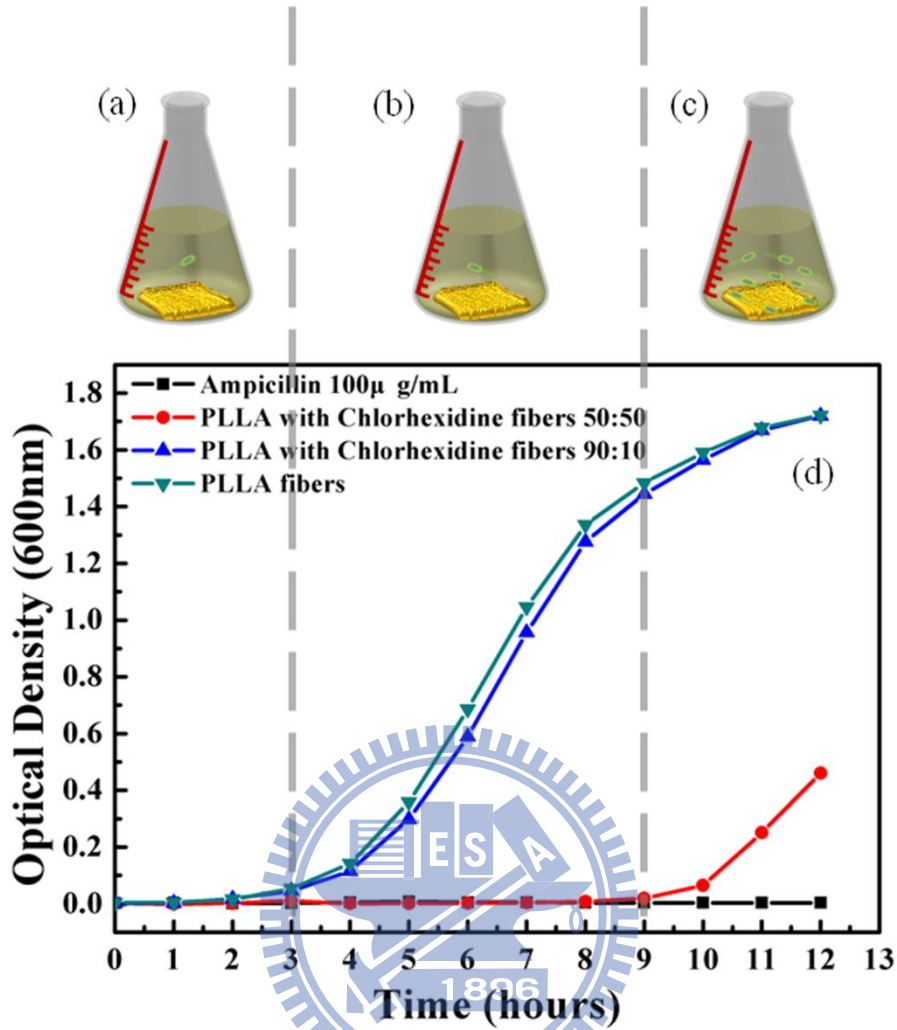


Figure 3- 5 (a) (b) (c) are illustrations of interaction between drug released by drug delivery membranes and growth rates of XL1-Blue in the (a) zero to third hours (b) fourth to ninth hours (c) tenth to twelfth hours (yellow membrane: PLLA/CHX(50:50 volume ratio), Green bacterial: XL1-Blue) (d) Growth curves of *XL1-Blue* in LB medium inoculated with 10^7 CFU of bacteria. The presence of different concentrations of (▲) PLLA/CHX fibers (90:10) and (●) PLLA/CHX fibers (50:50). Another two curves: one is only (▼) poly(L-lactic acid)s fibers; the other is (■) ampicillin-added 100 μg/mL.

Figure 3-6(a)(b)(c) were the illustrations of the interaction between PLLA/CHX (50:50) drug release membranes and TOPO XL1-Blue. Figure 3-6(d) was the bacteria growth curves of TOPO XL1-Blue derived by

observing the ODs of the 1mL broth extracted from flasks of various conditions at one-hour intervals. Although antibiotics, ampicillin, could effectively inhibit the growth of *E. coli*, a section of the genetic sequence of TOPO plasmid which was anti-ampicillin was inserted, and therefore TOPO XL1-Blue can still grow in broth with ampicillin. Microbial strains with plasmid could stay in the Lag Phase for one to two hours more than those without plasmid before they entered into the Log Phase. This characteristic was what this experiment needed. If the drug delivery membranes fabricated via electrospinning simply released CHX into the flasks through diffusion or permeation at steady rates, the 4 bacteria growth curves that reflected their interactions with TOPO XL1-Blue as illustrated in Figure 3-6(d) should be in line with Figure 3-5(d). In the zero to fourth hours in the Lag Phase, no significant bacterial growth was observed. Only in the fourth hour were minor OD increases observed in PLLA, PLLA/CHX (90:10), and ampicillin solution 100 μ g/mL (Optical Density 600nm = 0.023, 0.016, 0.011); ODs of PLLA/CHX (50:50) from the zero to fourth hours were maintained at the same level (Optical density 600nm = 0.003). We can further refer such results to Figure 3-6(a), the growth curves derived from the interaction between PLLA/CHX membranes and TOPO XL1-Blue. Figure 3-6(d) showed that there were not many bacteria in the flasks in the zero to fourth hours, and the release of CHX by PLLA/CHX (50:50) effectively inhibited the growth of bacteria during this period. In the following fifth to tenth hours, it was observed from the growth curves derived from the interaction between TOPO XL1-Blue and PLLA, PLLA/CHX (90:10), and ampicillin solution 100 μ g/mL that the Log Phase was initiated and XL1-Blue *E. coli* with TOPO plasmid

were growing exponentially. However, as PLLA/CHX (50:50) continued to release CHX, the concentration was maintained at a level that inhibited the growth of TOPO XL1-Blue (average Optical Density 600nm=0.002). We can further refer such results to Figure 3-6(b), the growth curves illustrating the interaction between the PLLA/CHX membranes and TOPO XL1-Blue in the fifth to tenth hours. If the PLLA/CHX (50:50) membranes released drug at a steady rate, CHX should be fully released from the membranes into the flasks with XL1-Blue or TOPO XL1-Blue in the ninth to tenth hours. The results should be similar to Figure 3-5(d), the illustration of the interaction between PLLA/CHX (50:50) and XL1-Blue, where XL1-Blue or TOPO XL1-Blue should start to grow in the tenth hour. However, this was not the case with TOPO XL1-Blue. It was observed in the eleventh to twelfth hours that the growth curves illustrating the interactions between TOPO XL1-Blue and PLLA, PLLA/CHX (90:10), and ampicillin solution 100 μ g/mL, still stayed in the Log Phase. TOPO XL1-Blue continued to grow in exponential multiples and ODs of PLLA/CHX (50:50) in this phase did not show significant increases (Optical density 600nm = 0.005), i.e. the growth of TOPO XL1-Blue was still inhibited. We can further refer the results to Figure 3-6(c), the illustration of the interactions between PLLA/CHX (50:50) and TOPO XL1-Blue. In addition to environmental factors, the concentration level of inhibiting drug was the main element contributing to the inhibiting capability. Given the assumption that the drug was released at a steady rate, the reason PLLA/CHX (50:50) could still effectively inhibit the growth of TOPO XL1-Blue in the eleventh to twelfth hours was TOPO XL1-Blue grew slower than XL1-Blue. Therefore, when CHX was first released into the flasks, there

was no TOPO XL1-Blue to interact with. CHX continued to stay in the flasks until XL1-Blue grew to a number that was too many for CHX to suppress [or there was not sufficient CHX to suppress TOPO XL1-Blue] (or until CHX concentration was lower than the effective inhibiting level). Then, it became possible for TOPO XL1-Blue to grow.

This study made use of bacterial growth curves to evaluate on a real-time basis the impacts of drug delivery speeds on the growth rates of bacteria in different phases. The growth curves of XL1-Blue and TOPO XL1-Blue were used to observe the impacts of drug delivery speeds of PLLA/CHX (50:50). The XL1-Blue growth curves showed that the concentration level of CHX in the ninth hour could no longer inhibit XL1-Blue, and XL1-Blue started to grow exponentially in the tenth to twelfth hours, demonstrating the common characteristics of a drug delivery system. According to Fick's law of diffusion, PLLA/CHX (50:50) released CHX into the flasks at a steady pace. Even though TOPO XL1-Blue grew slower, PLLA/CHX (50:50) kept on releasing CHX at a steady speed. When TOPO XL1-Blue grew to a number that was too many for CHX to suppress [or there was not sufficient CHX to suppress TOPO XL1-Blue] (or until CHX concentration was lower than the effective inhibiting level), it became possible for TOPO XL1-Blue to grow. there is not sufficient CHX to suppress TOPO XL1-Blue, it becomes possible for TOPO XL1-Blue to grow. Therefore, it could be concluded from this study that the biodegradable CHX delivery membranes fabricated via electrospinning were a rate-preprogrammed drug delivery system.

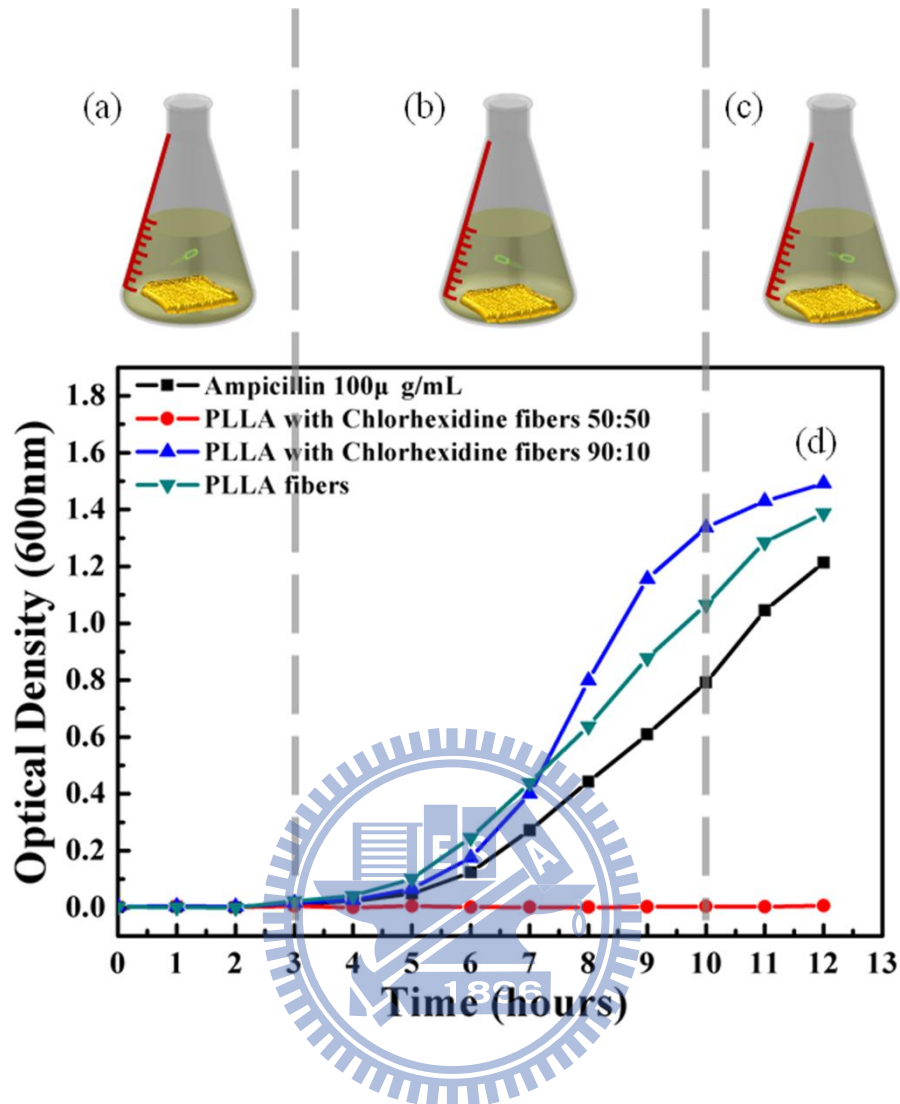


Figure 3- 6 (a) (b) (c) are illustrations of interaction between drug released by PLLA/CHX(50:50) membranes and growth rates of TOPO XL1-Blue in the (a) zero to fourth hours (b) fifth to tenth hours (c) eleventh to twelfth hours (yellow membrane: PLLA/CHX(50:50) volume ratio), Green bacterial: TOPO XL1-Blue. (d) Growth curves of *TOPO XL1-Blue* in LB medium inoculated with 10^7 CFU of bacteria. The presence of different concentrations of (▲) PLLA/CHX fibers (90:10) and (●) PLLA/CHX fibers (50:50). Another two curves: one is only (▼) poly(L-lactic acid)s fibers; the other is (■) ampicillin-added 100 μg/mL.

Polymeric drug delivery systems have numerous advantages compared to conventional dosage forms, such as improved therapeutic effect, reduced toxicity, convenience, and so on. However, the application of drug delivery

systems in dentistry is a comparatively new area of research. In addition to applications in wound dressing, PLLA/CHX is also added to mouth-wash and used in periodontal treatments as it not only is bio-degradable membrane but also contains CHX. It has been confirmed in pharmacology, microbiology, and toxicology that CHX is very powerful in killing or suppressing germs, such as gram-positive bacteria, gram-negative bacteria, anaerobic or aerobic bacterial, various bacilli, pseudomonas aeruginosa, albicans, etc. Furthermore, since it is not absorbable by human's gastrointestinal system, it practically has no systemic toxicity. At present, the practice of guided tissue regeneration (GTR) in treating periodontal diseases aims to stimulate the regeneration of alveolar bone and periodontal tissue. However, the infection of guided tissue regeneration membranes by bacteria often leads to poor surgery results. This explains why anti-bacteria agents, such as antibiotics or CHX, are usually used after surgery. If PLLA/CHX fiber membranes generated via electrospinning can be applied in GTR, the treatment of periodontal diseases can be brought up to another level.

In previous studies, it is known that Chlorhexidine (CHX) can effectively inhibit *E. coli* and *S. aureus*[75]. This experiment works with *E. coli* because it has a simpler physiology than other bacteria, and uses TOPO plasmid as control group to confirm that there is no human error during the process. Hence, future work can look into whether biodegradable PLLA/CHX membranes fabricated via electrospin have the same bacteria-inhibiting capability on the strains that CHX is known to inhibit.

Chapter 4 Membranes for Guided Bone Regeneration

4.1 Introduction

Guided bone regeneration (GBR) method is a well established therapy to repair mandible and alveolar bone defects infected by periodontal diseases. GBR membranes also have an important function which encourages bone growth. GBR membranes are occasionally utilized with dental implant or bone grafting materials[44]. The exposed implant or material filled area is covered by the membrane. In the market, conventional material of GBR membranes are non-degradable expanded—polytetrafluoroethylene (ePTFE: Gore-Tex)[78-80], degradable polylactide acid (Guidor)[81-82] and polyglatin (Vicryl)[83].

Polymorphism in materials science is the ability of a solid material to exist in more than one form or crystal structure. Polymorphism can potentially be found in any crystalline material including polymers, minerals, and metals, and is related to allotropy, which refers to elemental solids. The complete morphology of a material is described by polymorphism and other variables such as crystal habit, amorphous fraction or crystallographic defects. An example of an organic polymorph is glycine, which is able to form monoclinic and hexagonal crystals. Silica is known to form many polymorphs, the most important of which are; α -quartz, β -quartz, tridymite, cristobalite, coesite, and stishovite[84-85].

Biomineralization is the process by which living organisms produce minerals, often to harden or stiffen existing tissues. It is an extremely widespread phenomenon; all six taxonomic kingdoms contain members that are able to form minerals, and over 60 different minerals have been identified

in organisms[86-87]. Examples include silicates in algae and diatoms, carbonates in invertebrates, and calcium phosphates and carbonates in vertebrates. These minerals often form structural features such as sea shells and the bone in mammals and birds. Organisms have been producing mineralised skeletons for the past 550 million years. Other examples include copper, iron and gold deposits involving bacteria. Biologically-formed minerals often have special uses such as magnetic sensors in magnetotactic bacteria (Fe_3O_4), gravity sensing devices (CaCO_3 , CaSO_4 , BaSO_4) and iron storage and mobilization ($\text{Fe}_2\text{O}_3 \cdot \text{H}_2\text{O}$ in the protein ferritin). In terms of taxonomic distribution, the most common biominerals are the phosphate and carbonate salts of calcium that are used in conjunction with organic polymers such as collagen and chitin to give structural support to bones and shells. The structures of these biocomposite materials are highly controlled from the nanometer to the macroscopic level, resulting in complex architectures that provide multifunctional properties[88].

A major goal of periodontal regeneration therapy is the regeneration of lost supporting tissue, including the alveolar bone, periodontal ligament, and cementum around a previously diseased tooth root[38-39]. Guided tissue regeneration (GTR) has accomplished this goal, and has become a standard procedure for periodontal regeneration therapy since it was initially suggested for such therapy[40-42]. In addition, it has been applied to bone and peri-implant defects, and for bone augmentation procedures prior to implant placement. In such situations, it is sometimes termed guided bone regeneration (GBR)[42-44]. For the membrane to be effective, it must satisfy criteria such as excellent biocompatibility, controllable biodegradability, cytocompatibility,

suitable microstructure (pore size and porosity) and mechanical properties[45-47].



Figure 4- 1 Guided bone regeneration (GBR) membranes[40-42]

In previous studies, although present polymeric products show positive results in clinical studies, their weak mechanical properties and poor bone regeneration capacity are still major challenges[42]. To overcome these problems, recent research efforts have included the incorporation of bone-like ceramics into the membranes, e.g. hydroxyapatite, tricalcium phosphate and calcium carbonate[42, 44, 48-49]. Hydroxyapatite ($\text{HA}, \text{Ca}_{10}[\text{PO}_4]_6[\text{OH}]_2$) is the main mineral component of natural bone and has good biocompatibility, osteoconductivity and bioactivity, and thus it is suitable for making the guided bone regeneration membranes[50]. However, the brittleness of hydroxyapatite limits its applicability[51]. The co-precipitation of HA nanocrystals in soluble collagen has met with partial success in the fabrication of HA–collagen nanocomposites similar to the nanostructure of real bone, though with weaker mechanical properties. Calcium carbonate has been recognized as bone filling material and its good osteoconductivity has been approved in recent studies[44,

53-55].

Polymorphism in materials science is the ability of a solid material to exist in more than one form or crystal structure. Polymorphism can potentially be found in any crystalline material. Calcium carbonate is one of the most common biological minerals and has polymorphs of calcite, aragonite, and to a less extent amorphous state, vaterite or monohydrate in calcareous structures of organisms[56]. Calcium carbonate can be precipitated in aqueous solution as three anhydrous polymorphs, calcite, aragonite and vaterite, and three hydrated forms, amorphous calcium carbonate, calcium carbonate hexahydrate and calcium carbonate monohydrate[57-58].

The calcite has a trigonal and the aragonite has an orthorhombic crystal structure (Figure 4-2). The latter has typically higher elasticity modulus than the powder, better dispersibility due to the surface treatment, increased impact strength, tensile strength and elongation at break[59]. So far, most GTR/GBR membranes are made in the shape of porous foam, created by traditional methods such as particulate leaching, solvent casting or gas foaming[60]. Electrospinning is a simple and versatile method for fibers preparation, which employs electrostatic forces that strength a polymer jet to generate continuous fibers with diameters ranging from micrometers down to several nanometers[22]. Fibers obtained from electrospinning are in the range of 50 nm to a few microns in diameter and generally collected in the form of a non-woven structure[23]. It has already been shown that electrospun membranes have the potential to promote osteoblastic cell function and bone regeneration[42].

Poly(α -L-alanine) (PLLA) is one of the most promising biodegradable polymers owing to its mechanical property profile, thermoplastic processibility

and biological properties, such as biocompatibility and biodegradability[9]. Electrospinning is an interesting technique for spinning PLLA. The process offers an excellent opportunity for designing the surface morphology and porosity of the fibers to provide the most appropriate interface for biomedical application[25].

The scope of the present study is to increase the mechanical strength of the GBR membranes, because the good biocompatibility of PLLA as a biodegradable, aliphatic polyester has been proven, but its porous samples have low mechanical strength. In this study, biodegradable composites of PLLA and CaCO_3 have been prepared by mixing the powder of calcium carbonate (i.e. calcite or aragonite) with chloroform solutions of PLLA.

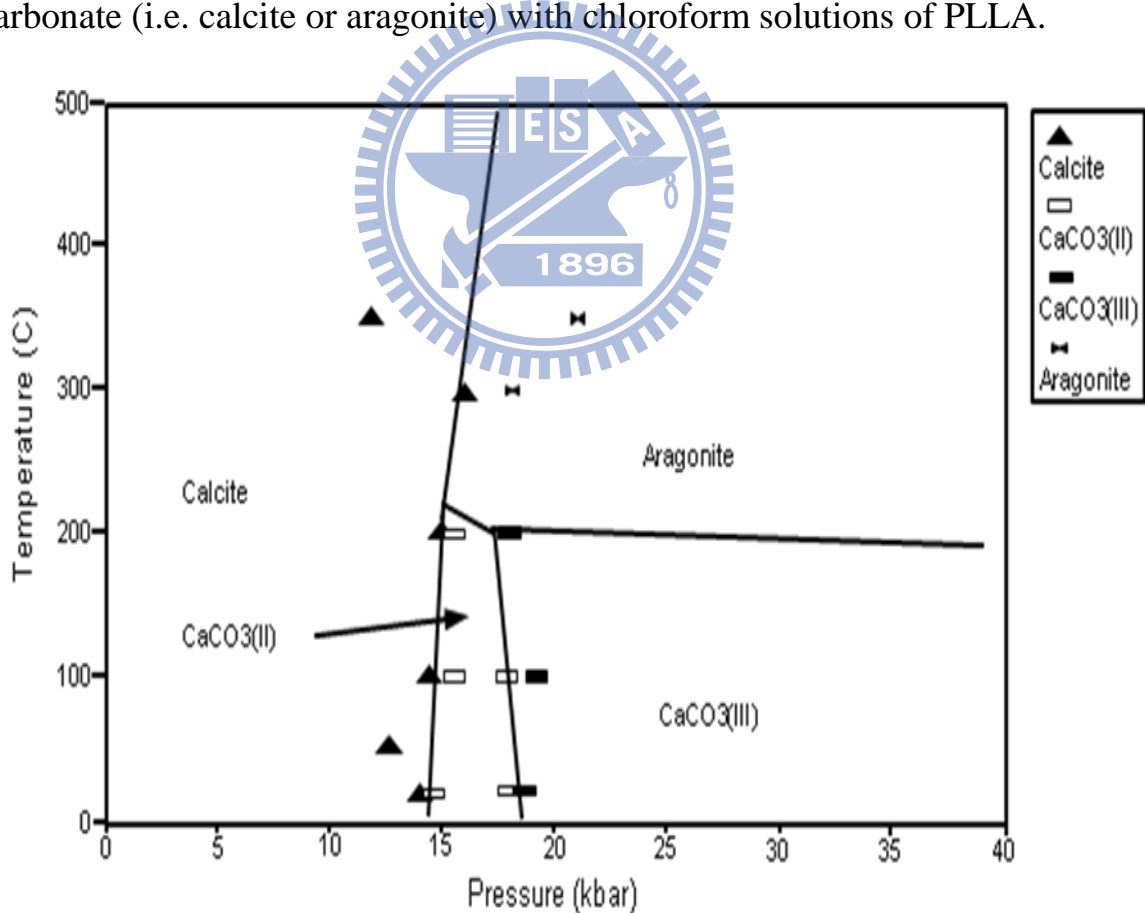


Figure 4- 2 Calcium carbonate phase diagram[56]

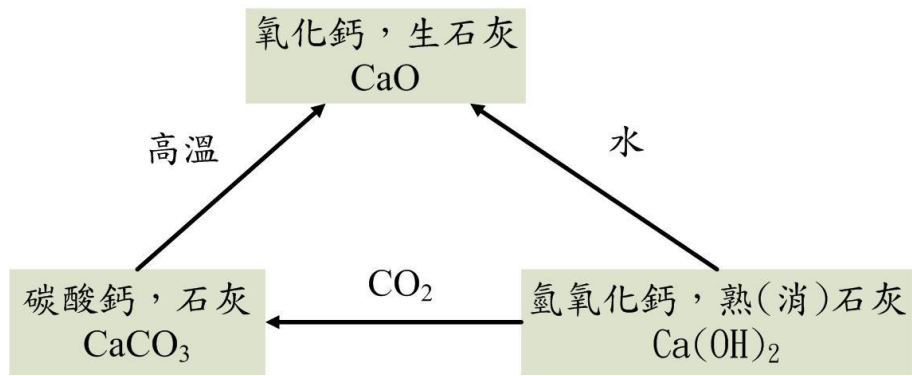


Figure 4- 3 Calcium carbonate Interaction diagram[42, 48]

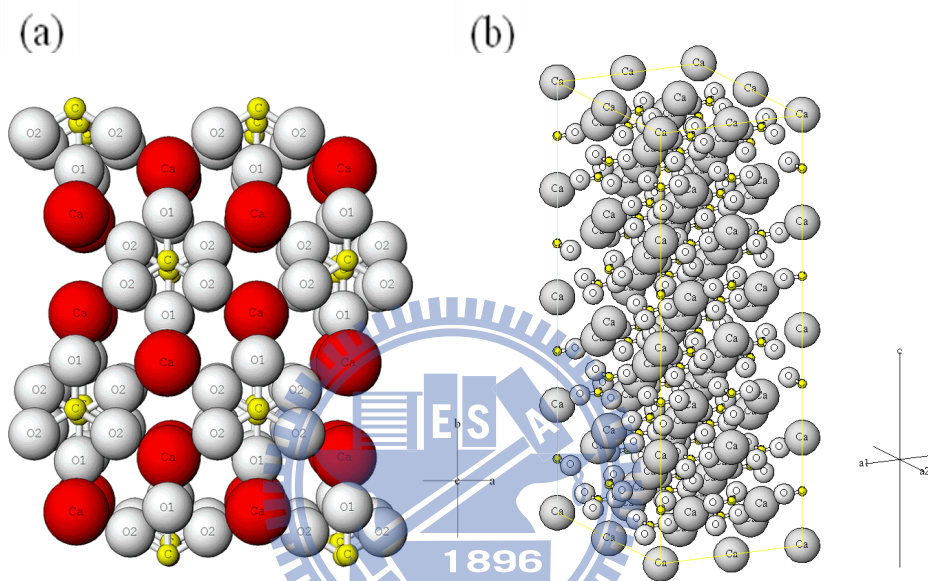


Figure 4- 4 lattice structure of (a)calcite and (b)aragonite[57]

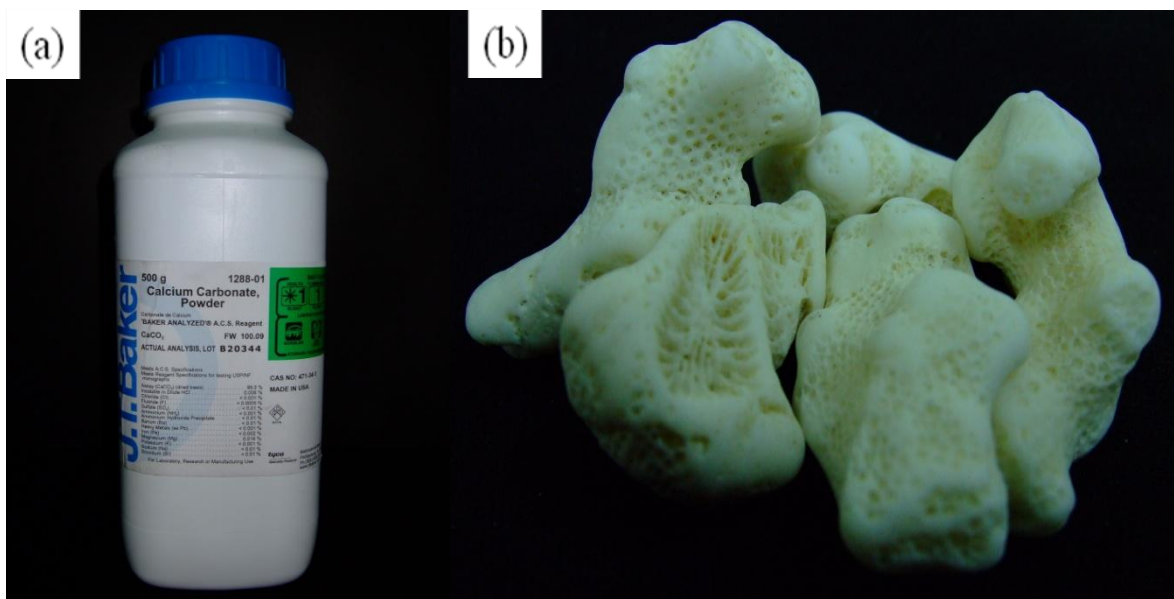


Figure 4- 5 Calcium carbonate of (a)calcite and (b)aragonite

4.2 Experimental procedure

4.2.1 Materials and Methods

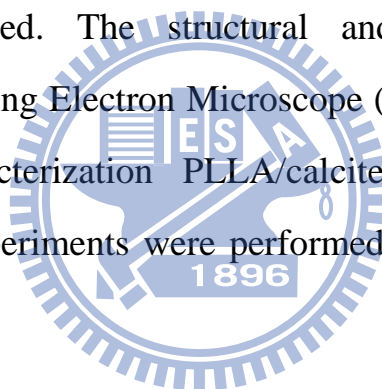
Poly(α -L-alanine) (PLLA) is a biodegradable, thermoplastic, aliphatic polyester derived from renewable resources, such as corn starch or sugarcane. PLLA with a molecular weight of 180~200 KDa, at a volume concentration of 12%, was 12g PLLA dissolved in 100ml ACS grade >99.8% chloroform. Calcium carbonate (Molecular Weight: 100.09, CAS No.:471-34-1) was purchased from J.T.Baker Taiwan(R.O.C). Calcium carbonate and nature coral (aragonite) at a volume concentration of 1-5%, was 1-5mg Calcium carbonate dissolved in 100ml 12% PLLA.

4.2.2 Fabrication of Calcium Carbonate Particles

First, commercial calcium carbonate & nature coral were placed into respective agate mortar and ground for one hour. The 2 kinds of ground powder were poured into different beakers with 100mL D.D. Water pH:7.0 and stirred with a magnetic stirring bar for 10 minutes. A 10mL syringe attached with a 0.45 μ filter at the tip was utilized to extract the solution out of the beakers by manually squeezing a (connected) plastic pump, and the solution flowing through the 0.45 μ filter was collected in new 50mL centrifuge tubes. The tubes were then put into a centrifuge machine to run for 30 minutes at 5000rpm. 48mL supernatant fluid was removed and the centrifuge tube with the remaining 2mL solution and pellet was moved into an oven at 37°C for 24 hours. White calcium carbonate powder was thus derived.

4.2.3 Fabrication of Guided Bone Regeneration membranes

The calcite-added PLLA and aragonite-added PLLA solution was injected into a 10mL syringe respectively. Next, the syringe pump was used to control the 10mL calcite-added PLLA and aragonite-added PLLA solution syringe at a flow rate of 0.2mL/hour. The syringe needle was stainless steel, while the collector was tinfoil paper. The distance between the syringe tip and the collector was 15cm. Then, the height power supply was connected to the syringe tip and the collector; the positive electrode was on the syringe tip side, and the negative electrode was on the collector side. The height power supply was turned on in the condition of 20KV and then the spinning fibers on the collector were observed. The structural and optical properties were investigated by a Scanning Electron Microscope (SEM), micro-Raman system and mechanical characterization PLLA/calcite or PLLA/aragonite fiber membranes. All the experiments were performed at room temperature, about 25°C.



4.2.4 Physical and chemical properties

1mg of white calcium carbonate powder, derived from ground, filtered, dried commercial calcium carbonate & nature coral, and 100mg of KBr powder were evenly mixed and ground in an agate mortar. Next, it was poured into the sample receiving place of KBr Pallet Die and pressed by a hydraulic press into a membrane of 10mm in diameter (10mmΦ KBr pellet). KBr pellet was then moved into a KBr Pellet Holder. FTIR Spectroscopy was measured in absorbance mode using a Perkin-Elmer Spectrum One FTIR Spectroscopy (Analytical & Bio Science Instrument Co., Ltd. Taipei Taiwan). FTIR

Spectroscopy was measured 500 (cm^{-1}) to 2000 (cm^{-1}) wavelength with a resolution of 4 cm^{-1} . The fibers were examined by a Field Emission Scanning Electron Microscope (FE-SEM) to visualize their morphology by using a JSM-6700F (JEOL Ltd.). The fiber samples were coated with a thin layer of palladium in 100sec at 20mA by the auto fine coater JFC-1600 (JEOL Ltd.). X-ray diffraction analysis was performed with a Max Science M18XHF (KXY-8019-1) X-ray powder diffractometer on finely powdered samples using Cu Ka radiation (50 kV and 200 mA) and an Ni filter with a scanning speed of $0.005^\circ 2\theta\text{s}^{-1}$. The time constant was set at 2 s. Raman scattering measurements were performed in the TRIAX 550 micro-Raman system. The 5145 Å line with a power of 0.2 W from the Coherent Innova Argon ion laser was focused to about $2 \sim 4 \mu\text{m}$ on the sample surface. The back-scattered signal was collected by a microscopic system and recorded with a JOBIN-YVON SPEX SPECTRUM ONE liquid nitrogen cooled CCD detector. All spectra were recorded by an OLYMPUS microscope objective and 3 accumulations at 300 seconds integration time with $\sim 50 \text{ mW}$ power on the sample for each Raman spectrum. Frequencies are to $\pm 2 \text{ cm}^{-1}$ accurately as determined from plasma emission lines. The frequency of each Raman band reported in this study was obtained using Lorentzian curve fitting.

4.2.5 Analysis of mechanical properties

The tensile mechanical property was tested by an Autograph IS-5000 Mechanical Tester (Shimadzu Co, Japan) with 100 kg load cell. The specimens were rectangular, about 25mm in width and about 70mm in length. The crosshead speed was set at 2.5 mm/min, and the load was applied until

ultimate fracture of the specimen. The elastic modulus was calculated as the slope of initial linear portion of the stress-strain curve. The tensile strength was determined as the maximum point of the stress-strain curve.

4.3 Results and Discussion

Calcite, Aragonite and Vaterite are isomers of calcium carbonate. The study aims to confirm the lattice structures of commercial calcium carbonate and natural coral reefs. KBr pellets of commercial calcium carbonate and those of natural coral reefs were first placed on KBr Pellet Holder to conduct FTIR spectra analyses. In the meantime, the lattice structure of the white calcium carbonate powder which had been ground in agate mortars and filtered with a 0.45μ filter was also analyzed via XRD spectra. The results are demonstrated in Figure 4-6. The absorption bands chosen for the quantitative analysis of a ternary mixture are the 713 cm^{-1} for calcite, the 700 and 712 cm^{-1} for aragonite. Aragonite displays a characteristic symmetric carbonate stretching vibration (ν_1) at 1083 cm^{-1} and a carbonate out-of plane bending vibration (ν_2) at 854 cm^{-1} and a carbonate In-plane bending vibration (ν_4) at $700,712\text{ cm}^{-1}$ in its FTIR spectrum. The out-of-plane bending (ν_2) vibrational mode is infrared active for all the three polymorphs, but there are some characteristic shifts among these. calcite and vaterite, the positions of the corresponding (ν_2) vibrations are very similar and appear at $\sim 875\text{ cm}^{-1}$. While the symmetric stretching (ν_1) vibration is both IR- and Raman-active for aragonite, it is only Raman-active in the case of calcite. Therefore, the peak around 1080 cm^{-1} is sometimes used to quantify aragonite from a mixture of aragonite and calcite[58, 89].

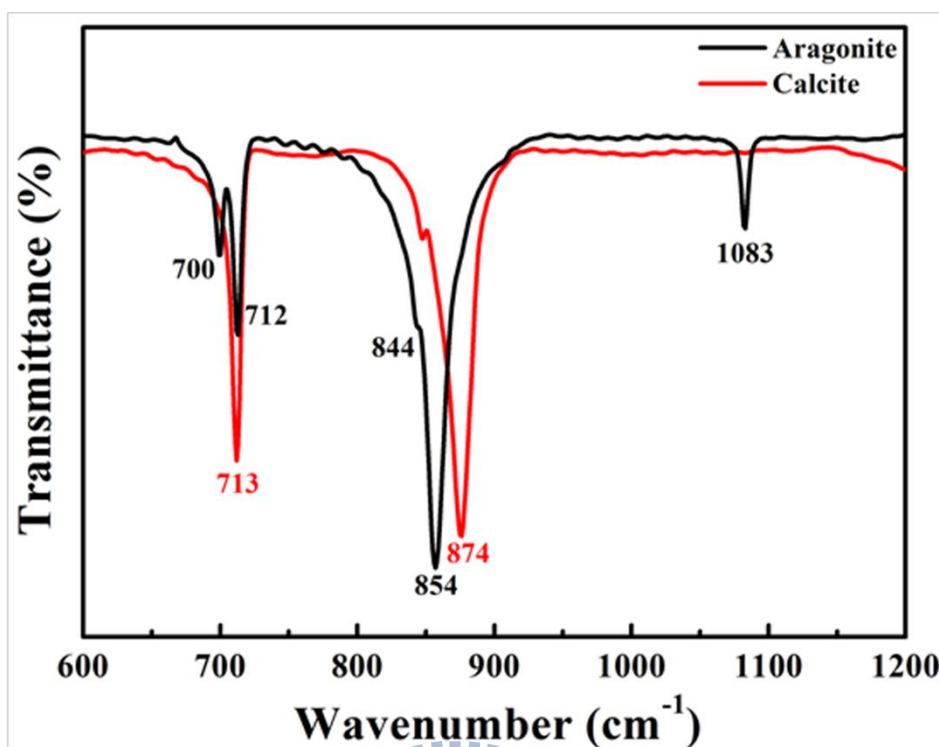


Figure 4- 6 FTIR spectra of calcite and aragonite showing their characteristic carbonate vibrational bands.

Figure 4-7 the XRD spectra of calcite, aragonite are shown in Fig. 4. The area under the principal XRD line at 3.39 Å (2θ : 26.3°) for aragonite samples. It is compared with the data from the JCPDS file No. 5-453 and all peaks of the obtained product can be assigned to those of aragonite crystals, indicating the formation of single-phase aragonite. calcite peak (2θ = 29.4°–29.58°) and the primary aragonite peak (2θ = 26.28°). JCPDS file No. 05-0586 and all peaks of the obtained product can be assigned to those of calcite crystals, indicating the formation of single-phase calcite. The calcium planes of calcite are (104) and (113) crystalline plane, while that of aragonite are the (111) and (221). The peaks attributed to the 104, 113 and 111, 221 reflections of calcite and aragonite, respectively, are also used for the quantitative analysis[58, 90-91].

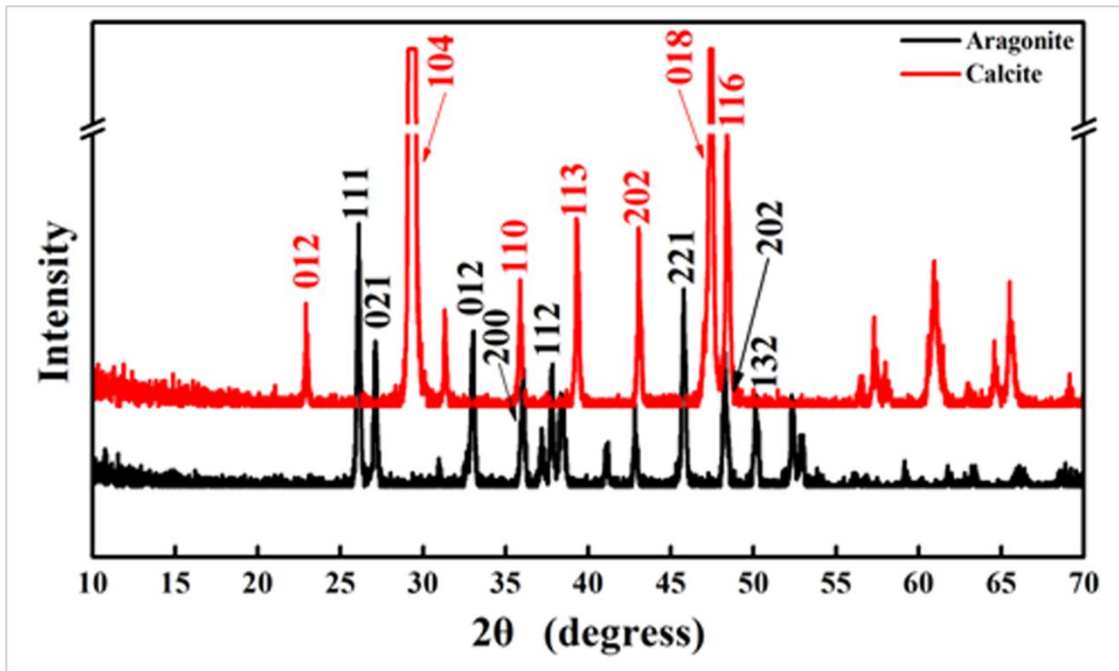


Figure 4- 7 Powder X-ray diffractograms of calcite and aragonite.

It can be observed from the electronic microscope that, in Figure 4-8(a), the fiber diameter of PLLA is approximately 3~5 μm and on the surface of the fibers are pores at the size of around 10nm. In Figure 4-8(b) where 5% of calcium carbonate is added with PLLA, other than the similarities in terms of the size of the fiber diameter (3~5 μm) and that of the surface pores (10nm), a 20 μm shuttle-like structure comes into being. In Figure 4-8(c) where 5% of coral is added with PLLA, other than the similarities (3~5 μm fiber diameter and 10nm surface pores), a 10 μm shuttle-like structure is created.

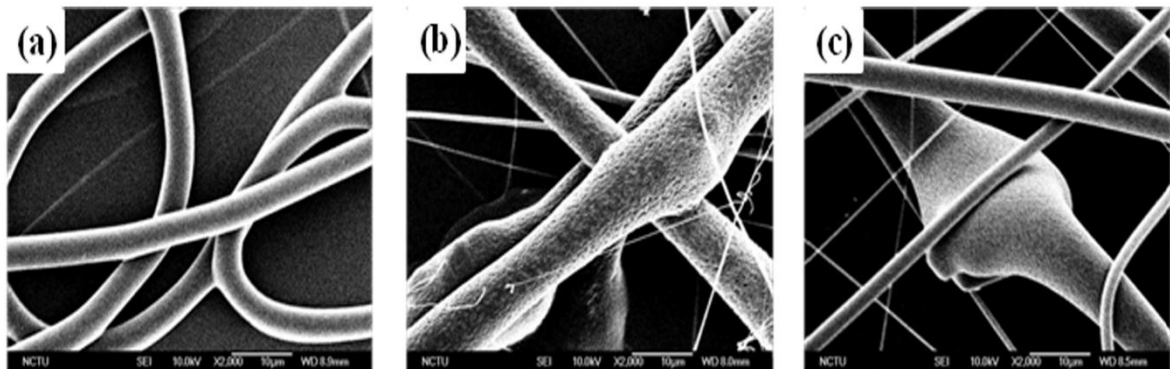


Figure 4- 8 Field Emission Scanning electron micrographs of the electrospinning

fibers: (a) PLLA fibers, (b) PLLA/calcite fibers(c) PLLA/aragonite fibers image.

Figure 4-9 is Micro-Raman spectra of the synthetically prepared PLLA fibers, PLLA/calcite fibers and PLLA/aragonite fibers. The CH_3 asymmetric deformation modes appear at about $1450 \pm 2 \text{ cm}^{-1}$, the same as intense Raman and IR bands would have detected in all the compounds[77]. The 1250-1400 cm^{-1} is region of the Raman spectra. Like in polypropylene and poly(α -L-alanine), this region is characterized by three group of bounds at 1390, 1360 and 1300 cm^{-1} . C=O stretching region. Presents the 1650-1850 cm^{-1} is region of the Raman spectra. Raman spectra (800-950 cm^{-1} region) of poly(L-lactic acid)s. Skeletal stretching and rCH_3 rocking region in figure 3 shows several strong absorption bands in the 1000-1250 cm^{-1} region. The Raman spectrum for the as-prepared sample is shown in Figure 3. Raman spectra can also be used to identify and distinguish aragonite from the other two calcium carbonate phases. The strongest line in each spectrum is the ν_1 symmetric stretch of CO_3^{2-} ion at $\sim 1080 \text{ cm}^{-1}$. Raman spectra of calcium carbonate (calcite) and coral (aragonite). The peaks chosen for analysis are the 711 cm^{-1} for calcite and 705 cm^{-1} for aragonite. The stronger and more highly resolved bands at $\sim 1085 \text{ cm}^{-1}$ are unable to be used in the analysis of the mixed systems due to extensive overlap between the three polymorphs in this region. The Raman spectra of calcite and aragonite are in good agreement with previous reports[58, 92].

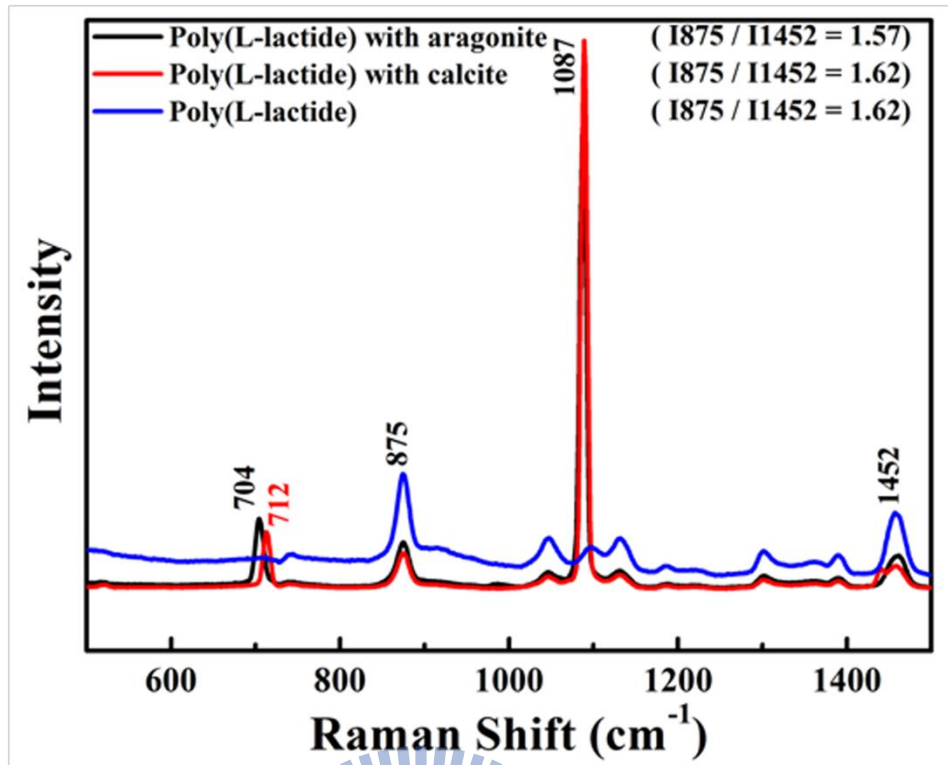


Figure 4- 9 Micro-Raman spectra of the synthetically prepared PLLA fibers, PLLA/calcite fibers and PLLA/aragonite fibers.

As mentioned in previous literature, I₈₇₅/I₁₄₅₂ Raman intensity ratios can signal results of bio-degradation and structural differences[77]. In this experiment, although both are bio-degradable membranes, the I₈₇₅/I₁₄₅₂ Raman intensity ratio of PLLA fiber membranes is 1.62, that of calcite-PLLA fiber membranes is 1.62, while that of aragonite-PLLA fiber membranes is 1.57.

RAMAN spectrum is utilized to confirm that calcite and aragonite have been successfully added with PLLA. Also, the I₈₇₅/I₁₄₅₂ Raman intensity ratios have indicated that they are biodegradable membranes, and Carbonic acid calcium salt, such as calcite and aragonite, does not interfere with the characteristics of PLLA.

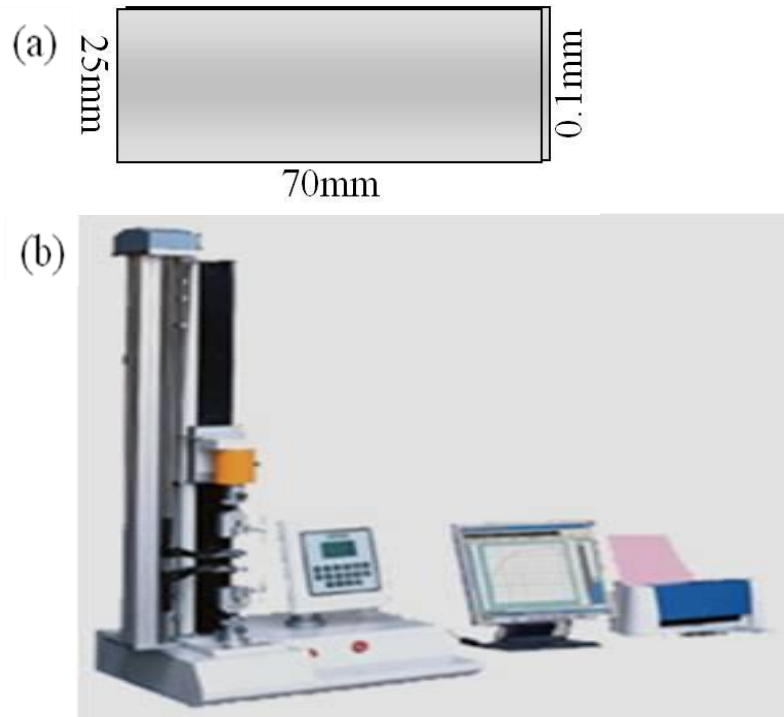


Figure 4- 10 Tensile tests (a) specimen size 25 mm× 70mm× 0.1mm (b) Instrument setup

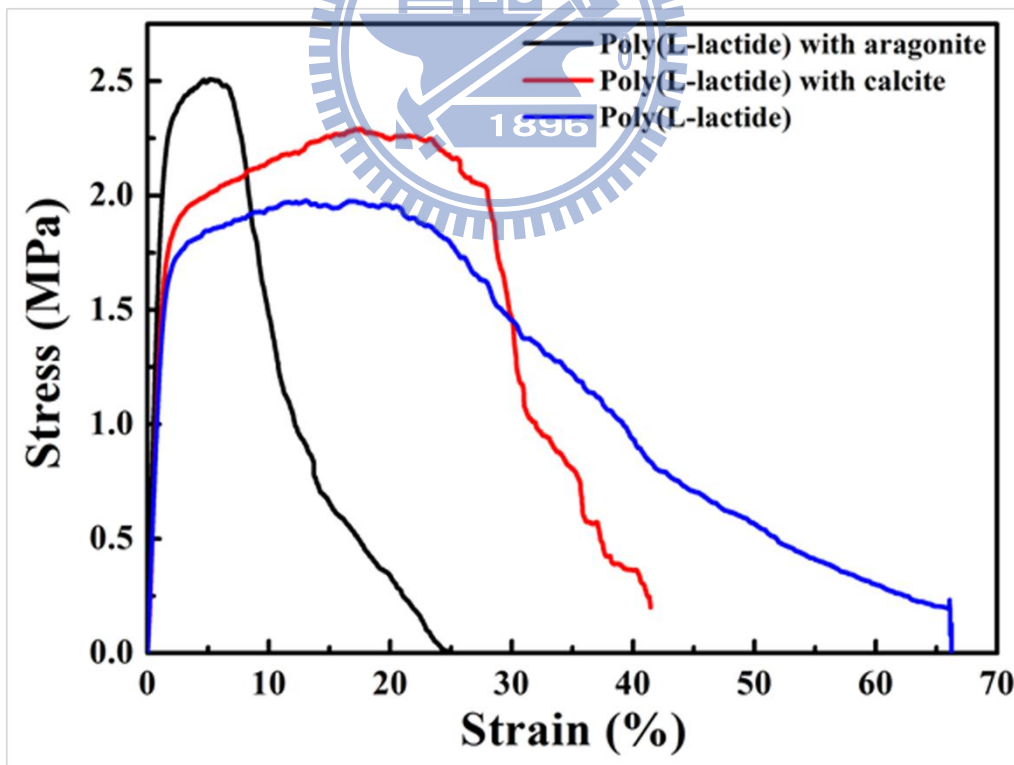


Figure 4- 11 Stress-strain curves of electrospun of PLLA, PLLA/calcite and PLLA/aragonite fiber.

Following the above experiment which confirms that the chemical properties of PLLA are not changed with the addition of calcite or aragonite, this experiment would produce calcite-PLLA or aragonite-PLLA membranes and conduct mechanical property analyses where tensile tests would be the main tool. Tensile tests are to measure the resistance capability of material bearing load or incremental load in a stationary status. During the process, both ends of the specimens are held tight and thus under axial stress. As a result, the specimens are stretched longer along axial direction. The specs of the rectangular tensile specimen membranes in this experiment were 25 mm×70mm× 0.1mm(Figure 4-10). Figure 4-11 demonstrates the stress-strain curves of PLLA, calcite-PLLA, and aragonite-PLLA membranes. Stress value can be derived by dividing load (Newton) by cross-section area (m^2), while strain value can be derived by dividing incremental length after stretch by original length. Table 3-1 demonstrates that the 0.2% offset yield strength of PLLA is 1.44MPa, that of PLLA with 5% calcite is 1.68MPa, and that of PLLA with 5% aragonite is 1.94MPa. Therefore, we can tell that PLLA with 5% calcite enjoys a higher 0.2% offset yield strength than pure PLLA by approximately 17%, and PLLA with 5% aragonite enjoys a higher 0.2% offset yield strength than pure PLLA by approximately 35%. Furthermore, the 0.2% offset yield strength of PLLA with 5% aragonite is higher than that of PLLA with 5% calcite by 18%. The reason is that although calcite and its polymorphism, aragonite, share the same chemical composition, aragonite is formed under higher environment pressure than calcite and could easily transform into calcite with lower energy state under atmospheric pressure (while calcite is

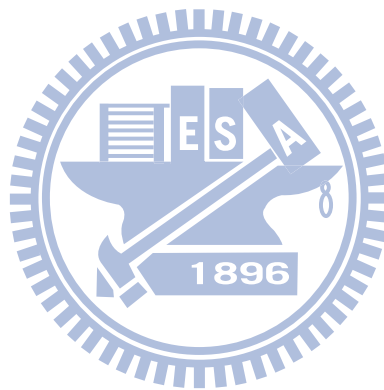
more stable under normal temperature and pressure). Therefore, diagenesis could easily turn aragonite into calcite. Previous studies by Hemming et al. have found that the anion vacancy of aragonite lattice (37.77\AA^3) is smaller than that of calcite lattice (40.87\AA^3). We can thus tell that aragonite is denser than calcite. Vacancy, a form of lattice imperfection, is categorized as a point defect. A point defect is defined as a departure from symmetry in the alignment of atoms in a lattice structure that affects only one or two lattice sites. It is the most common and important imperfection in lattice. As temperature has a bearing on the presence of vacancy, certain number of vacancy will exist per unit volume under heat balance ($T \neq 0^\circ\text{K}$). As temperature rises, heat increases, giving atoms enough energy to depart from lattice sites and making it more likely for vacancy to come into existence. The relation is as below:

$$\frac{n_v}{N} = e^{-E_v/kT} \quad (1)$$

n is the number of vacancy, N is the positional number of lattice, E_v is the energy needed to form vacancy, k is Boltzmann constant, while T is absolute temperature. According to the above relation, when temperature rises, vacancy concentration will increase and diffusion will accelerate. However, lattice imperfection usually impacts characteristics of materials, such as mechanical properties, conductivity, photovoltaic properties, magnetism, etc. This is the main factor contributing to the differences in the mechanical properties of guided tissue regeneration membranes under this experiment.

Table 4- 1: Mechanical properties of the electrospun PLLA, PLLA/calcite and PLLA/aragonite fiber.

Condition	UTS (MPa)	YS (MPa)	Young's Modulus (MPa)	Elongation (%)
PLLA/ Aragonite membrane	2.50	1.94	202.44	24.67
PLLA/ Calcite membrane	2.30	1.68	132.57	41.44
PLLA membrane	1.97	1.44	134.14	66.23



Chapter 5 Ultraviolet Resistant and Degradable Membranes

5.1 Introduction

Ultraviolet radiation, or UV, from the Sun can help with the synthesis of Vitamin D as well as the growth of bones, prevent rickets, and even sterilize so as to minimize bacteria infection on wounds. However, overall, UV does more harm than good on human bodies. Generally speaking, only 6% of UV from the Sun reaches the surface of the earth. Under normal circumstances, cells can repair themselves after exposure. Skin cells can absorb UV: 60%~80% by Stratum Corneum, 6%~11% by Epidermis, and 10%~20% by Dermis[93]. Stratum Corneum will then come off as a result of metabolism to rid harmful UV. Nevertheless, over exposure to UV can undermine DNA's repair ability[94], causing skin cells to age, progress to tumor, or die, leading to phototoxic skin disease, phototoxic reaction, & photosensitivity, and ultimately triggering skin cancer. It is fair to say that UV is the biggest threat to the health of the skin. In addition to skin damage, over exposure to UV can bring about acute keratitis, conjunctivitis, chronic cataract, etc[94-95].

Many polymers used in consumer products are degraded by UV light, and need addition of UV absorbers to inhibit attack, especially if the products are exposed to sunlight. The problem appears as yellowing discoloration or fading, cracking and sometimes, total product disintegration if cracking has proceeded sufficiently. The rate of attack increases with exposure time and sunlight intensity. It is known as UV degradation, and is one form of polymer degradation. UV absorption leads to chain degradation and loss of strength at sensitive points in the chain structure. They include tertiary carbon atoms, which

in polypropylene occur in every repeat unit. Sensitive polymers include thermoplastics, such as polypropylene and polyethylene[62].

Table 5- 1 Ultraviolet wave-lengths of maximum sensitivity for typical commercial polymers[62]

Polymer	Ultraviolet Wave-Length of Maximum Sensitivity
Polyesters	325 nm
Polystyrene	318 nm
Polyethylene	300 nm
Polypropylene	310 nm
Polyvinyl Chloride	310 nm
Vinyl Chloride/Acetate	295 nm
Polycarbonate	322-364 nm
Polymethyl Methacrylate	290-315 nm
Polyformaldehyde	300-320 nm

When plastics are used for outdoor applications, they often deteriorate fairly rapidly. Theoretical explanation is based upon absorption of ultraviolet energy, raising some bonds to an energy level which exceeds their stability, and thus initiating their breakdown, usually involving atmospheric oxidation and sometimes hydrolysis as well. Many of the newer engineering plastics offer high performance in their mechanical, thermal, and chemical properties, but still cannot be recommended for use out-of-doors[61].

Ultraviolet radiation can be classified into UV-A, UV-B, and UV-C regions. Much less is known about the biological effects of UV-A radiation (320–400

nm), which adjoins the visible light, so the waveband is usually not a topic of discussion. Most observed biological effects of UV-B (280–320 nm) radiation are extremely detrimental to living organisms[62]. Because solar UVR below wavelengths of 290 nm is effectively absorbed by stratospheric ozone, and no such radiation reaches living organisms from natural sources, the wavelength in the UV-C region (200–280 nm) is considered of little detriment to human beings. Ultraviolet radiation (UV-A、UV-B、UV-C can cause damage to C-H, C-C, O-H, C-Cl, etc. in living organisms, and substance with the same bond energy. In order to solve the polymer composite material is not suitable for outdoor issues, often in the processing additives are added to solve this problem a little[61-63]. Many common additives, such as : UV Absorber : Benzophenone、Phosphite Antioxidant、Hindered Amine Light Stabilizers (HALS) : Hindered Amine Light Stabilizer[64].

Many polymers used in consumer products are degraded by UV light, and need addition of UV absorbers to inhibit attack, especially if the products are exposed to sunlight. The problem appears as yellowing discoloration or fading, cracking and sometimes, total product disintegration if cracking has proceeded sufficiently. The rate of attack increases with exposure time and sunlight intensity. It is known as UV degradation, and is one form of polymer degradation. UV absorption leads to chain degradation and loss of strength at sensitive points in the chain structure. UV absorption and anti-oxidation agents are now the most prominent and effective ultraviolet resistance for plastics materials.

With the advances in technology and the increase in the global population,

plastic materials have found wide applications in every aspect of life and industries. However, most conventional plastics are non biodegradable, and their increasing accumulation in the environment has been a threat to the planet. To overcome all these problems, some steps have been undertaken. The first strategy involved production of plastics with high degree of degradability..

The majority of the studies on electrospinning fibers of PLLA to add Benzophenone -12[65-68] and Chemfos-168[69-70] from solutions, we have reported that molecular structures and antiultraviolet of electrospinning nanofibers. Benzophenone can be used as a photo initiator in UV-curing applications such as inks, imaging and clear coatings in the printing industry. Benzophenone prevents ultraviolet (UV) light from damaging scents and colours in products such as perfumes and soaps. It can also be added to the plastic packaging as a UV blocker. This allows manufacturers to package the product in clear glass or plastic. Without it, opaque or dark packaging would be used. In laboratories, solvents are often distilled with sodium and benzophenone as desiccants. The product of these two chemicals in the absence of air and water is a dark blue ketyl; a solution of this ketyl can be used to qualitatively test for the absence of air and water. Chemfos-168 is an antioxidant is a molecule capable of slowing or preventing the oxidation of other molecules. Oxidation is a chemical reaction that transfers electrons from a substance to an oxidizing agent. Oxidation reactions can produce free radicals, which start chain reactions that damage cells. Antioxidants terminate these chain reactions by removing free radical intermediates, and inhibit other oxidation reactions by being oxidized themselves. As a result, antioxidants are often reducing agents such as thiols or polyphenols.

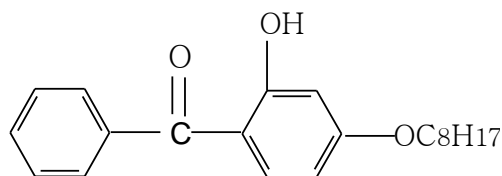
In this study, we investigated ultraviolet resistance of the PLLA, PLLA / UV absorption and PLLA / anti-oxidation agents by electrospinning. It is believed that this study could provide a good insight into ultraviolet resistance properties of the electrospinning polymer. We also hope to make the ultraviolet resistance electrospinning fibers and have high degree of degradability



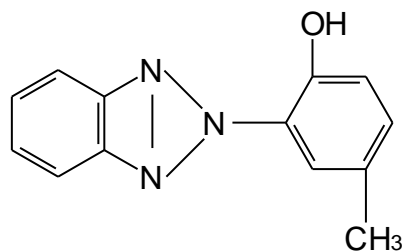
5.2 Experimental procedure

5.2.1 Materials and Methods

Poly lactide (PLA) is a biodegradable, thermoplastic, aliphatic polyester derived from renewable resources, such as corn starch or sugarcane. PLA with a molecular weight of 180~200 KDa, at a volume concentration of 12%, was 12g PLA dissolved in 100ml ACS grade >99.8 % chloroform. The Benzophenone structural studies of this material were done by Linnemann in 1865, who also reported its accurate melting point as 48–48.5 °C and described the stable orthorhombic phase. 2-Hydroxy-4-Octyloxy Benzophenone (bp12 CAS No.: 1843-05-06 $M_w = 326.42\text{Da}$), 2-(2'-hydroxy-5'-methylphenyl) benzotriazole (commercial name Tinuvin P or TIN) (chemsorb-p CAS No.: 2440-22-4 $M_w = 225\text{Da}$) and Phosphite Antioxidant Tris(2,4-di-tert-butylphenyl) phosphite (Irgafos 168 CAS No.: 31570-04-4 $M_w = 646.9\text{Da}$) was kindly supplied by Chembridge International Corp. Taipei, Taiwan (R.O.C.). The polymer fibers were injected in by using a 10mL glass syringe with a 22 needle gauge (0.7mm OD×0.4mm ID) at a flow rate of 0.2mL/hour, which was controlled by using a KDS100 pump YEONG-SHIN CO., LTD. Hsinchu, Taiwan (R.O.C.). The high voltage power supply used was a model 30KV/15W purchased from YOU-SHANG TECHNICAL CORP. Kaohsiung, Taiwan (R.O.C.). The equipment was attached to the needle tip through an alligator clip and voltage difference of 20KV was used; the tinfoil grounded target was placed at 15cm away from the needle tip.



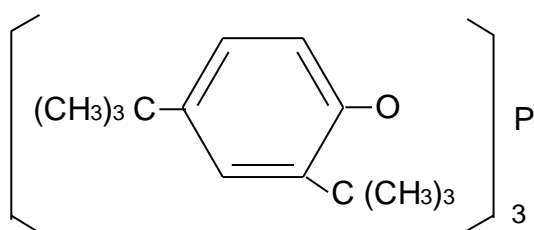
(a) 2-Hydroxy-4-Octyloxy Benzophenone



(b) 2-(2'-hydroxy-5'-methylphenyl) benzotriazole



(c) Tetrakis [Methylene(3',5'-Di-tert-Butyl-4-hydroxyphenyl) Propionate] methane



(d) Tris(2,4-di-tert-butylphenyl) phosphate

Figure 5- 1 The Ultraviolet resistance structure of (a) 2-Hydroxy-4-Octyloxy Benzophenone, (b) 2-(2'-hydroxy-5'-methylphenyl) benzotriazole, (c) Tetrakis [Methylene(3',5'-Di-tert-Butyl-4-hydroxyphenyl) Propionate] methane, and (d) Tris(2,4-di-tert-butylphenyl) phosphate

5.2.2 Fabrication of Composite ultraviolet resistant and high degree of degradable membranes

The polymer fibers were injected by using a 10mL glass syringe with a 22 needle gauge (0.7mm OD×0.4mm ID) at a flow rate of 0.2mL/hour, which was controlled by using a KDS100 pump (YEONG-SHIN CO., LTD. Hsinchu, Taiwan (R.O.C.)). The high voltage power supply used was a 30KV/15W model purchased from YOU-SHANG TECHNICAL CORP. Kaohsiung, Taiwan (R.O.C.). The equipment was attached to the needle tip through an alligator clip and voltage difference of 20KV was used; the tinfoil grounded target was placed at 15cm away from the needle tip.

First, the UV absorption (Benzophenone -12) -added PLLA and anti-oxidation agents (Chemfos-168)-added PLLA solution was injected into a 10mL syringe respectively. Next, the syringe pump was used to control the 10mL UV absorption (Benzophenone -12)-added PLLA and anti-oxidation agents (Chemfos-168)-added PLLA solution syringe at a flow rate of 0.2mL/hour. The syringe needle was stainless steel, while the collector was tinfoil paper. The distance between the syringe tip and the collector was 15cm. Then, the high power supply was connected to the syringe tip and the collector; the positive electrode was on the syringe tip side, and the negative electrode was on the collector side. The high power supply was turned on in the condition of 20KV and then the spinning fibers on the collector were observed. The structural and optical properties were investigated by a Scanning Electron Microscope (SEM), Micro-Raman system and Ultraviolet visible spectroscopy analyses fiber membranes. All the experiments were performed at room temperature, about 25°C

5.2.3 Physical and chemical properties

The fibers were examined by a Field Emission Scanning Electron Microscope (FE-SEM) to visualize their morphology by using a JSM-6700F (JEOL Ltd.). The fiber samples were coated with a thin layer of palladium in 100sec at 20mA by the auto fine coater JFC-1600 (JEOL Ltd.). Raman scattering measurements were performed in the TRIAX 550 micro-Raman system. The 5145 Å line with a power of 0.2 W from the Coherent Innova Argon ion laser was focused to about 2 ~ 4 µm on the sample surface. The back-scattered signal was collected by a microscopic system and recorded with a JOBIN-YVON SPEX SPECTRUM ONE liquid nitrogen cooled CCD detector. All spectra were recorded by an OLYMPUS microscope objective and 3 accumulations at 300 seconds integration time with ~50 mW power on the sample for each Raman spectrum. Frequencies are to ± 2 cm⁻¹ accurately as determined from plasma emission lines. The frequency of each Raman band reported in this study was obtained using Lorentzian curve fitting.

5.2.4 Ultraviolet Protection Factor (UPF)

The percent blocking of UV was determined for UVA in the range 315-400 nm, and for UV-B in between 280 and 315 nm. The UPF has been widely adopted by the textile and clothing industry to denote the protective ability of a textile based on instrumental measurements. The UPF values were calculated according to the AATCC test method using the following equation:

$$UPF = \frac{\sum_{\lambda=280}^{400} E_{\lambda} S_{\lambda} \Delta\lambda}{\sum_{\lambda=280}^{400} E_{\lambda} S_{\lambda} T_{\lambda} \Delta\lambda} \quad (2)$$

where E_{λ} is the relative erythemal spectral effectiveness; S_{λ} is the solar

spectral irradiance (W/cm²/nm); T_λ is the mean measured transmittance of the sample (%); and $\Delta\lambda$ is the measured wavelength interval (nm)[96].

Table 5- 2 UPF classification system of sun protective clothing[96]

UPF range	UV radiation protection category
15-24	Good
25-39	Very good
40-50, 50+	Excellent

5.2.5 UVA Effectiveness - The Boot's Star System

Boot's the Chemist, the largest producer of sunscreens in UK, has developed a label system that uses a four star rating based on spectrophotometric analysis[96]. The sunscreen samples are prepared according to a substrate method. The labeling system is already in use within the UK. The spectral transmittance values, T_λ , are converted to spectral absorbance values $A_\lambda = -\log(T_\lambda)$. A term called the "UVA ratio" is calculated, which is the ratio of the total absorption in the UVA to that in the UVB:

$$A_\lambda = -\log(T_\lambda) \quad (3)$$

$$\frac{\alpha_{UVA}}{\alpha_{UVB}} = \frac{\int_{320\text{nm}}^{400\text{nm}} A_\lambda d\lambda}{\int_{290\text{nm}}^{320\text{nm}} A_\lambda d\lambda} \quad (4)$$

The method specifically calls for the A_λ data to be measured in 5 nm increments and for the integrals to be solved using Simpson's rule for area approximation. The limits of the UVA and UVB spectral regions also vary

slightly from those previously noted. This sort of discrepancy for UVA and UVB is frequently encountered within scientific publications. The star rating, and its associated claim for UVA protection, is determined from the measured UVA ratio:

Table 5- 3 UVA Effectiveness[96]

UVA ratio	Star category	Category descriptor
0.0 to <0.2	-	too low for UVA claim
0.2 to <0.4	*	MODERATE
0.4 to <0.6	**	GOOD
0.6 to <0.8	***	SUPERIOR
0.8 to ≥ 0.8	****	MAXIMUM

5.2.6 UVA Effectiveness - Critical Wavelength

Similar to the Boots Star method, a sample is prepared according to a substrate technique, its spectral transmittance is measured, T_λ , and converted to spectral absorbance values $A_\lambda = -\log(T_\lambda)$. A ratio is calculated as follows which determines the total absorption in incremental wavelength bands and compares it to the total UV absorption. The ratio recorded for each wavelength, λ is:

$$R = \frac{\int_{290\text{nm}}^{\lambda\text{nm}} A_\lambda d\lambda}{\int_{290\text{nm}}^{400\text{nm}} A_\lambda d\lambda} \quad (5)$$

The critical wavelength, λ_c , is the first value where the ratio $R \geq 0.9$.

Table 5- 4 Level of Protection (Critical Wavelength)[96]

λ_c	Level of Protection
$340\text{nm} \leq \lambda_c < 370\text{nm}$	Some
$\lambda_c > 370\text{nm}$	More (broad-spectrum)

5.3 Results and Discussion

It could be observed by the electronic microscope that, in Figure 5-2(a), the fiber diameter of PLLA was approximately $4.92 \pm 2.23\mu\text{m}$ and on the surface of the fibers were pores at the size of around 10nm. In Figure 5-2(b), the fiber diameter of PLLA/0.3% Benzophenone-12 was approximately $3.56 \pm 0.6\mu\text{m}$ and on the surface of the fibers were pores at the size of around 10nm. In Figure 5-2(c), the fiber diameter of PLLA/0.3% Chemfos-168 was approximately $1.25 \pm 0.6\mu\text{m}$ and on the surface of the fibers were pores at the size of around 10nm.. In Figure 5-2(d), the fiber diameter of PLLA/0.3% Chemsorb-p was approximately $1.25 \pm 0.6\mu\text{m}$ and on the surface of the fibers were pores at the size of around 10nm.

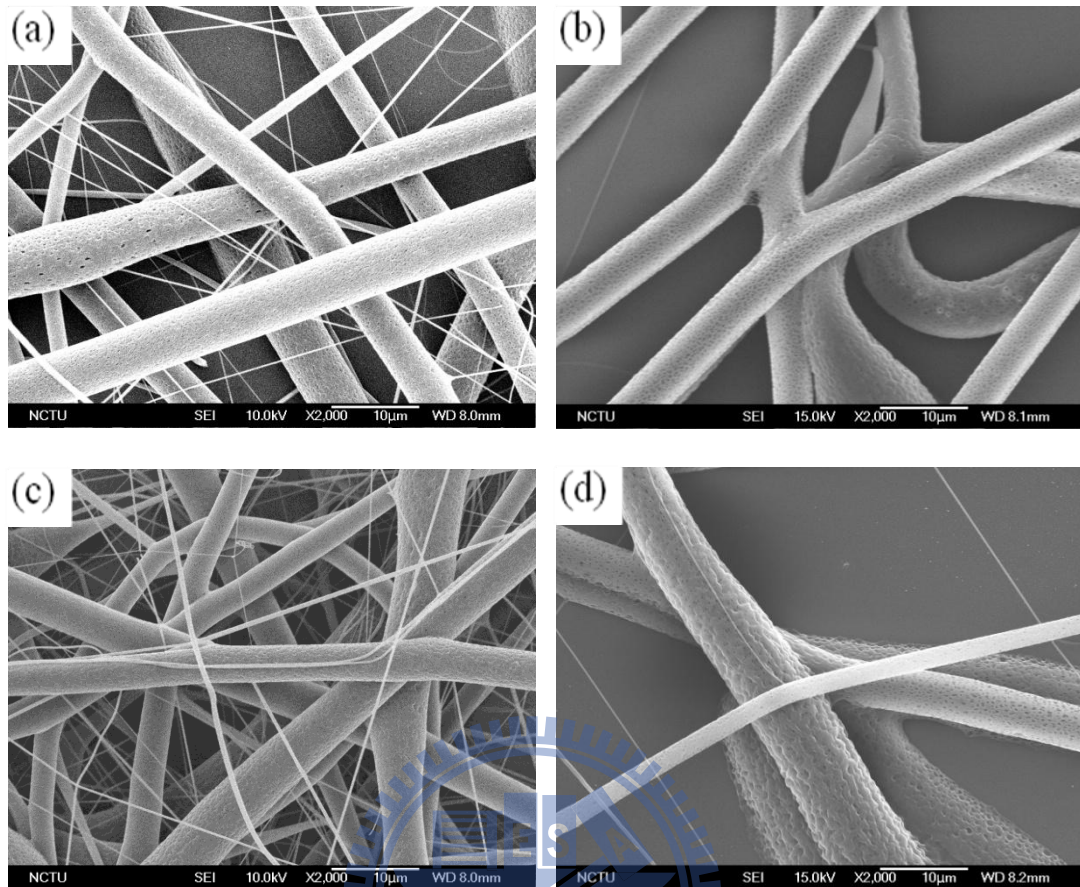


Figure 5- 2: SEM Image (a) PLLA , (b) PLLA/Benzophenone-12 , (c) PLLA/Chemfos-168(d) PLLA/Chemsorb-p

In Figure 5-3(a), Micro-Raman spectra of PLLA fibers. (b), Micro-Raman spectra of PLLA/Benzophenone-12 fibers. (c), Micro-Raman spectra of PLLA/Chemfos-168 fibers. (d), Micro-Raman spectra of PLLA/ Chemsorb-p. Micro-Raman Spectroscopy is utilized to conduct fiber membrane analyses at CH_3 and CH bending region. The CH_3 asymmetric deformation modes appeared at about $1450 \pm 2 \text{ cm}^{-1}$ as intense Raman and IR bands in all the compounds. The $1250\text{-}1400 \text{ cm}^{-1}$ region of the Raman spectra. Like in polypropylene and poly(α -L-alanine), this region was characterized by three groups of bands at 1390 , 1360 and 1300 cm^{-1} . $\text{C}=\text{O}$ stretching region. Presents the $1650\text{-}1850 \text{ cm}^{-1}$ region of the Raman spectra. Raman spectra ($800\text{-}950 \text{ cm}^{-1}$ region) of

poly(L-lactic acid)s. Skeletal stretching and rCH_3 rocking region. Figure 5-3 shows several strong absorption bands in the $1000\text{-}1250\text{ cm}^{-1}$ region.

In Figure 5-3(b), Micro-Raman spectra of PLLA/Benzophenone-12 fibers. BP crystallizes in two polymorphic forms with stable α -phase and metastable β -phase[67]. The deformation vibrations of the phenyl ring at 564, 625, 627 and 724 cm^{-1} (measured: 565, 616, 619 and 723 cm^{-1}) and the out-of-plane C–H deformation vibration at 770 cm^{-1} (measured: 768 cm^{-1}) are predicted quite correctly. The very intense lines at 1002 and 1029 cm^{-1} in the experimental Raman spectra are predicted as the deformation vibration of the phenyl ring (1006 cm^{-1}) and as the C–C stretching vibration of the phenyl ring (1038 cm^{-1}). Most likely, the deformation vibration at 1006 cm^{-1} is appreciably affected by the phenyl ring C–C stretching vibrations leading to increase of its intensity. In such a case the mixed character of the 1006 cm^{-1} vibration becomes apparent. The next quite intense modes of the BP molecule appear to be the stretching CB–C–CA vibrations at 1154 and 1276 cm^{-1} (measured: $1145\text{-}1166$, and 1279 cm^{-1}). Some discrepancies between calculated and measured frequencies is seen in the spectra, however they are not too large. The most intensive lines in the experimental Raman spectra are at 1596 , 1601 and 1650 cm^{-1} . Theoretical calculations predict these modes as corresponding to the phenyl ring C–C stretching vibrations (1594 and 1614 cm^{-1}) and to the C=O stretching vibration (1707 cm^{-1}). Whereas the intensities of these vibrations are predicted quite correctly, nevertheless, the large deviations between the measured and calculated frequencies are observed.

In Figure 5-3(c), Micro-Raman spectra of PLLA/ phosphite Chemfos-168 fibers. We initially chose to use Raman spectroscopy of the polymer film.

Several absorption bands of 168 (1213, 1196, 1083, 854 and 776 cm^{-1})[69-70] are candidates for monitoring the 168 concentration as they are resolvable from the polymer. In practice the peak at 1083 cm^{-1} was most clearly defined when analysing a Polymer film containing dissolved 168 and this peak was chosen for analysis.

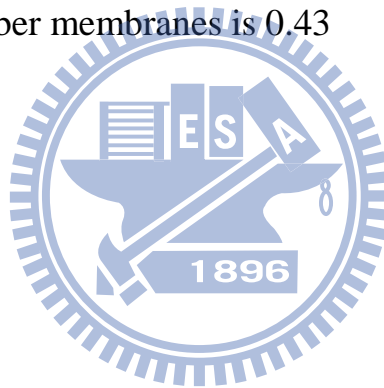
In Figure 5-3(d), Micro-Raman spectra of PLLA/ Chemsorb-p. A strong deuteration effect is evident for the two lines at 1604 and 1422 cm^{-1} . The latter becomes a doublet on deuteration. The fundamentals at 1296 cm^{-1} collapse on deuteration and the 1342 cm^{-1} fundamental band in the protonated molecule reveals a double-peak structure. Analogous to the situation for TIN, the spectra of HBT and HBO show strong effects on deuteration near 1600 cm^{-1} with a large downshift of about 10 cm^{-1} . Around 1450 cm^{-1} , strong intensity redistribution occurs together with wavenumber shifts, indicating a strong alteration in the normal coordinate for the respective modes. Concentrating on deuteration effects on the skeletal vibrations of the molecules, we exclude the spectral region of the X-H stretching modes from our discussion. A characteristic phenolic OH stretching mode is observed in all three molecules, pointing to strong intramolecular hydrogen bonding in a non-polar solvent. It displays the large isoshifts of the respective band, characteristic of a localized mode. There is a simple physical explanation for the isoshift effects in the two modes which occur in all three molecules around 1600 and 1450 cm^{-1} . They derive their large Raman intensities from coupling of the phenolic C-O-H group to two spectrally neighbouring degenerate modes of the six-membered ring which is part of the phenolic group. Degeneracy is broken by either a stretching or a deformation of the C-O bond from the attached C-O-H group. In benzene, the E_{2g} mode at

1595 cm^{-1} is strongly Raman active. The analogous mode for TIN lies at 1604 cm^{-1} . The degeneracy is broken by coupling of the C-O stretching coordinate. The 1422 cm^{-1} of TIN is connected with a C-O-H deformation movement coupled to the E_{1u} mode, being at 1485 cm^{-1} in benzene. The latter benzene mode is not Raman active by itself and the intensity comes from coupling to the remainder of the molecule. The essential downshift of δ_{COH} on deuteration brings about a reorganization of the normal coordinates for the mode near 1422 cm^{-1} and is connected with strong redistribution of intensities in the neighbouring bands. Raman excitation at the high-wavenumber side of the resonant molecular 0-0 transition results in the appearance of a distinct combination tone spectrum beyond 1650 cm^{-1} in which a grouping of bands is discernible. It pertains up to the C-H stretching range. This was shown previously for TIN and it also holds for HBT and HBO, although the high quality of the TIN spectra could not be attained for the other molecules. Applying Raman excitation at 363.8 nm, which is slightly above the 0-0 transition of TIN at 366.8 nm, a good-quality overtone spectrum was obtained. The doublet found on deuteration around the 1422 cm^{-1} mode is repeated in the combination tone spectrum. This holds for combinations with the 469 cm^{-1} mode up to four orders.

Vibrational spectroscopy has been extensively used also for investigating the *in vitro* and *in vivo* degradation mechanism and kinetics of different biomedical devices composed of PLAs. The I875/I1452 Raman intensity ratio was utilized for a relative quantitative evaluation of polymeric chain length. The I875/I1452 Raman intensity ratio was useful for studying the *in vitro* and *in vivo*

degradation of PLA devices. The ratio was identified as a spectroscopic marker of the partial and progressive breakdown of the polymeric chain during degradation, spectroscopically confirming hydrolysis of ester linkage as the primary mechanism of PLA degradation.

As mentioned in previous literature, the I875/I1452 Raman intensity ratio signals results of bio-degradation and structural differences[77]. In this experiment, although both are bio-degradable membranes, the I875/I1452 Raman intensity ratio of PLA fiber membranes is 1.59; I875/I1452 Raman intensity ratio of PLLA/Benzophenone-12 fiber membranes is 0.61; I875/I1452 Raman intensity ratio of PLLA/Chemfos-168 fiber membranes is 1.53 while that of PLLA/Chemsorb-p fiber membranes is 0.43



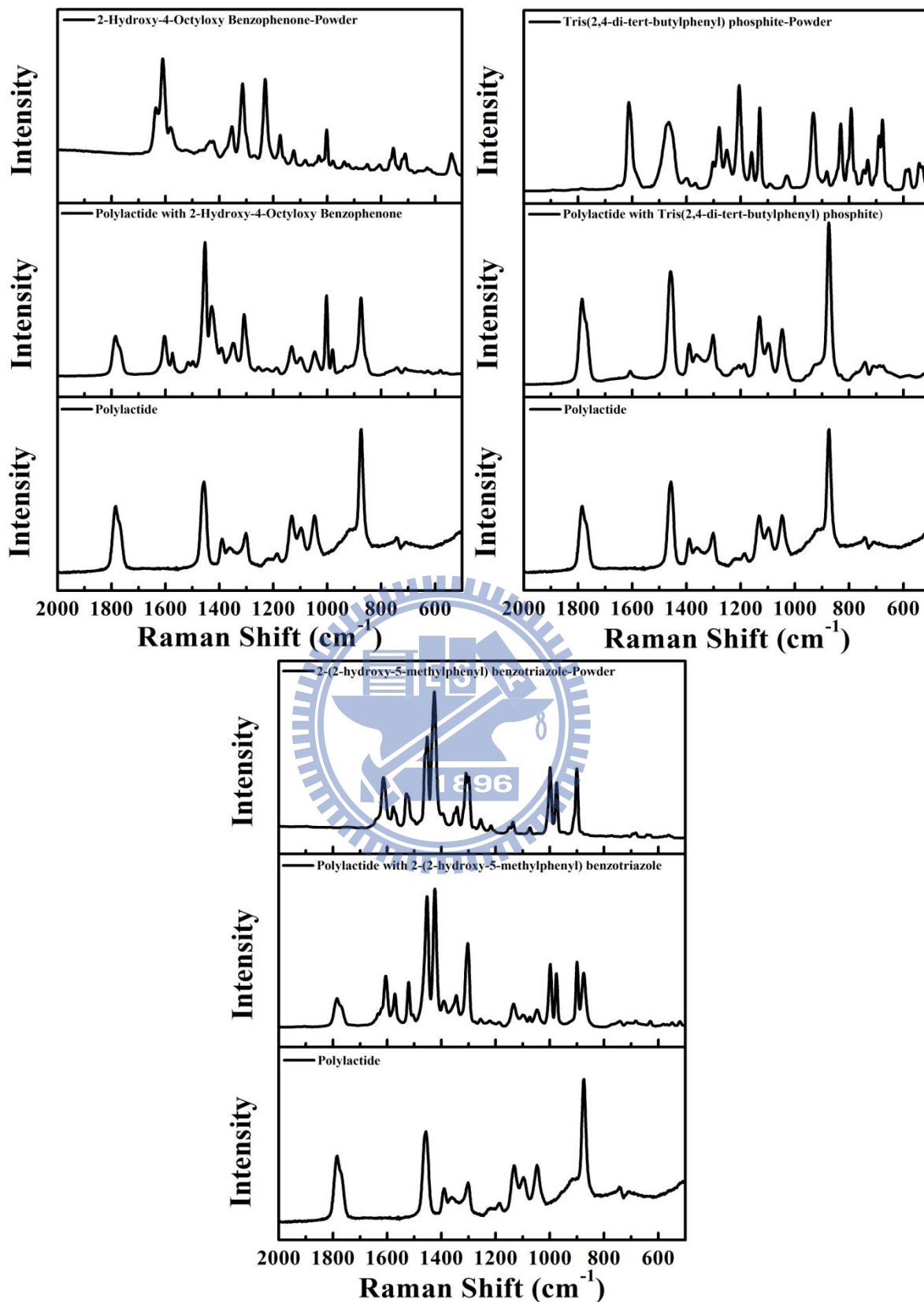


Figure 5- 3 Micro-Raman spectra of PLLA fibers, PLLA/Benzophenone-12 fibers, PLLA/Chemfos-168 fibers and PLLA/ Chemsorb-p fibers.

In Figure 5-4 The PLLA, PLLA/ Benzophenone-12 and PLLA/ Chemfos-168 fibers were characterized by UV transmission. The characteristic UV transmission peaks from 200 to 400 nm wavelength. The PLLA/ Benzophenone-12 fibers has single sharp peak between 250 to 300 nm than other fibers. PLLA/ Benzophenone-12 has nano structure than PLLA and PLLA/ Chemfos-168 fibers.

Boots the Chemist, the largest producer of sunscreens in the UK, has developed a label system that uses a four star rating based on spectrophotometric analysis. The spectral transmittance values, T_λ , are converted to spectral absorbance values $A_\lambda = -\log(T_\lambda)$. A term called the UVA ratio is calculated which is the ratio of the total absorption in the UVA to that in the UVB (Eq 4,5) The method specifically calls for the A_λ data to be measured in 5 nm increments and for the integrals to be solved using Simpson's Rule for area approximation. The limits of the UVA and UVB spectral regions also vary slightly from those previously noted. This sort of discrepancy for UVA and UVB is frequently encountered within scientific publications. The star rating, and its associated claim for UVA protection, is determined from the measured UVA ratio (Table 5-5)[96].

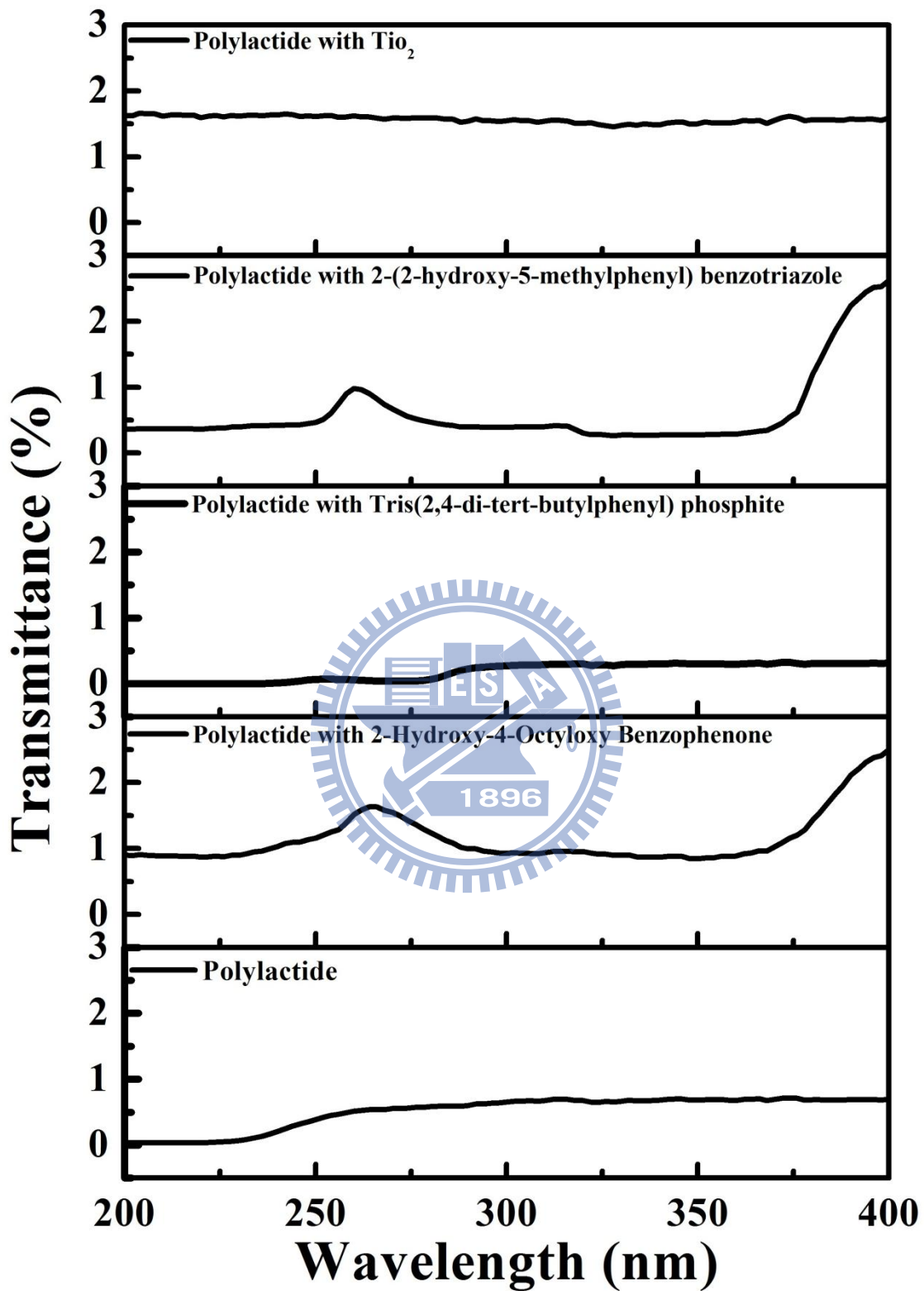


Figure 5- 4 The transmission spectra of (A) PLA , (B) PLA/Benzophenone-12 , (C) PLA/ Chemfos-168 fibers.

Table 5- 5 UVA Effectiveness - UPF and Critical Wavelength

Condition	Ratio (UVA / UVB)	λ_c (nm)	UVA %	UVB %	UPF	UV protection category
PLA membrane	2.65	388	99.31	99.36	148.78	Excellent broad-spectrum
PLA / BP12 membrane	2.56	386	98.79	99.01	87.52	Excellent broad-spectrum
PLA / Chemfos168 membrane	2.63	388	99.70	99.76	350.55	Excellent broad-spectrum
PLA / Chemsorb-p membrane	2.54	384	99.23	99.59	151.82	Excellent broad-spectrum

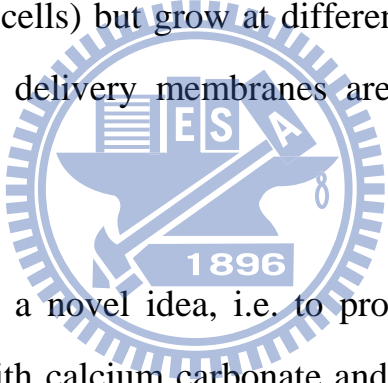
The PLLA has a good ability in anti-ultraviolet. We use the elements (UV absorption and anti-oxidation agents) composite with PLLA by electrospinning in our study. We observed the PLLA/ UV absorption (Benzophenone-12) fiber membranes higher than PLLA membrane 14.9% in UVA ratio and PLLA/ anti-oxidation agents (Chemfos-168) fiber membranes higher than PLLA membrane 17.9% in UVA ratio. As mentioned in previous literature, the I875/I1452 Raman intensity ratio signals results of bio-degradation and structural differences. In this experiment, although both are bio-degradable membranes, the the PLLA/ UV absorption (Benzophenone-12) fiber membranes higher than PLLA membrane 61.6% in I875/I1452 Raman intensity ratio and PLLA/ anti-oxidation agents (Chemfos-168) fiber membranes higher than PLLA membrane 3.7% in I875/I1452 Raman intensity ratio. So PLLA Add UV absorption (Benzophenone-12) fiber membranes can achieve good UV resistance and fast bio-degradation.

Chapter 6 Conclusions

Electrospinning is a simple and versatile method for fibers preparation, which employs electrostatic forces that strength a polymer jet to generate continuous fibers with diameters ranging from micrometers down to several nanometers. Electrospinning is an interesting technique for spinning PLLA. The process offers an excellent opportunity for designing the surface morphology and porosity of the fibers to provide the most appropriate interface for biomedical application. In most of these applications, the properties of polymers are modified using fillers and fibers to suit the high strength/specific properties requirements. Polymer composites offer advantages over other conventional materials when specific properties are compared.

[1] The study found that biodegradable drug delivery membranes that were fabricated from Poly(α -L-alanine) (PLLA) and chlorhexidine (CHX)-gluconate via electrospinning could steadily and continuously inhibit the growth of bacteria. Bacterial growth curves were used to evaluate on a real-time basis the relationship between drug delivery speeds of the membranes and growth rates of bacteria in different phases. The results of this experiment show that CHX drug delivery membranes fabricated via electrospinning are a typical rate-preprogrammed drug delivery system, which can effectively inhibit the growth of bacteria. In this experiment where bacteria growth curves are used to evaluate the inhibiting capability of CHX releasing membranes, it is found that (1) biodegradable CHX delivery membranes can be fabricated via electrospinning, CHX can effectively inhibit the growth of bacteria, and the concentration level of CHX released by the delivery membranes can have a say over the

inhibiting duration; (2) previous studies have focused on the delivery efficiency of Polymer/CHX or simply on the drug delivery efficiency. Only a few of them have evaluated the inhibiting capability of Polymer/CHX matrix (Inhibition Zone), but evaluations of bacteria inhibiting capability based on Inhibition Zone are only qualitative, not quantitative. Therefore, this experiment proposes to evaluate on a real-time basis the impacts of drug delivery speeds of the membranes on the growth rates of bacteria in different phases; (3) as growth curves of a single bacterium can only conclude whether the membranes possess characteristics of drug delivery systems, bacteria that are of the same strain (competent cells and plasmid inserted competent cells) but grow at different speeds are used to evaluate whether such drug delivery membranes are a rate-preprogrammed drug delivery system.

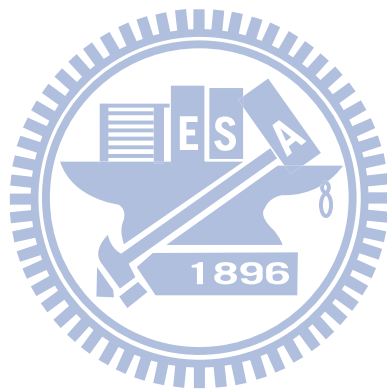
- 
- [2] This study proposes a novel idea, i.e. to produce bio-degradable GTR or GBR membranes with calcium carbonate and its polymorphism, aragonite, through electrospinning. Biomineralization is the formation process of minerals within organisms. With huge organic molecules, organisms can limit the crystallization of inorganic minerals within to nanometers. Some organisms transform minerals into calcite, some transform minerals into aragonite, while some have dual formations. Calcium carbonate enjoys fair bio-compatibility, while its polymorphism has a different lattice structure which means different mechanical properties. This experiment shows that the addition of calcium carbonate and its polymorphism which have different lattice structure, to PLLA can produce GBR membranes or

GTR membranes with different mechanical properties. We can tell that PLLA with 5% calcite enjoys a higher 0.2% offset yield strength than pure PLLA by approximately 17%, and PLLA with 5% aragonite enjoys a higher 0.2% offset yield strength than pure PLLA by approximately 35%. Furthermore, the 0.2% offset yield strength of PLLA with 5% aragonite is higher than that of PLLA with 5% calcite by 18%. There is no doubt that, be GTR membranes or GBR membranes, excellent biocompatibility, controllable biodegradability, cytocompatibility, suitable microstructure (pore size and porosity), and mechanical properties are required as long as medical applications are involved. The polymer PLLA experimented in this study is biocompatible and biodegradable, and calcite as well as aragonite added is calcium carbonate. Calcium carbonate has been recognized as bone filling material and its good osteoconductivity has been approved in recent studies. In this study, electrospinning is utilized to produce membranes as previous studies have pointed out that such method can create suitable microstructure (pore size and porosity) with the potential to promote osteoblastic cell function and bone regeneration. As a result, the biggest challenge with GTR membranes or GBR membranes is how to adjust(change) the mechanical properties of the membranes in accordance with locations and functions of such membranes. This study proposes a novel idea, i.e. to produce bio-degradable GTR or GBR membranes with calcium carbonate (calcite) and its polymorphism, aragonite, through electrospinning. Calcium carbonate enjoys fair bio-compatibility, while its polymorphism has a different lattice structure which means different

mechanical properties. Therefore, calcite or aragonite can be opted based on different application purposes. Moreover, calcite and aragonite can be mixed to various percentage to generate bio-degradable membranes that can meet needs/objectives of different applications.

[3] Many polymers used in consumer products are degraded by UV light, and need addition of UV absorbers to inhibit attack, especially if the products are exposed to sunlight. UV absorption and anti-oxidation agents are now the most prominent and effective ultraviolet resistance for plastics materials. This article provides a comprehensive review of the ultraviolet resistance ability, bio-degradation and structural differences of UV absorption and anti-oxidation agents. The PLLA has a good ability in anti-ultraviolet. We use the elements (UV absorption and anti-oxidation agents) composite with PLLA by electrospinning in our study. We observed the PLLA/ UV absorption (Benzophenone-12) fiber membranes higher than PLLA membrane 14.9% in UVA ratio and PLLA/ anti-oxidation agents (Chemfos-168) fiber membranes higher than PLLA membrane 17.9% in UVA ratio. As mentioned in previous literature, the I875/I1452 Raman intensity ratio signals results of bio-degradation and structural differences. In this experiment, although both are bio-degradable membranes, the the PLLA/ UV absorption (Benzophenone-12) fiber membranes higher than PLLA membrane 61.6% in I875/I1452 Raman intensity ratio and PLLA/ anti-oxidation agents (Chemfos-168) fiber membranes higher than PLLA membrane 3.7% in I875/I1452 Raman intensity ratio. So PLLA Add UV absorption (Benzophenone-12) fiber membranes can achieve good UV

resistance and fast bio-degradation.



Chapter 7 Future work

Over the past few decades, polymers have replaced many of the conventional materials in a variety of applications. Ease of processing, productivity, and decrease in cost of the materials are the most important advantages of using polymers in a number of fields. In most of these applications, the properties of polymers are modified using fillers and fibers to suit the high strength/specific properties requirements. Polymer composites offer advantages over other conventional materials when specific properties are compared. We use the fillers (chlorhexidine-gluconate, calcium carbonate, UV absorption and anti-oxidation agents) with biodegradable polymer Poly(α -L-alanine) by electrospinning in our study. This is possible because of the polymer composites membranes via electrospinning offer over conventional materials. In addition to the field of applied biomedical we believe that this way of processing of polymer composite materials can also be applied to other areas such as: Dye-Sensitized Solar Cell, Piezoelectric film.

References

- [1] L. A. Pilato and M. J. Michno, *Advanced composite materials*. New York, USA: Springer-Verlag, 1934.
- [2] R. B. Seymour, *New concepts in polymer science*. Netherlands: VSP BV, 1990.
- [3] S. M. Lee, "Handbook of Composite Reinforcements," ed: John Wiley & Sons, 1993.
- [4] M. M. Bergshoef and G. J. Vancso, "Transparent Nanocomposites with Ultrathin, Electrospun Nylon-4,6 Fiber Reinforcement," *Advanced Materials*, vol. 11, pp. 1362-1365, 1999.
- [5] S. A. Carter, *et al.*, "Enhanced luminance in polymer composite light emitting devices," *Applied Physics Letters*, vol. 71, pp. 1145-1147, 1997.
- [6] D. N. Saheb and J. P. Jog, "Natural fiber polymer composites: A review," *Advances in Polymer Technology*, vol. 18, pp. 351-363, 1999.
- [7] Z.-M. Huang, *et al.*, "A review on polymer nanofibers by electrospinning and their applications in nanocomposites," *Composites Science and Technology*, vol. 63, pp. 2223-2253, 2003.
- [8] C.-M. Chan, *et al.*, "Polypropylene/Calcium carbonate Nanocomposites," United States Patent US 2003/0060547 A1, 2003.
- [9] H. Tsuji, "Poly(lactide) Stereocomplexes: Formation, Structure, Properties, Degradation, and Applications," *Macromolecular Bioscience*, vol. 5, pp. 569-597, 2005.
- [10] B. Gupta, *et al.*, "Poly(lactic acid) fiber: An overview," *Progress in Polymer Science*, vol. 32, pp. 455-482, 2007.
- [11] H. Tsuji, *et al.*, "Electrospinning of Poly(lactic acid) Stereocomplex Nanofibers," *Biomacromolecules*, vol. 7, pp. 3316-3320, 2006.
- [12] S. François, *et al.*, "A poly(l-lactic acid) nanofibre mesh scaffold for endothelial cells on vascular prostheses," *Acta Biomaterialia*, vol. 5, pp. 2418-2428, 2009.
- [13] O. N. Tretinnikov, *et al.*, "Adsorption of Enantiomeric Poly(lactide)s on Surface-Grafted Poly(l-lactide)," *Langmuir*, vol. 20, pp. 6748-6753, 2004.
- [14] J. F. Cooley, "Apparatus for electrically dispersing fluids " United States Patent 692631, Feb 4, 1902.
- [15] W. J. Morton, "Method of Dispersing Fluids," United States Patent 705691, Jul 29, 1902.
- [16] J. Zeleny, "The Electrical Discharge from Liquid Points, and a Hydrostatic Method of Measuring the Electric Intensity at Their Surfaces," *Physical Review*, vol. 3, p. 69, 1914.
- [17] G. Taylor, "Disintegration of Water Drops in an Electric Field," *Proceedings of the Royal Society of London. Series A. Mathematical and Physical Sciences*, vol. 280, pp.

- 383-397, July 28, 1964.
- [18] G. Taylor, "Electrically Driven Jets," *Proceedings of the Royal Society of London. A. Mathematical and Physical Sciences*, vol. 313, pp. 453-475, December 2, 1969 1969.
- [19] J. Doshi and D. H. Reneker, "Electrospinning process and applications of electrospun fibers," *Journal of Electrostatics*, vol. 35, pp. 151-160, 1995.
- [20] D. Li and Y. Xia, "Electrospinning of Nanofibers: Reinventing the Wheel?," *Advanced Materials*, vol. 16, pp. 1151-1170, 2004.
- [21] S. Ramakrishna, *et al.*, *An Introduction to Electrospinning and Nanofibers*. Singapore: world scientific publishing Co. Pte. Ltd., 2005.
- [22] D. Li, *et al.*, "Electrospinning: A Simple and Versatile Technique for Producing Ceramic Nanofibers and Nanotubes," *Journal of the American Ceramic Society*, vol. 89, pp. 1861-1869, 2006.
- [23] D. H. Reneker and A. L. Yarin, "Electrospinning jets and polymer nanofibers," *Polymer*, vol. 49, pp. 2387-2425, 2008.
- [24] R. Inai and *et al.*, "Structure and properties of electrospun PLLA single nanofibres," *Nanotechnology*, vol. 16, p. 208, 2005.
- [25] S. Agarwal, *et al.*, "Use of electrospinning technique for biomedical applications," *Polymer*, vol. 49, pp. 5603-5621, 2008.
- [26] R. A. Thakur, *et al.*, "Electrospun nanofibrous polymeric scaffold with targeted drug release profiles for potential application as wound dressing," *International Journal of Pharmaceutics*, vol. 364, pp. 87-93, 2008.
- [27] J. M. Corey, *et al.*, "The design of electrospun PLLA nanofiber scaffolds compatible with serum-free growth of primary motor and sensory neurons," *Acta Biomaterialia*, vol. 4, pp. 863-875, 2008.
- [28] V. Pornsopone, *et al.*, "Electrospun Methacrylate-Based Copolymer/Indomethacin Fibers and Their Release Characteristics of Indomethacin," *Journal of Polymer Research*, vol. 14, pp. 53-59, 2007.
- [29] J. Zeng, *et al.*, "Biodegradable electrospun fibers for drug delivery," *Journal of Controlled Release*, vol. 92, pp. 227-231, 2003.
- [30] I. Sondi and B. Salopek-Sondi, "Silver nanoparticles as antimicrobial agent: a case study on E. coli as a model for Gram-negative bacteria," *Journal of Colloid and Interface Science*, vol. 275, pp. 177-182, 2004.
- [31] X. Xu, *et al.*, "Biodegradable electrospun poly(L-lactide) fibers containing antibacterial silver nanoparticles," *European Polymer Journal*, vol. 42, pp. 2081-2087, 2006.
- [32] J. D. Schiffman and C. L. Schauer, "One-Step Electrospinning of Cross-Linked Chitosan Fibers," *Biomacromolecules*, vol. 8, pp. 2665-2667, 2007.
- [33] M. Spasova, *et al.*, "Electrospun Chitosan-Coated Fibers of Poly(L-lactide) and Poly(L-lactide)/Poly(ethylene glycol): Preparation and Characterization,"

- Macromolecular Bioscience*, vol. 8, pp. 153-162, 2008.
- [34] J. Xu, *et al.*, "Preparation of chitosan/PLA blend micro/nanofibers by electrospinning," *Materials Letters*, vol. 63, pp. 658-660, 2009.
- [35] D. S. Jones, *et al.*, "Examination of the physical state of chlorhexidine within viscoelastic, bioadhesive semisolids using raman spectroscopy," *Journal of Pharmaceutical Sciences*, vol. 89, pp. 563-571, 2000.
- [36] L. Chen, *et al.*, "Electrospun cellulose acetate fibers containing chlorhexidine as a bactericide," *Polymer*, vol. 49, pp. 1266-1275, 2008.
- [37] I. C. Yue, *et al.*, "A novel polymeric chlorhexidine delivery device for the treatment of periodontal disease," *Biomaterials*, vol. 25, pp. 3743-3750, 2004.
- [38] R. C. d. Oliveira, *et al.*, "Tissue response to a membrane of demineralized bovine cortical bone implanted in the subcutaneous tissue of rats," *Brazilian Dental Journal*, vol. 15, pp. 3-8, 2004.
- [39] D. B. Jill and W. Hom-Lay, "Periodontal and Endodontic Regeneration," *Journal of endodontics*, vol. 35, pp. 321-328, 2009.
- [40] S. Nyman, *et al.*, "Healing following implantation of periodontitis-affected roots into gingival connective tissue," *Journal of Clinical Periodontology*, vol. 7, pp. 394-401, 1980.
- [41] T. Karring, *et al.*, "Development of the biological concept of guided tissue regeneration — animal and human studies," *Periodontology 2000*, vol. 1, pp. 26-35, 1993.
- [42] F. Yang, *et al.*, "Development of an electrospun nano-apatite/PCL composite membrane for GTR/GBR application," *Acta Biomaterialia*, vol. 5, pp. 3295-3304, 2009.
- [43] C. H. F. Hämmerle and T. Karring, "Guided bone regeneration at oral implant sites," *Periodontology 2000*, vol. 17, pp. 151-175, 1998.
- [44] K. Fujihara, *et al.*, "Guided bone regeneration membrane made of polycaprolactone/calcium carbonate composite nano-fibers," *Biomaterials*, vol. 26, pp. 4139-4147, 2005.
- [45] M. Dewair, *et al.*, "Use of immunoblot technique for detection of human IgE and IgG antibodies to individual silk proteins," *Journal of Allergy and Clinical Immunology*, vol. 76, pp. 537-542, 1985.
- [46] S. Kurosaki, *et al.*, "Fibroin allergy IgE mediated hypersensitivity to silk suture materials," *Journal of Nippon Medical School*, vol. 66, pp. 41-44, 1999.
- [47] K.-H. Kim, *et al.*, "Biological efficacy of silk fibroin nanofiber membranes for guided bone regeneration," *Journal of Biotechnology*, vol. 120, pp. 327-339, 2005.
- [48] S. Liao, *et al.*, "A three-layered nano-carbonated hydroxyapatite/collagen/PLGA composite membrane for guided tissue regeneration," *Biomaterials*, vol. 26, pp.

- 7564-7571, 2005.
- [49] F. Schwarz, *et al.*, "Guided bone regeneration at dehiscence-type defects using biphasic hydroxyapatite+beta tricalcium phosphate (Bone Ceramic®) or a collagen-coated natural bone mineral (BioOss Collagen®): an immunohistochemical study in dogs," *International Journal of Oral and Maxillofacial Surgery*, vol. 36, pp. 1198-1206, 2007.
- [50] H. H. K. Xu and C. G. Simon, "Self-hardening calcium phosphate composite scaffold for bone tissue engineering," *Journal of Orthopaedic Research*, vol. 22, pp. 535-543, 2004.
- [51] Z.-H. Dong, *et al.*, "A guided bone regeneration membrane composed of hydroxyapatite and polyurethane," *Journal of Ceramic Processing Research*, vol. 9, pp. 478-487, 2008.
- [52] L. Wang and C. Li, "Preparation and physicochemical properties of a novel hydroxyapatite/chitosan-silk fibroin composite," *Carbohydrate Polymers*, vol. 68, pp. 740-745, 2007.
- [53] A. Piattelli, *et al.*, "Clinical and histological results in alveolar ridge enlargement using coralline calcium carbonate," *Biomaterials*, vol. 18, pp. 623-627, 1997.
- [54] H. Liao, *et al.*, "Tissue responses to natural aragonite (Margaritifera shell) implants in vivo," *Biomaterials*, vol. 21, pp. 457-468, 2000.
- [55] W. R. Walsh, *et al.*, "A resorbable porous ceramic composite bone graft substitute in a rabbit metaphyseal defect model," *Journal of Orthopaedic Research*, vol. 21, pp. 655-661, 2003.
- [56] N. J. Hess, *et al.*, *Raman spectroscopy at simultaneous pressure and temperature: Phase relations and lattice dynamics of CaCO₃*, 1991.
- [57] F. Huang, *et al.*, "Controlled deposition and transformation of amorphous calcium carbonate thin films," *Crystal Research and Technology*, vol. 44, pp. 818-822, 2009.
- [58] D. Chakrabarty and S. Mahapatra, "Aragonite crystals with unconventional morphologies," *Journal of Materials Chemistry*, pp. 2953-2957, 1999.
- [59] L. Olah, *et al.*, "Synthesis, structural and mechanical properties of porous polymeric scaffolds for bone tissue regeneration based on neat poly(ϵ -caprolactone) and its composites with calcium carbonate," *Polymers for Advanced Technologies*, vol. 17, pp. 889-897, 2006.
- [60] C. Nublat, *et al.*, "Ammonium bicarbonate as porogen to make tetracycline-loaded porous bioresorbable membranes for dental guided tissue regeneration: failure due to tetracycline instability," *Journal of Biomaterials Science, Polymer Edition*, vol. 17, pp. 1333-1346, 2006.
- [61] R. D. Deanin, *et al.*, "Mechanism of ultraviolet degradation and stabilization in plastics," *Polymer Engineering & Science*, vol. 10, pp. 228-234, 1970.

- [62] C. Teng and M. Yu, "Preparation and property of poly(ethylene terephthalate) fibers providing ultraviolet radiation protection," *Journal of Applied Polymer Science*, vol. 88, pp. 1180-1185, 2003.
- [63] F. Urbach, "Chapter 3 The negative effects of solar radiation: a clinical overview," in *Comprehensive Series in Photosciences*. vol. Volume 3, U. G. Paolo, Ed., ed: Elsevier, 2001, pp. 39-67.
- [64] Izhar Halahmi, *et al.*, "UV resistant multilayered cellular confinement system " Tel Aviv, IL Patent US 7648754 B2 2010.
- [65] L. M. Ilharco, *et al.*, "Infrared Approach to the Study of Adsorption on Cellulose: Influence of Cellulose Crystallinity on the Adsorption of Benzophenone," *Langmuir*, vol. 13, pp. 4126-4132, 1997.
- [66] S. E. Blanco, *et al.*, "Conformation, hydrogen bonding and UV solvatochromic shifts of benzophenones in primary alcohols," *Journal of Molecular Structure: THEOCHEM*, vol. 582, pp. 91-105, 2002.
- [67] W. Szaśiadek, *et al.*, "Polarized IR and Raman study and DFT chemical quantum calculations of the vibrational levels for benzophenone single crystal," *Journal of Raman Spectroscopy*, vol. 36, pp. 912-923, 2005.
- [68] L. Babkov, *et al.*, "Raman spectra of metastable phase of benzophenone," *Journal of Molecular Structure*, vol. 792-793, pp. 73-77, 2006.
- [69] N. C. Billingham and P. Garcia-Trabaja, "Physical chemistry of a phosphite processing stabilizer in polypropylene. Part 1: Solubility," *Polymer Engineering & Science*, vol. 41, pp. 417-425, 2001.
- [70] D. H. Jeon, *et al.*, "Antioxidants and their migration into food simulants on irradiated LLDPE film," *LWT - Food Science and Technology*, vol. 40, pp. 151-156, 2007.
- [71] S. S. Biju, *et al.*, "Dual coated erodible microcapsules for modified release of diclofenac sodium," *European Journal of Pharmaceutics and Biopharmaceutics*, vol. 58, pp. 61-67, 2004.
- [72] A. K. Bajpai, *et al.*, "Responsive polymers in controlled drug delivery," *Progress in Polymer Science*, vol. 33, pp. 1088-1118, 2008.
- [73] V. V. Ranade and M. A. Hollinger, "Role of polymers in drug delivery," in *Drug Delivery Systems, Second Edition*, ed: CRC Press, 2003.
- [74] P. D. Riggs, *et al.*, "Chlorhexidine release from room temperature polymerising methacrylate systems," *Biomaterials*, vol. 21, pp. 345-351, 2000.
- [75] G. Rölla and B. Melsen, "On the Mechanism of the Plaque Inhibition by Chlorhexidine," *Journal of Dental Research*, vol. 54, pp. B57-B62, June 1, 1975.
- [76] G. Kister, *et al.*, "Effects of morphology, conformation and configuration on the IR and Raman spectra of various poly(lactic acid)s," *Polymer*, vol. 39, pp. 267-273, 1998.
- [77] P. Taddei, *et al.*, "Vibrational spectroscopy of polymeric biomaterials," *Journal of*

- Raman Spectroscopy*, vol. 32, pp. 619-629, 2001.
- [78] A. Piattelli, *et al.*, "Bone formation inside the material interstices of e-PTFE membranes: a light microscopical and histochemical study in man," *Biomaterials*, vol. 17, pp. 1725-1731, 1996.
- [79] C. H. F. Hämmerle, *et al.*, "Temporal dynamics of healing in rabbit cranial defects using guided bone regeneration," *Journal of oral and maxillofacial surgery : official journal of the American Association of Oral and Maxillofacial Surgeons*, vol. 53, pp. 167-174, 1995.
- [80] H. A. Marouf and H. M. El-Guindi, "Efficacy of high-density versus semipermeable PTFE membranes in an elderly experimental model," *Oral surgery, oral medicine, oral pathology, oral radiology, and endodontics*, vol. 89, pp. 164-170, 2000.
- [81] A. Piattelli, *et al.*, "Evaluation of guided bone regeneration in rabbit tibia using bioresorbable and non-resorbable membranes," *Biomaterials*, vol. 17, pp. 791-796, 1996.
- [82] A. V. Imbronito, *et al.*, "Healing of alveolar bone in resorbable and non-resorbable membrane-protected defects. A histologic pilot study in dogs," *Biomaterials*, vol. 23, pp. 4079-4086, 2002.
- [83] M. Soncini, *et al.*, "Experimental procedure for the evaluation of the mechanical properties of the bone surrounding dental implants," *Biomaterials*, vol. 23, pp. 9-17, 2002.
- [84] Wöhler and Liebig, "Untersuchungen über das Radikal der Benzoesäure," *Annalen der Pharmacie*, vol. 3, pp. 249-282, 1832.
- [85] G. M. Day, *et al.*, "Investigating the latent polymorphism of maleic acid," *Chemical Communications*, pp. 54-56, 2006.
- [86] A. Sigel, *et al.*, *Biomineralization: From Nature to Application* vol. 4: John Wiley & Sons Ltd, The Atrium, Southern Gate, Chichester, 2008.
- [87] H. A. Lowenstam and S. Weiner, *On Biomineralization* Oxford University Press, Inc., 1989.
- [88] M. Sarikaya, "Biomimetics: Materials fabrication through biology," *Proceedings of the National Academy of Sciences of the United States of America*, vol. 96, pp. 14183-14185, December 7, 1999.
- [89] N. V. Vagenas, *et al.*, "Quantitative analysis of synthetic calcium carbonate polymorphs using FT-IR spectroscopy," *Talanta*, vol. 59, pp. 831-836, 2003.
- [90] C. G. Kontoyannis and N. V. Vagenas, "Calcium carbonate phase analysis using XRD and FT-Raman spectroscopy " *The Analyst*, vol. 125, pp. 251-255, 2000.
- [91] H. Wei, *et al.*, "Crystallization habit of calcium carbonate in presence of sodium dodecyl sulfate and/or polypyrrolidone," *Journal of Crystal Growth*, vol. 260, pp. 545-550, 2004.

- [92] C. G. Kontoyannis, *et al.*, "Quantitative Analysis of Sulfated Calcium Carbonates Using Raman Spectroscopy and X-ray Powder Diffraction," *The Analyst*, vol. 122, pp. 33-38, 1997.
- [93] R. R. Anderson and J. A. Parrish, "The Optics of Human Skin," *J Investig Dermatol*, vol. 77, pp. 13-19, 1981.
- [94] N. Agar and A. R. Young, "Melanogenesis: a photoprotective response to DNA damage?," *Mutation Research/Fundamental and Molecular Mechanisms of Mutagenesis*, vol. 571, pp. 121-132, 2005.
- [95] T. M. Nolan, *et al.*, "The Role of Ultraviolet Irradiation and Heparin-Binding Epidermal Growth Factor-Like Growth Factor in the Pathogenesis of Pterygium," *The American Journal of Pathology*, vol. 162, pp. 567-574, 2003.
- [96] A. Springsteen, *et al.*, "In vitro measurement of sun protection factor of sunscreens by diffuse transmittance," *Analytica Chimica Acta*, vol. 380, pp. 155-164, 1999.

